POLITECNICO DI TORINO

Master's Degree in Civil Engineering

SEISMIC DESIGN AND LIFE CYCLE COST ANALYSIS OF A STEEL MRF BUILDING

Supervisors:

Prof. Gianpaolo Cimellaro

Prof. Fabio Freddi

Candidate:

Mattia Sabatini

Academic Year: 2024/2025

Abstract

Nowadays, the increasing demand for resilient and sustainable structures leads to design strategies that go beyond probabilistic criteria based on building's life-safety. Performance-based seismic design approach assesses building and determines the probability of experiencing a certain loss. The current work examines a steel Moment Resisting Frame (MRF) office building, located in L'Aquila, Italy, by applying FEMA P-58 framework. Losses assessment is performed, comparing the EC8 design scenario (PACT's intensity-based analysis) and 2009 L'Aquila earthquake scenario (PACT's scenario-based analysis). Annualized probabilities are computed as well through PACT's time-based performance assessment, developing building's life cycle cost analysis. The Moment Resisting Frame is designed through EC3 and EC8 rules, attending to ductility criteria and capacity design (i.e. hierarchy of strength). HEB400 and IPE360 sections are assigned respectively to the MRF's columns and beams and an Openseespy model to represent the lateral seismic resistant frame is created. Columns are modelled as fiber-section elements to consider distributed plasticity, whereas end-beams are represented by non-linear hysteretic springs referring to the Lignos model. Firstly, non-linear static analyses are conducted to establish elements capacity and pushover curve. Then, non-linear time history analyses are carried out by amplitude/scaling a suite of ground motion to the target EC8 spectrum, with the purpose to deeply understand cyclic behavior of the dissipative elements. Finally, IDAs are performed and fragilities curves referred to both local and global EDP, such as roof plastic hinge rotation and interstory drift, are obtained. Building's damage states are thus depicted, and collapse fragility is obtained. FEMA P-58 framework is subsequently implemented to conduct the various PACT analyses (intensity, scenario, time-based). Non-linear analyses results are incorporated and arranged with a Monte Carlo procedure to develop hundreds of statistically obtained demand vectors. The study shows that L'Aquila scenario, compared to the design situation, results in 34% increase in median repair time and 52% increase in median repair cost. Moreover, structural components make a larger contribution to the overall losses than the design situation. However, time-based assessment illustrates the total repair time and cost evolution with the seismic intensity. Low intensities result in losses controlled by non-structural elements damage. As the seismic level increases, structural components make the dominant contribution, with occasional collapses and not repairable realization due to exceeding residual drift limits. At near median collapse intensities, residual drift and structural damage govern the losses.

Table of Contents

List of Figures

1. INTRODUCTION

1.1. Seismic Design and Performance Based Assessment Background

The increasing development in structural earthquake resistance systems and the pressing demand for resilient and sustainable structures leads to design structure with the purpose of achieving selected target performance level. Northridge's 1994 earthquake, which resulted in approximately 45 billion $ direct losses, was the first to highlight the need for consideration on post-event functionality. Guidelines on performance-based design (PBD) were created (e.g. ATC 40, FEMA 350) and incorporated into structural engineering practice [1]. Unlike Code-based design requirement, which deals with building's life-safety (i.e. strength and stiffness requirement), Performance-Based Seismic Design (PBSD) first generation allowed consideration on the structural response in terms of discrete performance levels, such as operational (OP), immediate occupancy (IO), life safety (LS) and collapse prevention (CP) [2]. These performance levels were damage-based and derived from EDP (e.g. plastic hinge rotation, story drift). Second generation of performance-based earthquake engineering (PBEE) was developed to extend these considerations and predict consequences, including repair cost, repair time (i.e. downtime), risk to human life and environmental impacts [1]. The purposes are to reduce costs due to post-events repair and determine the probability of experiencing a certain loss so that owners and designers can select performance to be achieved. Such performances are thus measured in terms of probability of incurring casualties, unsafe placards, repair time and repair cost [3].

1.2. Research Motivation

Over the years, the development of performance-based seismic design highlighted significant advantages in assessing post-event functionality and economic losses. However, its practical application in Europe has not been widely adopted, using force-based design method which mainly focuses on forces as design parameters. Indeed, even though EC8 acknowledges PBSD approach, there is not an extended use of it [4]. Recognizing this gap, the present work describes a detailed implementation of the FEMA P-58 performance-based seismic design methodology within an EC8 design contest. The combined results provide a deeper understating of the expected performance, quantifying downtime and repair costs for different earthquakes intensities over the building's life period.

1.3. Study Framework

The current work consists in a seismic design and life-cycle assessment of a steel Moment Resisting Frame office building located in L'Aquila, Italy. The structural design was carried out according to both EC8 and EC3, following capacity design and hierarchy of strength for the MRF dimensioning and EC3 provision for the gravity frame. A detailed Openseespy model was developed to analyze global behavior of the seismic resistant system by means of pushover, IDAs and Fragility curves. Columns were modelled as fiber-section, while beam as elastic elements. Lignos model is assigned to the expected plastic hinges to consider hysteretic joint behavior. Pushover analysis shown the progressive loss of building strength, whereas IDAs derived fragilities was used to determine the building global dynamic behavior and collapse fragility as well. FEMA P-58 was implemented by first develop seismic hazard for the 3 main PACT's analysis: intensity, scenario and time-based assessment. The seismic hazard was defined through the following approaches:

- EC8 code-based spectrum for the intensity-based analysis
- Deterministic-obtained spectrum for the scenario-based analysis, using ground motion prediction equations representing L'Aquila, 2009, earthquake
- Hazard curve considering the MAFE (mean annual frequency of exceedance) integrated by EFEHR for time-based assessment

Through the PACT tool implementation, repair cost and time fragilities are obtained and component losses distribution analyzed. Results show a comparison between code-based and scenario (L'Aquila, 2009) assessment, as well as a building's life period global and local losses evolution.

2. METHODOLOGY

Eurocode 8 (EN 1998 – 1) provides design criteria to ensure that structures achieve required level of safety and ductility in seismic region, with the objective of preventing collapse and controlling possible damage incurring. Concurrently Performance-Based approaches allow to extend the analysis with complementary tools that go beyond the design checks, evaluating the global response in terms of demand, capacity and expected losses [5], [6]. Integrating these two approaches provides a connection between code-based design and performance-based assessment to achieve a more complex, comprehensive and accurate evaluation of the structure response.

2.1. EC8 Moment Resisting Frame Design

Among the different strategies for seismic-resistant building, one of the most used is a particular type of structural systems equipped with Moment Resisting Frames (MRFs). The main feature of this approach is the erection of a gravity frame which is intended to carry only vertical load, whereas the whole horizontal seismic demand and lateral forces are resisted by the Moment Resisting Frame. This system relies on rigid beam-to-column joints which withstand seismic action and promote energy dissipation in predetermined zones, typically with the formation of plastic hinge.

2.1.1. Ductility

Ductility is a fundamental concept when energy dissipation is required in seismic engineering as it describes the capability of structures to achieve significant deformation without loss of strength. It's defined as the ratio between the ultimate and the yield deformation:

$$\mu = \frac{\varepsilon_u}{\varepsilon_y} \tag{2.1}$$

This feature allows structures to dissipate energy during strong excitation through controlled inelastic deformation, avoiding brittle failure and achieving reliable and predictable ductile behavior.

2.1.1.1. Material Ductility

As defined in (2.1), in order to achieve significant deformation without loss of strength, ductile materials dissipate energy by increasing their inelastic deformation during plastic

branch. Figure 2.1 illustrates this behavior, the post-yield branch where inelastic deformation occurs while the stress level remains constant. Ductile elements are designed to yield under seismic action while other structural elements are designed to resist the maximum action transferred by these dissipative zones.

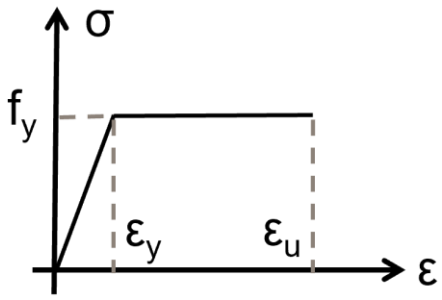

Figure 2.1: material stress-strain law (elastic-perfectly plastic)

2.1.1.2. Section Ductility

Cross-section ductility is defined by classification in four section compactness classes. They are based on requirements for plastic analysis according to slenderness and on the capability to reach some bending moment levels. Class 4 section is the lower one in terms of structural performance, since they develop local buckling before reaching yielding. Class 3 section is defined as semi-compact, they are able to reach yielding bending moment, but they can't reach the plastic one. Class 2 section are considered "compact", they can reach plastic bending moment with a limited rotation capacity. Class 1 section is called "plastic" and they can reach both plastic bending moment and significant rotation. Figure 2.2 Illustrates moment-rotation features among the four section classes.

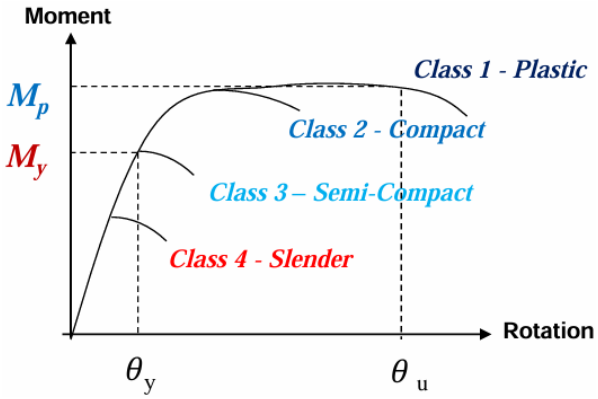

Figure 2.2: moment-rotation features for each cross-section classes (adapted from Freddi, UCL, lecture notes)

2.1.1.3. Structure Ductility

Ductility is both a material and structure's property; the use of ductile materials doesn't necessarily mean that the structure will behave in a ductile manner. Therefore, EC8 Capacity Design requires to attend a good Hierarchy of Strength where the weakest element will be the first to reach plastic behavior. The optimal global behavior would be the formation of the first plastic hinge on the beams, while the last at the base columns. Figure 2.3 Shows two possible mechanisms: the first one is the optimal while the second one, so called soft story mechanism, is the one to avoid. Dealing with global ductility it's important to refer also to local ductility. The hinge created in the edge beam must be able to develop the minimum required rotation capacity before the last base column's plastic hinge is formed.

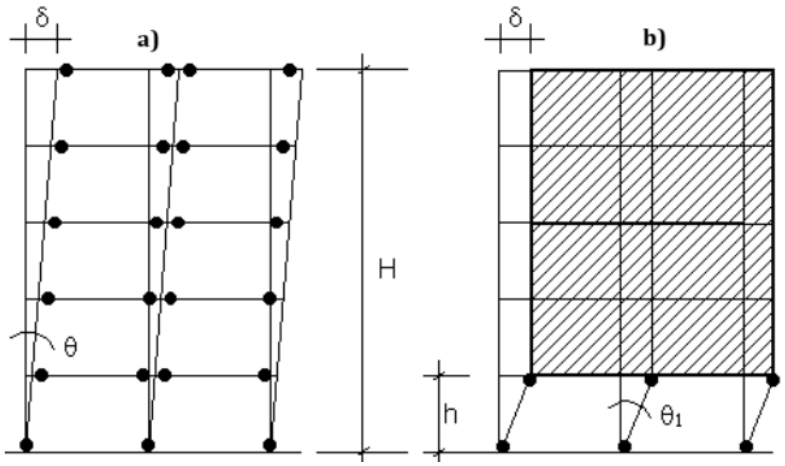

Figure 2.3: plasticisation mechanism a) optimal mechanism b) soft story mechanism (adapted from Ceravolo, Polytechnic of Turin, lecture notes)

2.1.1.4. Behavior Factor

When design concerns with ductility, the behavior factor "q" must be considered. It is used to divide the elastic response spectrum obtaining the inelastic design response spectrum, an approach widely used to perform elastic analysis also when structure is supposed to response inelastically [7]. Behavior factor goes from 1.5-2 for structures belongings to low ductility class (DCL) to 6-6.5 for high ductility class (DCH) structures. Moment Resisting Frame "q" with high ductility is defined as:

$$q = 5 * \frac{\alpha_u}{\alpha_1} \tag{2.2}$$

Where α_i factor is defined by the structural system as in Figure 2.4:

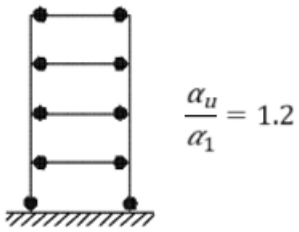

Figure 2.4: single span moment resisting frame regular in elevation (adapted from Freddi, UCL, lecture notes)

Whereas DCL structure is designed to respond in the elastic range, DCH Moment Resisting Frame design attends both EC3 and EC8 requirement due to the dissipative behavior of the structural system.

2.1.2. Response Spectrum Analysis Principles

Once the structural system and gravity load are defined, it must be computed lateral load intensity due to the earthquake. Lot are the strategies to compute these forces: FEM software like sap2000 are able to compute, just by inputting elastic response spectrum and structure data like element size and vertical load, solicitation diagram. These are obtained by superposition of effect, as shown in Figure 2.5, and will be required for EC8 checks. Displacement, rotation, and deformation are computed as well. The resulting displacement obtained in the analysis ($\delta_{e,i}$, Figure 2.6), multiplied by the behavior factor to take into account spectral acceleration reduction passing from the elastic to inelastic design response spectrum, will be used in the damage and second order effect checks.

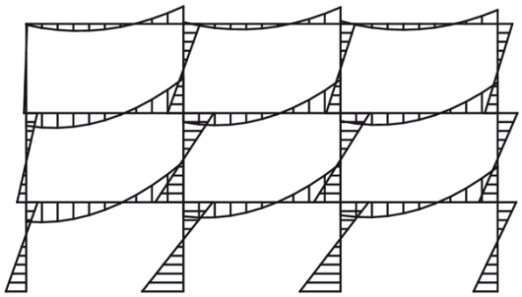

Figure 2.5: bending moment due to gravity and earthquake load: effect superposition (adapted from Freddi, UCL, lecture notes)

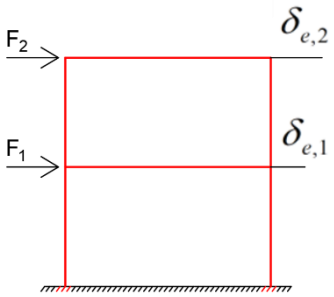

Figure 2.6: response spectrum analysis elastic displacement (to be multiplied by "q")

2.2. Hazard Analysis

Seismic hazard analysis is considered an effort to quantify seismic hazard like ground shaking, fault rupture, soil liquefaction, and their associated uncertainty in time and space, providing estimates for seismic risk assessment, that's the probability of occurrence of any consequence both to humans and their built environment [8]. The first step of this process is defining the site, which means define soil condition represented by shear wave velocity:

$$V_s = \frac{30}{\sum_{i=1}^{n} \frac{h_i}{\upsilon_i}} \tag{2.3}$$

As an illustration, NTC2018 establish five different categories based on the mentioned physical property of the ground: "A" category deal with topography where shear wave velocity are considered at least 800 m/s [9]. Another set of fundamental parameters are distance measurements such as the Joyner-Boore distance (R_{jb}: distance to the surface projection in the direction of the dip), the rupture distance (R_{rup}: closest distance to the rupturing fault plane) and the distance along the fault strike ($R_{x,i}$) [10]. These parameters are all considered equal to zero if the building is located inside the fault's surface projection (Figure 2.7).

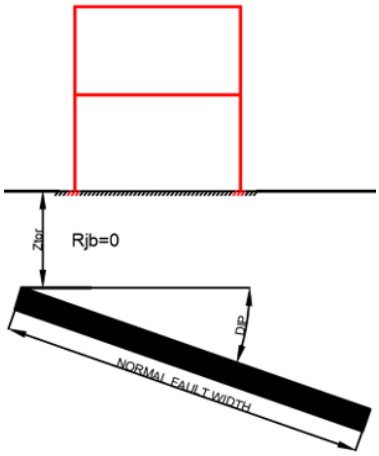

Figure 2.7: Joyner-Boore distance of a building located on the fault surface projection

The last parameter to be considered in the site-source characterization is the magnitude of the potential seismic scenario (M_w). Earthquake magnitude is fundamental both in the probabilistic hazard analysis and in the deterministic hazard analysis. In the first case it represents a possible scenario to be included into the statistical integration constructing probabilistic curves (MAFE, probability of exceedance along a specific period) where the probabilistic hazard spectrum is derived. In the deterministic approach, instead, M_w represents the main scenario considered in the prediction equation constructing the deterministic hazard spectrum.

2.2.1. Attenuation Relationship

In order to compute probabilistic and deterministic spectrum is required to develop some equation, also called ground motion prediction equation, that allows to convert single ground motion record (M_i, $R_{jb,i}$, R_{rup}) into a prevision of seismic intensity like PGA, PGV, 5%-damped spectral acceleration. Bindi et al [11] developed such equations from the ITACA strong motion database, updating the existing ITA08 with a larger number of records, including only earthquake whose M_w is avaiable and avoiding single station earthquake's record. The regression is made considering magnitude going from 4 to 6.9 and site-to-sources distances up to 200km. Figure 2.8 extracted by Bindi et al [11] shows the whole data set considered by the autors in the new ITA10, comparing it with ITA08:

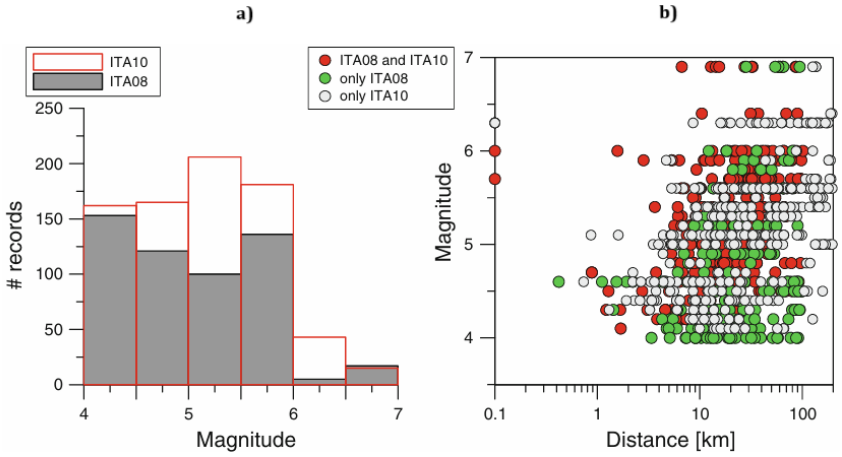

Figure 2.8: Bindi et al. dataset a) number of record over specific magnitude b) magnitude of record over specific distance

Once the database containing the records is defined it's possible to compute each seismic parameter of interest. Equation (2.4) developed by Bindi et al is based on Boore and Atkinson model [12] modifying site classification including a term linearly decreasing with the distance and neglecting non-linear terms [11]:

$$\log_{10} Y = e_1 + F_D(R,M) + F_M(M) + F_S + F_{Sof} \tag{2.4}$$

Where e_1 is a regression coefficient, F_D is a distance function presented as follows:

$$F_D(R,M) = [c_1 + c_2 * (M - M_{ref})] * \log_{10}\left(\frac{\sqrt{R_{JB}^2 + h^2}}{R_{ref}}\right) - c_3 * \left(\sqrt{R_{JB}^2 + h^2} - R_{ref}\right) \tag{2.5}$$

Where c_1, c_2, c_3, h are regression coefficients as e_1, M_{ref} is equal to 5 and R_{ref} is chosen as 1 km. Joyner-Boore distance depends on the location of the site as mentioned above. F_M represents the magnitude function that is:

$$F_M(M) = \begin{cases} b_1 * (M - M_h) + b_2 * (M - M_h)^2 \\ b_3 * (M - M_h) \end{cases} \tag{2.6}$$

M_h is equal to 6.75 while b_1, b_2, b_3 are regression coefficients as well. F_S represents the site amplification, and it's given by:

$$F_S = s_j * C_j \tag{2.7}$$

With j going from 1 to 5, s_j are regression coefficients and C_j are dummy variables used to denote the five EC8 site classes. Finally, F_{sof} represents the style of faulting:

$$F_{sof} = f_j * E_j \tag{2.8}$$

For j=1,…,4, considering f_j as regression coefficients and again E_j are dummy variables taking in consideration the fault classes. The four style of faulting considered by Bindi et al are: normal (N), reverse (R), strike slip (SS) and unknown (U) [11]. By means of attenuation relationship defined above it's possible to compute different curves representing seismic intensity (and the decrease of its soil parameter intensity) related to the event's magnitude and distance source-to-site, as is shown in Figure 2.9:

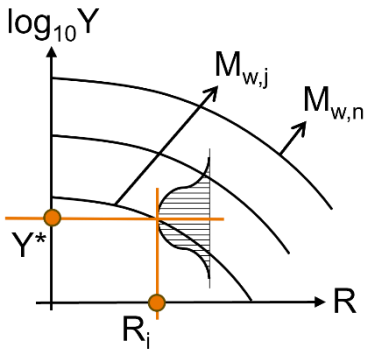

Figure 2.9: GMPE (ground motion prediction equation) curves, attenuation of the ground motion parameter Y with the distance

These obtained curves is the representation of the predicted seismic ground motion parameter (vertical axis) attenuation related to the site-to-source distance (horizontal axis) for a costant magnitude. Each curve includes the lognormal uncertainty of the parameter around the mean value [10].

2.2.1.1. Deterministic Spectrum (PACT Scenario-Based Spectrum)

One of the existing approaches to define seismic hazard is to create a deterministic response spectrum by fixing specific couple M-R in Figure 2.9 and compute for each spectral period (0.2s-2s, [11]) the spectral acceleration [10]. Each defined value is considered as a mean and must be take into accoun with his dispersion. This approach is particularly interesting analyzing structural responses against specific earthquake events: that's how the scenario-based spectrum is defined in PACT (Performance Assessment Calculations Tool).

2.2.2. Hazard Curves

Alternatively, a classical procedure to define seismic hazard is developing probabilistic response spectrum. Firstly, is computed an hazard curve which describes the probability or frequency of exceedance of a certain seismic intensity level for a certain period T_i. Successively it's possible to extrapolate spectral accelerations and create the probabilistic spectrum by fixing an interest time period with the same probability/frequency of exceedance.

2.2.2.1. Probability of Exceedance

The process of deriving an hazard curve for T_i and a probabilistic spectrum consequently consists of a triple integration. Like in the deterministic approach, the first step want to consider a couple M-R (Figure 2.9) corresponding to a single seismic source, and this time evaluate the probability the ground motion parameter Y*, corresponding to the mean of the chosen couple M-R, exceed a certain target seismic intensity level y* as described in equation (2.9) and Figure 2.10.

$$z = \frac{y^* - Y^*}{\sigma_{Y^*}} \qquad (2.9)$$

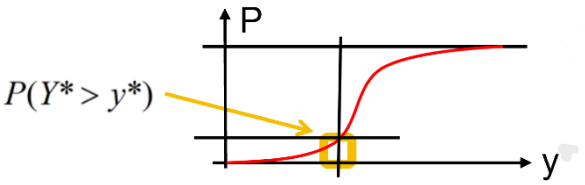

*Figure 2.10: probability of exceeding a certain seismic intensity level y**

The second step consist in integrating over the whole possible seismic source considering the mean annual frequency of exceedance of the lower event magnitude occurring "υ" (equation 2.10, Figure 2.11) and finally integrate over the all seismic intensity level y* as shown in Figure 2.12.

$$\lambda_{y^*} = \sum_k \nu^* \sum_j M^* \sum_i R^* [P(Y^* > y^*) \mid m_j, r_i] * [P(M = m_j)] * [P(R = r_i)] \qquad (2.10)$$

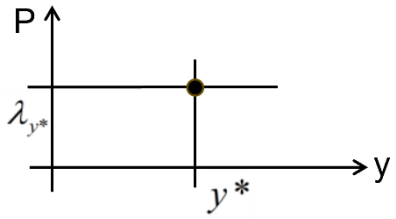

Figure 2.11: probability of exceeding of a specific site a certain value y considering the various possible seismic sources*

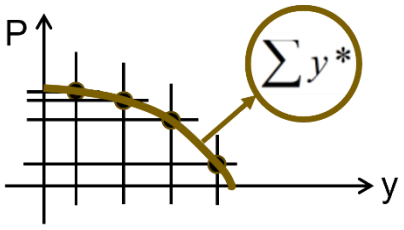

*Figure 2.12: probability of exceedance of a specific site considering the various possible seismic sources and seismic intensity level y**

2.2.2.2. MAFE Curve (PACT Time-Based hazard)

Figure 2.12 represents the probability of exceedance, for a certain site, of the whole possible incurring seismic intensity level y*, for a specific spectral period T_i. The process could be repeated to create different curves such as describing the site behavior for different spectral periods. As discussed above, the ground motion parameters Y* and y* could represent PGA, PGV or 5%-damped spectral acceleration. Figure 2.13 shows as an illustration spectral acceleration's hazard curve: each curve, represented by different color, is the probability of exceeding a certain spectral acceleration over 50 years (e.g. considering the orange curve (T_i) there's 10% probability $S_a(T_i)$ will be exceeded within 50 years).

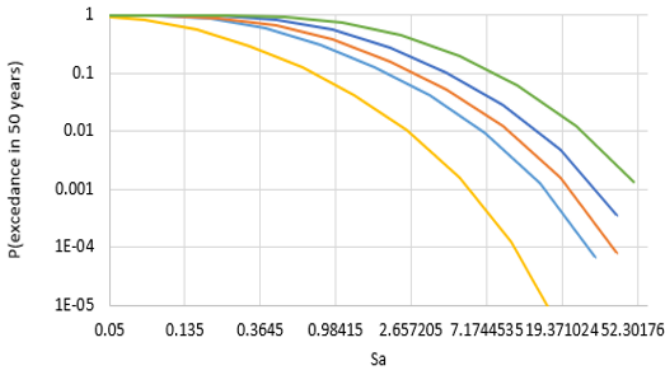

Figure 2.13: site specific hazard curves describing probability of exceeding a certain spectral acceleration over 50 years

Figure 2.13 curves can be manipulated to obtain the a curve where, instead of the probability of exceedance within 50 years, the MAFE (Mean Annual Frequency of Exceedance) is inserted in the vertical axis Figure 2.14. This procedure is made using the following equation:

$$P(Y^* > y^*) = 1 - e^{-\lambda T} \tag{2.11}$$

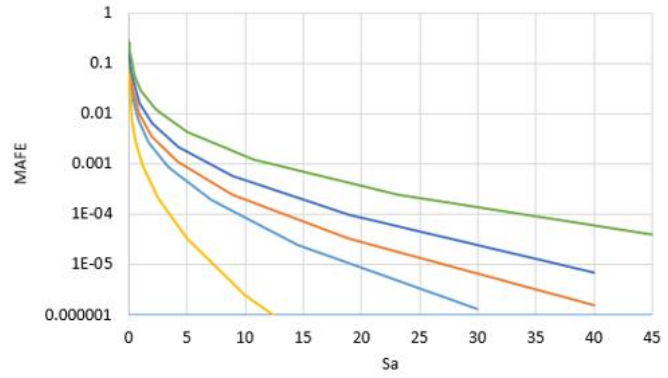

Figure 2.14: site specific hazard curves describing the mean annual frequency of exceedance of a certain spectral acceleration

Such curves are commonly used to describe site hazard: PACT (Performance Assessment Calculation Tool) makes use of them as well to correlate the mean annual frequency of

exceedance of certain intensity level with the possible damage to be sustained by the analyzed building.

2.2.2.3. Probabilistic Hazard Consistent Spectrum (EC8 & PACT Intensity-Based Spectrum)

Another consideration to be made is the development of probabilistic hazard-derived spectrum from hazard curves as Figure 2.13. Fixing a target probability level (e.g. 10% probability within 50 years) the corresponding spectral accelerations can be extracted from each T_i curve. These values define the hazard-derived spectrum. It's also interesting to compare it with some code-based spectrum (e.g. NTC2018 spectrum considering 475 years return period, which corresponds to 10% probability of exceedance within 50 years) Figure 2.15:

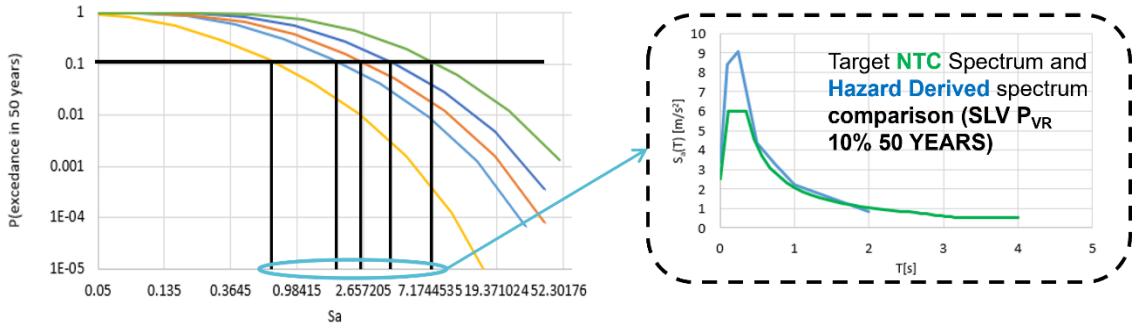

Figure 2.15: hazard-derived spectrum compared with NTC 2018 target spectrum

Probabilistic spectrum is the starting point for each PACT intensity-based analysis and for building's seismic design as well.

2.3. PACT

PACT (Performance Assessment Calculation Tool) is a software developed by FEMA P-58 containing a user-friendly platform to carry out intensity, scenario and time-based loss calculation. PACT scope is to reduce costs due to earthquake damage occurring providing an alternative strategy to code-based design, which only deals with life-safety of the building. PBSD (Performance-based Seismic Design) is based on an assessment of the building design to evaluate the probability of experiencing different damage and losses amount, measured in terms of casualties, repair and replace cost, repair and replace time, unsafe placards. The main process of the analysis consists of capturing main building data, input earthquake shaking, applying building fragilities and consequences to some pre-established components and presenting results of a huge number of loss estimations runs [3].

2.3.1. Building Model

Defining the model means inputting all the data required to characterize the size, construction costs and occupation of the designed building. Building data key points are reported below in Figure 2.16:

Building Data	Description
story number and floor area	A floor level and the story above is represented by the same number. Usually basement story are considered rugged and not counted in the numeration
total replace cost & time	cost to be substained to demolish, remove the damaged building and replace it
shell replace cost	replacement of the basic building structure before of the tenants improvements
occupation	establish the number of people present in the building at different times and days, depending also in the population model (healtcare, office ecc), determine type and quantity of non-structural component

Figure 2.16: mean building data to be inserted in PACT

The second fundamental step in characterizing the building is to define the components that is supposed to be damaged by earthquake events. All the structural and non-structural vulnerable components are characterized by fragility functions and included into performance groups to define components quantities. It's possible to derive these quantities into building inventory. An excel workbook has been created containing normative quantities based on typical values as well [3].

2.3.1.1. Component fragilities

PACT fragilities components are divided into categories: A – substructure, B – shell, C – interiors, D – equipment and furnishings, E – special construction and demolition. Each fragility establishes the probability a certain component will reach or exceed some damage state (DS), as a function of an EDP (engineering demand parameter). The main PACT's EDP are interstory drift ratio and floor acceleration. As an illustration Figure 2.17 shows a typical fragility function reporting its damage states. These curves are usually modeled by lognormal cumulative density function and defined by the key parameters median (θ), which defines 50% probability of exceeding the selected damage state and dispersion (β), representing damage uncertainty.

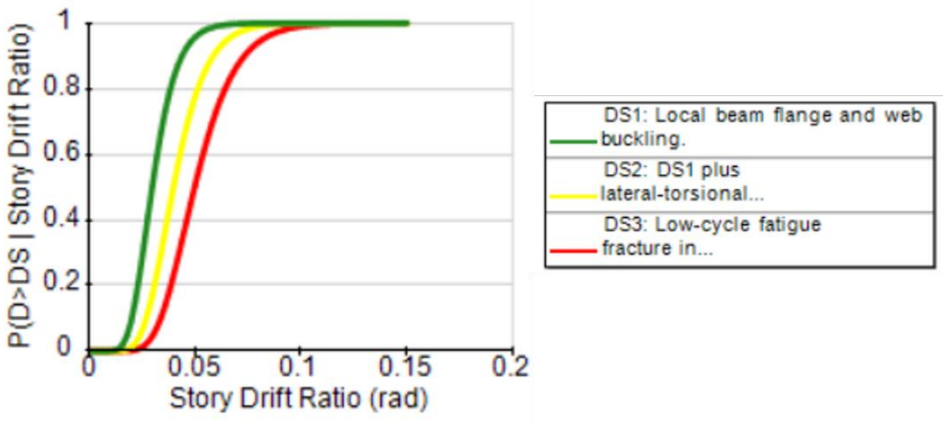

Figure 2.17: PACT's component fragility example

Units of measurements are associated with performance group to well estimate consequences and damages. The quantities of components in a performance group are given by the total number of components present in the building divided by the related unit of measurement. Components can be defined in units of “each” (e.g. elevators), “lineal feet” (e.g. 100 LF for partition walls), “square feet” (e.g. 100 SF for ceiling) and others. As an illustration, a building floor containing 350 meters of partition walls will result, as PACT input quantity, in 3.5 (i.e. 350/100). Rugged components are not included in the building performance model because they are considered as not damageable [3].

2.3.1.2. Building Fragilities

It’s necessary to consider the probability the entire structure may experience critical performance level. Building collapse is the main cause of earthquake induced casualties and, even if collapse has not occurred, excessive residual drift could represent an issue resulting in the convenience to replace the whole building [3]. Whereas there is a default PACT’s residual drift fragility available, building collapse fragility must be determined. The first step consists in defining the various possible collapse mechanisms and their related probability of occurrence. Figure 2.18 shows a simplified representation for a 2-story frame.

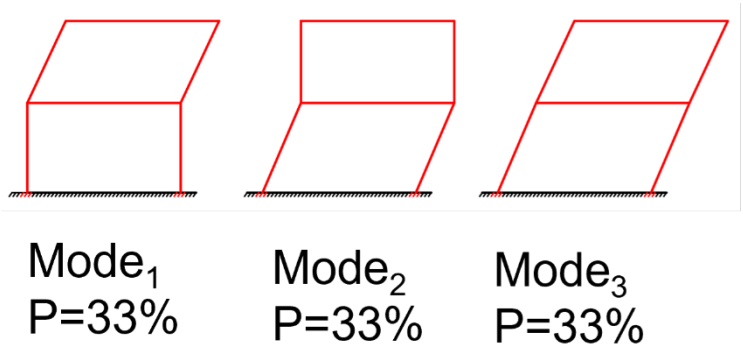

Figure 2.18: 2-story frame's collapse modes example

PACT requires the obtained collapse modes and the median and dispersion value of the Collapse fragility. This fragility defines the probability of incurring structural collapse as a function of ground motion intensity. There are several strategies to develop collapse fragility; among them, one of particular interest is IDA (Incremental Dynamic Analysis). IDA involves subjecting a structural model to a suite of ground motion records, each scaled to different intensity levels, producing curves describing the relationship between the increase of the intensity and the corresponding generated EDP [3], [13].

2.3.2. Performance Assessment

Since the model has been defined and compiled, the results of the analysis need to be incorporated into the PACT's framework to successively allow loss computation. What's mainly the tool procedure deals with is transforming a few sets of analysis results, obtained either through NLTHA (Non-Linear Time History Analysis) or simplified procedures, into a huge number of demand vectors to be analyzed in a statistical manner within the loss analysis.

2.3.2.1. Earthquake Hazard

Earthquake ground shaking is characterized by target response spectrum. For intensity-based analysis the response spectrum could be any code-based probabilistic spectrum as discussed in "Probabilistic Hazard Consistent Spectrum (EC8 & PACT Intensity-Based Spectrum)". Scenario-based ground shaking is represented by deterministic response spectrum derived from specified distance-magnitude pairs by means of ground motion prediction equations, as seen "in Deterministic Spectrum (PACT Scenario-Based Spectrum)". For time-based analysis, hazard curves such Figure 2.14 must be developed for the specific site of interest. Once the spectrum has been derived, a suite of ground motion spectrum-consistent must be selected and scaled to the spectral acceleration $S_a(T_1)$ of the target spectrum. Figure

2.19 gives an illustration of the scaled ground motion's spectrum. During the analysis, to achieve a more reliable solution, at least 7 ground motion sets must not result in structural collapse [3].

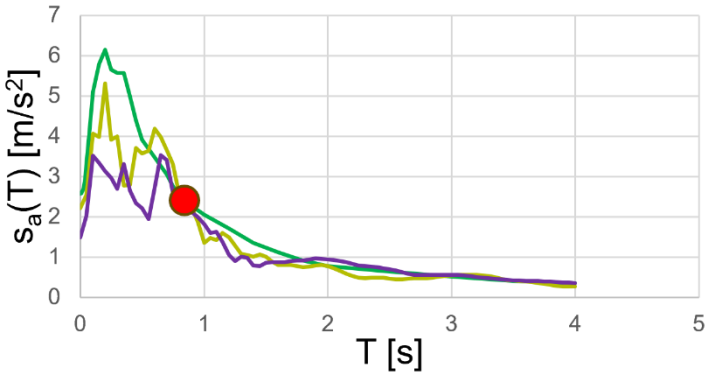

Figure 2.19: ground motion scaling to target spectral acceleration

2.3.2.2. Demand Set Developing: Monte Carlo Simulation

Monte Carlo simulation is the procedure used by PACT to develop many demand vectors starting from the analysis results. Considering "X" as the matrix of the results obtained from the analysis (NLTHA or Simplified), "Y" the matrix of the natural logarithm of the results and "M_Y" the vector containing the mean of "Y", "Σ_{YY}" the covariance matrix of "Y", "D_Y" and "L_Y" the matrix containing the square roots of the eigenvalue and the eigenvector of "Σ_{YY}", then the new matrix "W" containing the huge number of statistically obtained demand vector is given by the exponential of Z:

$$Z = L_Y * D_Y * U + M_Y \tag{2.12}$$

Where "Z" is a vector of natural logarithm of demand parameters with the same statistical distribution as "Y" and "U" is a vector of uncorrelated standard normal random variables. Both the model uncertainty "β_m" and the uncertainty on the shape of the scenario-based spectrum "β_{gm}" is considered inflating the "Σ_{YY}" using a SRSS (Square Root of the Sum of the Square) [3].

2.3.2.3. Performance Calculation

The last step of the performance assessment consists of analyzing the damage that occurred in each realization and evaluating the losses. Firstly, collapse occurring check is carried out: if the spectral acceleration of the realization exceeds the median collapse spectral acceleration, the run is considered as collapsed, a random number is generated for choosing the collapse mechanism and losses are calculated with total replacement values. If collapse does not occur, the total realization cost is computed summing the repair cost corresponding to the damage

occurred by each component in the current realization. Consequence function is used for this purpose as shown in Figure 2.20:

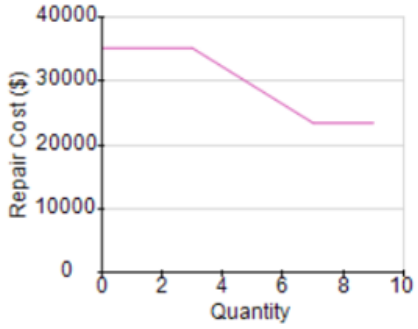

Figure 2.20: PACT conseuquence cost function example

The result consists of a set of time and cost fragilities curves, obtained by aggregating the repair costs and repair times from the single realizations.

3. STEEL MRF CASE STUDY

The present work focuses on the design of a 2-story steel moment resisting frame building, followed by non-linear analysis using Openseespy. Then FEMA P-58 framework is implemented comparing the various PACT's methodology and developing a life cycle cost analysis. Before performing the various PACT analysis, it's therefore necessary to obtain a rigorous and accurate structural model of the building. The 2-story steel moment resisting frame building has been designed attending EC8 and EC3 rules, whereas the Openseespy model has been created to analyze the structural response and better understand its behavior under real ground motion excitation. By means of IDAs, global fragility curves for different damage states have been derived and implemented in PACT.

3.1. Building Design

The case study consists of a 2-story commercial office building located in L'Aquila, Italy, designed as a moment resisting frame. The lateral load is carried only by the MRF (shown as the red lines in Figure 3.1, Figure 3.2), whereas the vertical load is carried by the gravity frame (drawn as the black lines Figure 3.1, Figure 3.2). The building has a square plant composed of 3 bays 6 meters each. The first story height is 3.5 meters whereas the second one is 3.2 meters (Figure 3.1, Figure 3.2).

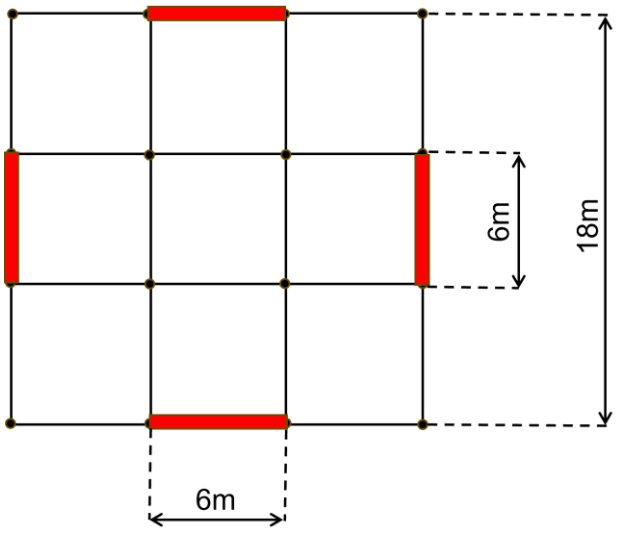

Figure 3.1: case study building's plant view

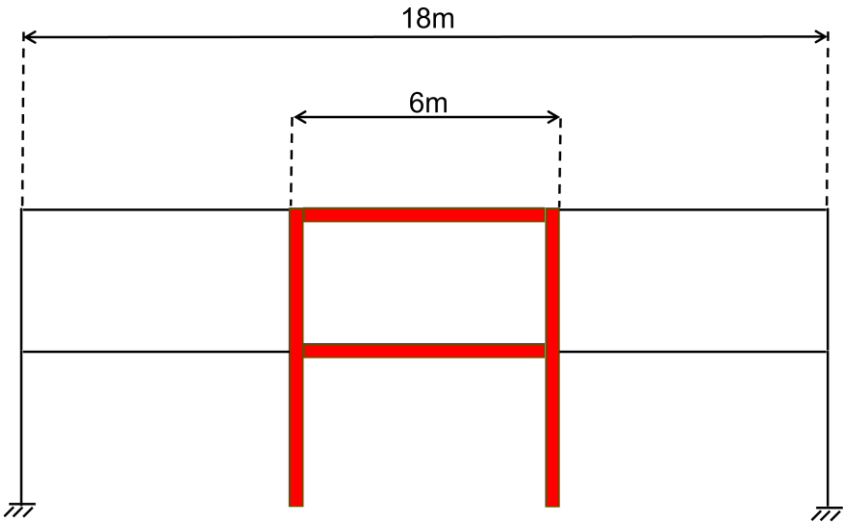

Figure 3.2: case study building's frontal view

Since in the structural system adopted, seismic resistance is provided by the Moment Resisting Frame, the gravity frame has to sustain only vertical loads (i.e. connections considered as pinned and, therefore, bending moment is not transmitted). The design for the structural systems is carried out simultaneously with two different strategies. MRF is designed performing a beam and column section optimization using sap2000, while gravity frame is designed attending EC3 rules and performing the calculation on the most solicited columns and beams system.

3.1.1. MRF Load Analysis

Before developing any calculations, it's fundamental to define areas of interest to establish how many fractions of a certain load a structural system will be required to resist. Each moment resisting frame will sustain half of the whole seismic mass of the building in the corresponding direction of excitation. Both seismic and vertical load's tributary area is depicted as follow : blue hatched area (Figure 3.3) represent the seismic tributary area, whereas the green one (Figure 3.4) defines the vertical loads area (it should be noted that area "A_1" will be used for the calculation of the distributed load acting on the beams while the "A_2" area will deal with the computation of the concentrated forces acting on the columns).

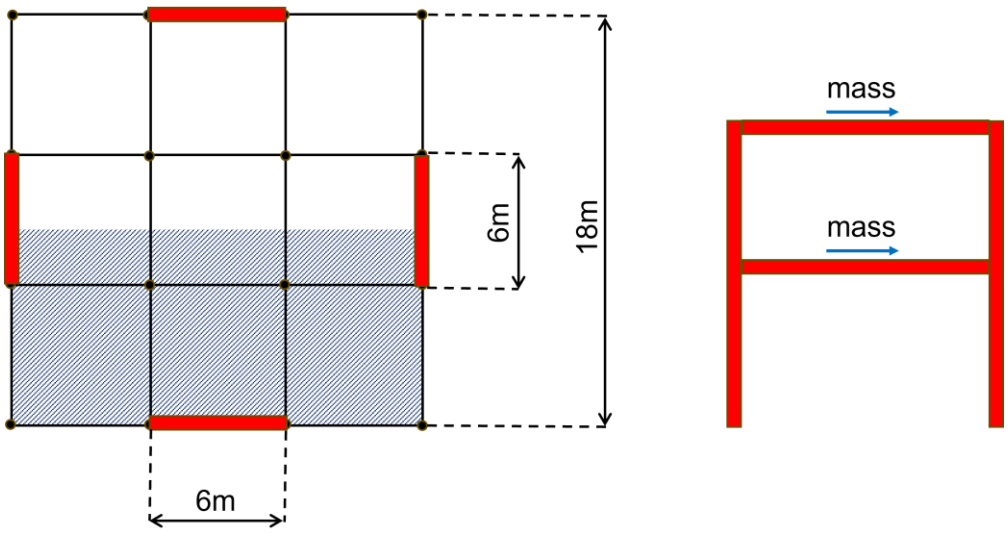

Figure 3.3: MRF's seismic tributary area

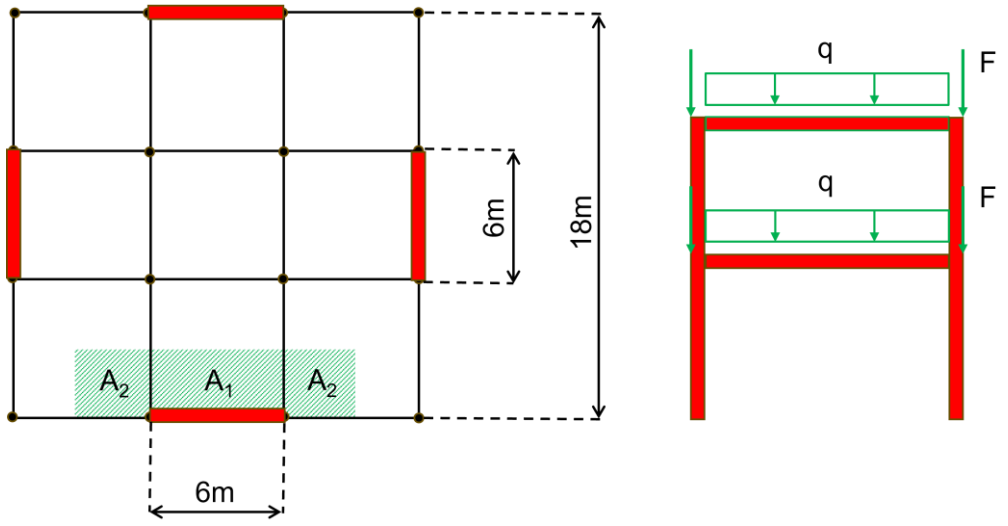

Figure 3.4: MRF's vertical load tributary area

Both the seismic mass (3.3), concentrated forces (3.4) and distributed load (3.5) on the Moment Resisting Frame are obtained from the combination of action for seismic design situation, EC0 [14], equation (3.1):

$$\sum_{j\geq 1} G_{k,j} \text{"+"} P \text{"+"} A_{Ed} \text{"+"} \sum_{i\geq 1} \psi_{2,i} * Q_{k,i} \tag{3.1}$$

Before evaluating the actual value of the mass and forces it's necessary define the amount of permanent and variable load acting on the structure, as follow in equation (3.2):

$$\begin{aligned} G_{k,floor} &= 4.5KN/m^2 \\ G_{k,cladding} &= 2KN/m \\ Q_k &= 2KN/m^2 \end{aligned} \tag{3.2}$$

Consequently, the resulting mass and forces are (equation 3.3-3.5):

$$m = [G_1 * A + G_2 * A + \psi * Q * A + 0.1(G_1 * A + G_2 * A + \psi * Q * A)] * 100 = 98 ton \quad (3.3)$$

$$q = \frac{G_1 * A_1 + G_2 * A_1 + \psi * Q * A_1 + 0.1(G_1 * A_1 + G_2 * A_1 + \psi * Q * A_1)}{L} = 19 KN / m \quad (3.4)$$

$$F = G_1 * A_2 + G_2 * A_2 + \psi * Q * A_2 + 0.1(G_1 * A_2 + G_2 * A_2 + \psi * Q * A_2) = 57 KN \quad (3.5)$$

Where the permanent loads of beams and columns is assumed equal to 10% of the supported weight and the "ψ" coefficient is taken equal to 0.3. The gravity frame design is made in a similar way, but using the combination of action for persistent design situation as illustrated in the following equation (3.6) [14]:

$$\sum_{j \geq 1} \gamma_{G,j} * G_{k,j} \text{"+"} \gamma_P * P \text{"+"} \gamma_{Q,1} * Q_{k,1} \text{"+"} \sum_{i \geq 1} \gamma_{Q,i} * \psi_{0,i} * Q_{k,i} \quad (3.6)$$

3.1.2. MRF Seismic analysis

During the seismic analysis the section optimization has been performed to find the best solution. Since the whole building seismic mass is carried by the Moment Resisting Frame and the connection between the gravity frame and the lateral load resisting system is considered as pinned, only the MRF is modeled on sap2000. The gravity frame will be analyzed and designed successively. Just from the beginning, to attend EC8 suggestion and limitation on the section resistance, it's been decided to assign as beam's steel s235, while s355 it's chosen for columns. Moreover, to guarantee an overstrength in column section, IPE section is chosen for beams, while HEB section is chosen for columns. Finally, to select the more appropriate sections dimension, all combinations of IPE profiles ranging from 240 to 400 (240, 270, 300, 330, 360, 400) and all HEB profiles going from 300 to 450 (300, 320, 340, 360, 400, 450) were analyzed.

3.1.2.1. Modal Analysis

MRF has been modelled in sap2000, concentrating the floor mass in the beam midpoint and considering structural steel self-weight in this mass as well, to better control the structure behavior during the analysis. Check on the modal analysis is made by comparing sap2000 results with a MATLAB code created to compute eigenvector "[Phi]" and eigenvalue "[Ω]" matrix. The script calculates these matrices solving the eigen-problem (equation 3.7) through the implementation shown in equation (3.8):

$$\det(K - w_k * M) = 0 \quad (3.7)$$

$$[Phi, Omega] = eig(K, M) \quad (3.8)$$

Results obtained by sap2000 and MATLAB related to the modal analysis are close each other, T_1 is equal to 0.88s.

3.1.2.2. Response Spectrum Analysis

Since the modal analysis gives reliable results the next step on sap2000 analysis is to assign an elastic response spectrum and a behavior factor that will take into account the ductility of the system in the various runs. The building is located, as mentioned above, in L'Aquila, Italy, belonging to EC8 site class A, T1. Moreover, as discussed in "Behavior Factor", "q" is inputted equal to 6. The resulting elastic spectrum will be divided by this factor (Figure 3.5):

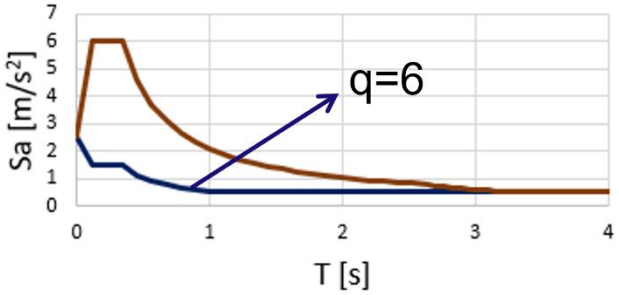

Figure 3.5: L'Aquila elastic and inelastic response spectrum

Sap2000 response spectrum analysis makes an effect superposition between the gravity load acting on the MRF and the computed lateral forces to derive solicitations diagrams. As for the modal analysis, a MATLAB code has been created to compute static equivalent forces starting from the first eigenmodes, with the purpose of checking the results. Equation (3.9) illustrates how to obtain static equivalent forces:

$$\{F_{h,i}\} = \Gamma_i * M * \phi_i * S_a(T_i) \tag{3.9}$$

Once static equivalent forces have been obtained for the first and the second floor and for both the first and second mode of vibration, an SRSS (Square Roots of the Sum of the Squares) is performed to generate the solicitation diagrams. Also in this case, the results are close each other and the section optimization procedure is performed many times, considering three main checks, illustrated in the following equations (3.10-3.12):

$$\theta = \frac{P * d_r}{V_{tot} * h} \leq 0.1 \tag{3.10}$$

$$d_r * \upsilon \leq 0.01 * h \tag{3.11}$$

$$\sum_{j}^{n} M_{Rd,column} \geq 1.3 * \sum_{i}^{m} M_{Rd,beam} \qquad (3.12)$$

Equation (3.10) represents the ultimate limit state EC8 requirement on second order effect because of the possibility that gravity loads could increase the internal action due to their influence on the deformed configuration. Equation (3.11) is the damage limitation requirement and equation (3.12) represent the beam-column member hierarchy that assure the plastic hinge creation in beams rather than in columns. Limit of resistance exceedance is considered too, but usually steel building design is governed by displacement. The Moment Resisting Frame's profile chosen in the late process are IPE360 for beams and HEB400 for columns as shown in Figure 3.6:

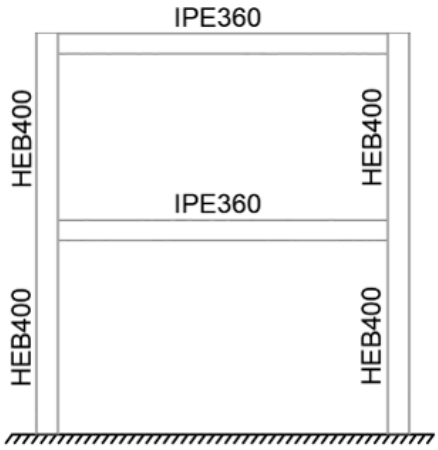

Figure 3.6: Moment Resisting Frame beams and columns section

The forces corresponding to the chosen frame profiles resulting both from sap2000 and MATLAB SRSS process are illustrated in Figure 3.7:

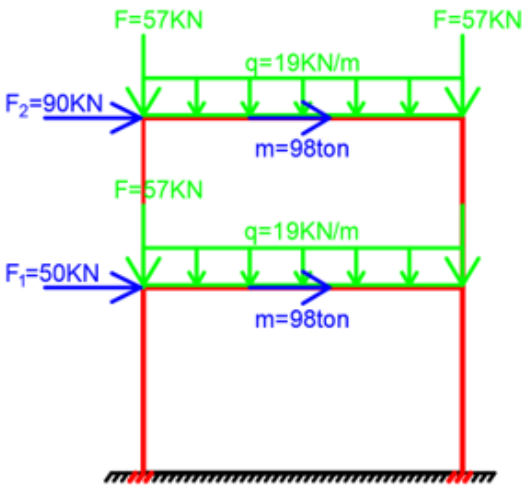

Figure 3.7: forces acting on the Moment Resisting Frame corresponding to IPE360, HEB400 profiles

Equation (3.10) and (3.11) are satisfied both for the first and second story as follows (equation 3.13-3.14):

$$\theta = \frac{P * d_r}{V_{tot} * h} = 0.04 \leq 0.1$$
$$\theta = \frac{P * d_r}{V_{tot} * h} = 0.043 \leq 0.1 \quad (3.13)$$

$$d_r * \upsilon = 21.9 \leq 0.01 * h = 35$$
$$d_r * \upsilon = 28.2 \leq 0.01 * h = 32 \quad (3.14)$$

3.1.2.3. Internal Forces

The resulting solicitations diagrams are illustrated for the shear and the bending moment in Figure 3.8:

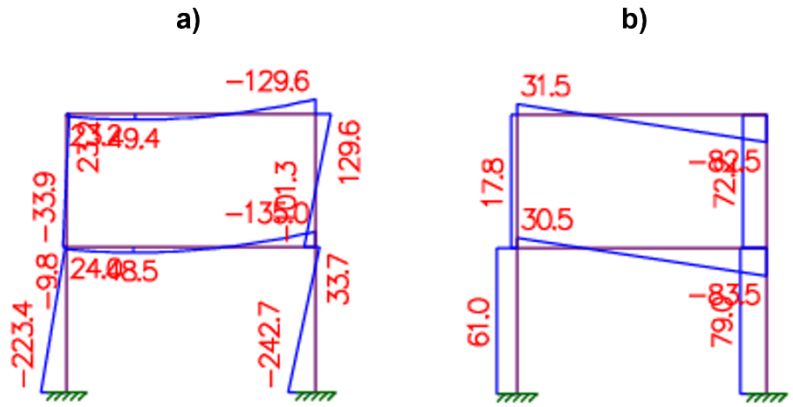

Figure 3.8: Moment Resisting Frame solicitations diagrams obtained by the effect superposition a) bending moment b) shear

3.1.3. Gravity frame's load analysis

Similarly to what's been done in the chapter "MRF Load Analysis", tributary areas for the gravity frame's beams and columns are defined. The purpose of this process is, again, to establish the amount of load a certain structural element is required to carry. Tributary areas represent zones that deliver their weight to the selected element (Figure 3.9, Figure 3.10).

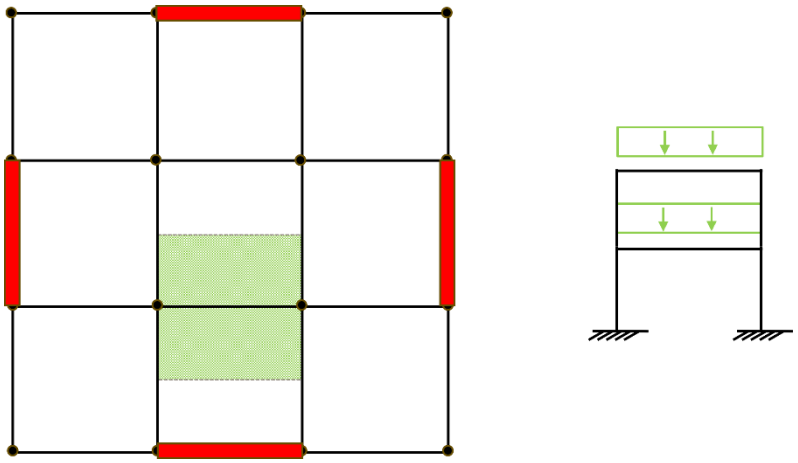

Figure 3.9: most solicited gravity frame beam's tributary area

The green area represents the weight the gravity beam is intended to sustain. The gravity frame design is carried out using the combination of action for persistent design situation as illustrated in the following equation (3.15) [14].

$$\sum_{j\geq 1}\gamma_{G,j} * G_{k,j} "+" \gamma_P * P "+" \gamma_{Q,1} * Q_{k,1} "+" \sum_{i\geq 1}\gamma_{Q,i} * \psi_{0,i} * Q_{k,i} \tag{3.15}$$

Permanent and variable loads are the those mentioned in the previous section, equation (3.2). Consequently, the distributed load is expressed as follows in the equation (3.16):

$$\begin{aligned} q_1 &= \frac{\gamma_{G,1} * G_1 * A + \gamma_{G,2} * G_2 * 6 + \gamma_{Q,1} * Q * A}{L} \\ q_2 &= \frac{0.1(\gamma_{G,1} * G_1 * A + \gamma_{G,2} * G_2 * 6 + \gamma_{Q,1} * Q * A)}{L} \\ q &= q_1 + q_2 = 60 KN/m \end{aligned} \tag{3.16}$$

Where $\Upsilon_{G,1}$ and $\Upsilon_{G,2}$ is equal to 1.35 and $\Upsilon_{Q,1}$ is equal to 1.5. Figure 3.10, on the other hand, shows the most solicited column under its carried weight. In this work, the shear force provided by each connected beam is considered to design the column profile. Base column must sustain its self-weight and the sum of the 8 beam's shear.

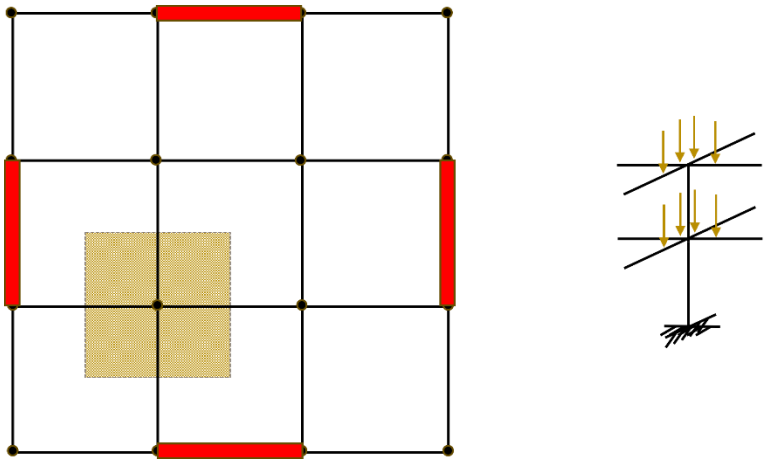

Figure 3.10: most solicited gravity frame column's tributary area

3.1.4. Structural Design

The structural design is carried out attending both EC3 and EC8 principles, which prescribes ultimate and serviceability limit states verifications.

3.1.4.1. MRF Capacity Design

Moment Resisting Frames resist lateral seismic action with elements able to dissipate energy during cyclic loading. Columns, beams and connections must thus be able to dissipate and sustain flexural bending during cyclic excitation. EC3 defines resistance criteria while EC8 add check to guarantee local and global ductility and a good hierarchy of strength as well. Plastic hinge occurring must concern beams, and the global ductile behavior has to be provided by local elements which minimum rotation capacity must be higher than a certain value [14],[15],[5]. The following checks are carried out to verify the MRF's profiles (HEB400 s355, IPE360 s235) chosen in "Response Spectrum Analysis".

3.1.4.1.1. ULS

3.1.4.1.1.1. Second Order Effect

The following equation (3.17) represent the verifications respectively for the first and second floor:

$$\theta = \frac{P * d_r}{V_{tot} * h} = 0.04 \le 0.1 \qquad OK \qquad (3.17)$$
$$\theta = \frac{P * d_r}{V_{tot} * h} = 0.043 \le 0.1$$

3.1.4.1.1.2. Beam-Column Members Hierarchy

$$\sum M_{Rd,column} > 1.3 * \sum M_{Rd,beam} \quad OK$$
$$2 * 663.38 > 1.3 * 271.76 KNm$$

3.1.4.1.1.3. Beam Detailing

Before conducting the various checks, it's fundamental to define the actions (E_d). Whereas M_{ed} and N_{ed} are those obtained by the superposition effect process during sap2000 analysis "Response Spectrum Analysis", Figure 3.8, and drift/displacement are those related to that actions, V_{ed} is computed differently. Indeed, it's considered as the summation of two contributions:

1. Shear obtained in the seismic combination, without considering the lateral force influence (i.e. shear computed applying Figure 3.7 vertical loads alone)
2. Shear obtained in a beam configuration where two plastic bending moment $M_{pl,Rd}$ are applied to both its edges

Figure 3.11 shows the load distribution described in the previous points and the resulting shear internal actions for the MRF's beams verifications:

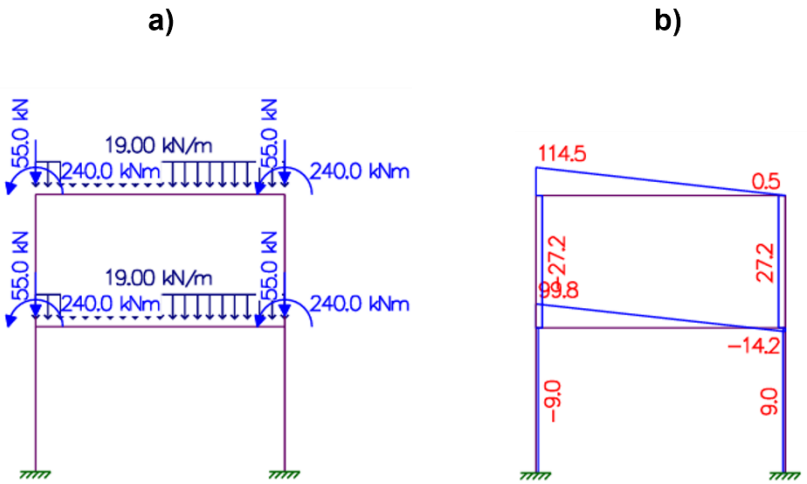

Figure 3.11: MRF's ULS beam detailing a) load distribution for the shear (V_{ed}) computation b) shear internal actions

$$\frac{M_{Ed}}{M_{pl,Rd}} < 1$$
$$M_{Ed} = 130 KNm \quad OK \quad ()$$
$$M_{pl,Rd} = \frac{W_{pl,Rd} * f_y}{\gamma_{M0}} = 239.5 KNm$$

$$\frac{V_{Ed}}{V_{pl,Rd}} < 0.5$$
$$V_{Ed} = 114KN \qquad OK \qquad (3.18)$$
$$V_{pl,Rd} = \frac{A_v * (\frac{f_y}{\sqrt{3}})}{\gamma_{M0}} = 585.85KN$$

$$\frac{N_{Ed}}{N_{pl,Rd}} < 0.15$$
$$N_{Ed} = 57.2KN \qquad OK \qquad (3.19)$$
$$N_{pl,Rd} = \frac{A * f_y}{\gamma_{M0}} = 1709.14$$

MRF's beams are checked for lateral torsional buckling as well. It's necessary for the beams to develop plastic hinges and not to buckle before the inflection.

$$\frac{M_{Ed}}{M_{buck,Rd}} < 1$$
$$M_{Ed} = 130KNm$$
$$M_{cr} = \frac{\pi}{L} * (G * J_P * E * I_T)$$
$$\lambda_{LT} = \sqrt{\frac{f_y * W_{pl,y}}{M_{cr}}} \qquad FAIL \qquad (3.20)$$
$$\theta_{LT} = 0.5 * (1 + 0.34(\lambda_{LT} - 0.2) + \lambda_{LT}^2)$$
$$\chi_{LT} = \min(\frac{1}{\theta_{LT} + \sqrt{\theta_{LT}{}^2 - \lambda_{LT}^2}}; 1) = 0.448$$
$$M_{buck,Rd} = \frac{\chi_{LT} * f_y * W_{el,y}}{\gamma_{M1}} = 107.52KNm$$

To avoid buckling problems it's necessary to insert steel diaphragms along the beam span, providing effective lateral restrain to the web. Two steel diaphragms are inserted, giving a critical length of 2 m and a buckling resisting moment of 180 KNm.

3.1.4.1.1.4. Column Detailing (Overstrenght Factor)

Columns verifications are carried out with different actions with respect to those obtained by effect superposition, Figure 3.8. Actions are defined as follows:

$$E_d = E_{d,G} + 1.1 * \gamma_{OV} * \Omega * E_{d,E} \qquad (3.21)$$

That's the sum of the actions obtained by gravity loads and the lateral seismic actions multiplied by the "Υ_{OV} and Ω" factors. "Υ_{OV}" is the overstrength factor and is equal to 1.25 [5]. "Ω" is another factor provided by EC8 which considers the minimum capacity-to-demand ratio among the dissipative beam joints. In the current work "Ω" is defined as follows:

$$\Omega = \frac{M_{pl,Rd}}{M_{Ed}} = \frac{239.5}{130} = 1.75 \tag{3.22}$$

The final resulting actions are illustrated in Figure 3.12:

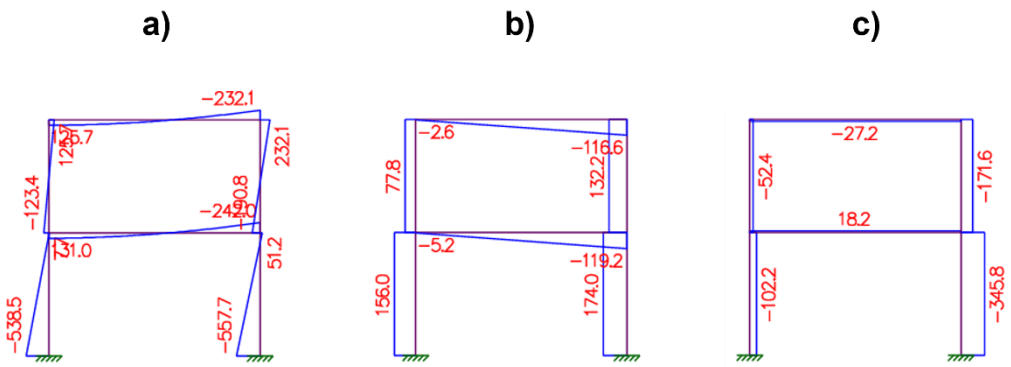

Figure 3.12: MRF's ULS column detailing (E_d) a) bending moment b) shear c) axial force

$$\frac{V_{Ed}}{V_{pl,Rd}} < 0.5$$
$$V_{Ed} = 175KN \qquad OK \tag{3.23}$$
$$V_{pl,Rd} = \frac{A_v * (\frac{f_y}{\sqrt{3}})}{\gamma_{M0}} = 2951.41KN$$

$$\frac{N_{Ed}}{N_{pl,Rd}} < 0.15$$
$$N_{Ed} = 346KN \qquad OK \tag{3.24}$$
$$N_{pl,Rd} = \frac{A * f_y}{\gamma_{M0}} = 7021.11$$

$$\frac{M_{Ed}}{M_{N,Rd}} < 1$$
$$M_{Ed} = 558KNm \qquad OK \tag{3.25}$$
$$M_{N,Rd} = M_{pl,Rd} * [1 - (\frac{N_{Ed}}{N_{pl,Rd}})^2] = 1139.1KNm$$

3.1.4.1.2. DLS

In seismic design, the interstory drift limitation is a DLS verification. To carry this check out with the same load combination of the ULS situations, EC8 introduce the "υ" factor, dividing the obtained drift by 0.5 instead of changing the seismic action (i.e. instead of considering the appropriate return period for the DLS spectrum and, thus, instead of reducing spectral ordinates) [5].

3.1.4.1.2.1. Interstory Drift Limitation

For the first and second floor respectively, the checks are then:

$$\begin{aligned} d_r * \upsilon = 21.9 \le 0.01 * h = 35 \\ d_r * \upsilon = 28.2 \le 0.01 * h = 32 \end{aligned} \quad OK \qquad (3.26)$$

It should be noticed that verifications compliance with resistance is over satisfied, for example equation (3.23) or (3.24). Steel structures design is governed by displacement, drift ratios and second order effects, as it is shown in equation (3.17) and (3.26).

3.1.4.2. Gravity Frame Design

The gravity frame, as mentioned in the previous sections, carries only vertical loads. Therefore, it has only to guarantee adequate strength against the prescribed load combinations [14],[15]. The chosen profiles are (HEB300, s355) for gravity columns and (IPE400, s235) for beams. $\Upsilon_{M,0}$ and $\Upsilon_{M,1}$ is considered equal to 1.05. The following equations summarize the conducted checks.

3.1.4.2.1. ULS

3.1.4.2.1.1. Beam Detailing

During the bending moment verification (equation 3.27) is used the elastic section modulus because of the IPE400 profile classification (i.e. class 3 that's not able to develop the plastic resistance):

$$\begin{aligned} \frac{M_{Ed}}{M_{pl,Rd}} < 1 \\ M_{Ed} = 260 KNm \qquad OK \\ M_{pl,Rd} = \frac{W_{el} * f_y}{\gamma_{M0}} = 271.76 KNm \end{aligned} \qquad (3.27)$$

$$\frac{V_{Ed}}{V_{pl,Rd}} < 1$$
$$V_{Ed} = 170KN \qquad OK \qquad (3.28)$$
$$V_{pl,Rd} = \frac{A_v * (\frac{f_y}{\sqrt{3}})}{\gamma_{M0}} = 659.39KN$$

And for the lateral torsional buckling (LTB) is checked regard the weak axis (z-z):

$$\frac{M_{Ed}}{M_{buck,Rd}} < 1$$
$$M_{Ed} = 260KNm$$
$$M_{cr} = \frac{\pi}{L} * (G * J_P * E * I_T)$$
$$\lambda_{LT} = \sqrt{\frac{f_y * W_{el,y}}{M_{cr}}} \qquad FAIL \qquad (3.29)$$
$$\theta_{LT} = 0.5 * (1 + 0.34(\lambda_{LT} - 0.2) + \lambda_{LT}^2)$$
$$\chi_{LT} = \min(\frac{1}{\theta_{LT} + \sqrt{\theta_{LT}{}^2 - \lambda_{LT}^2}}; 1) = 0.495$$
$$M_{buck,Rd} = \frac{\chi_{LT} * f_y * W_{el,y}}{\gamma_{M1}} = 134.64KNm$$

To avoid buckling problems it's necessary to insert steel diaphragms along the beam span, providing effective lateral restrain to the web. To increase the amount of buckling resistance moment from 134.6 KNm to a minimum of 260 KNm, 10 steel diaphragms are required.

3.1.4.2.1.2. Column Detailing

The base column, as mentioned above, sustains its whole self-weight and the axial force corresponding to the sum of 8 transmitted shear (1320 KN). Since the building size is contained and presents only 2 floors, it's decided to keep the same column section for both the first and second story.

$$\frac{N_{Ed}}{N_{pl,Rd}} < 1$$
$$N_{Ed} = 1320KN \qquad OK \qquad (3.30)$$
$$N_{pl,Rd} = \frac{A * f_y}{\gamma_{M0}} = 5292.26KN$$

Because the gravity frame carries only vertical load, column is checked for pure compression buckling:

$$\frac{N_{Ed}}{N_{buck,Rd}} < 1$$
$$N_{Ed} = 1440KNm$$
$$\lambda = \frac{L_{cr}}{i} * \sqrt{\frac{f_y}{\pi^2 * E}}$$
$$\theta = 0.5 * (1 + 0.49(\lambda - 0.2) + \lambda^2) \quad OK \tag{3.31}$$
$$\chi = \min(\frac{1}{\theta + \sqrt{\theta^2 - \lambda^2}}; 1) = 0.605$$
$$N_{buck,Rd} = \frac{\chi * A * f_y}{\gamma_{M1}} = 3201KN$$

3.1.4.2.2. DLS

Damage limit state verification requires a different load combination with respect to ULS. Permanent and variable loads are the those mentioned in the previous section, equation (3.2). The following equation (3.32) illustrates the adopted combination and the corresponding distributed load to be used in the verifications:

$$\sum_{j>1} G_{k,j} + Q_{k,1} + \sum_{i>1} \psi_{0,i} * Q_{k,i}$$
$$q = G_1 * A + G_2 * 6 + Q * A = 40KN / m \tag{3.32}$$

3.1.4.2.2.1. Deflection

The maximum deflection is assumed to be:

$$\delta < \delta_{\max}$$
$$\delta_{\max} = \frac{L}{200} = 30mm \qquad OK \tag{3.33}$$
$$\delta = \frac{5 * q * L^4}{384 * E * I} = 14mm$$

3.2. Non-Linear Analysis

Unless building design is usually carried out using elastic analysis, most of the times structures undergo large inelastic displacement and deformation during seismic excitation. Non-Linear analysis allows calculation considering strength and stiffness deterioration associated with inelastic material behavior. A fundamental requirement is the definition of component's force-deformation diagrams to capture and better understand element's response and property. The strong column-weak beam requirement during non-linear analysis is implemented by modelling such elements supposed to yield with their expected strength

permitting design with the maximum expected demand [16]. In this work, non-linear analysis is performed to capture these aspects and develop some curves such IDAs and fragilities that will be used in the FEMA P-58 framework.

3.2.1. Openseespy Model

Non-linear numerical model has been implemented in Openseespy using python interface (Openseespy). In line with the assumption made during the code-based design, only the Moment Resisting Frame has been modelled, since it represents the unique lateral resisting structural system. Figure 3.13 shows the frame model. The green hinge represents the panel zone model, the pink hinge on the other hand represents the expected plastic hinge in the beam. Blue lines are the connection, modelled as extremely rigid. Red and black lines are respectively the elastic beam-column and the non-linear beam-column.

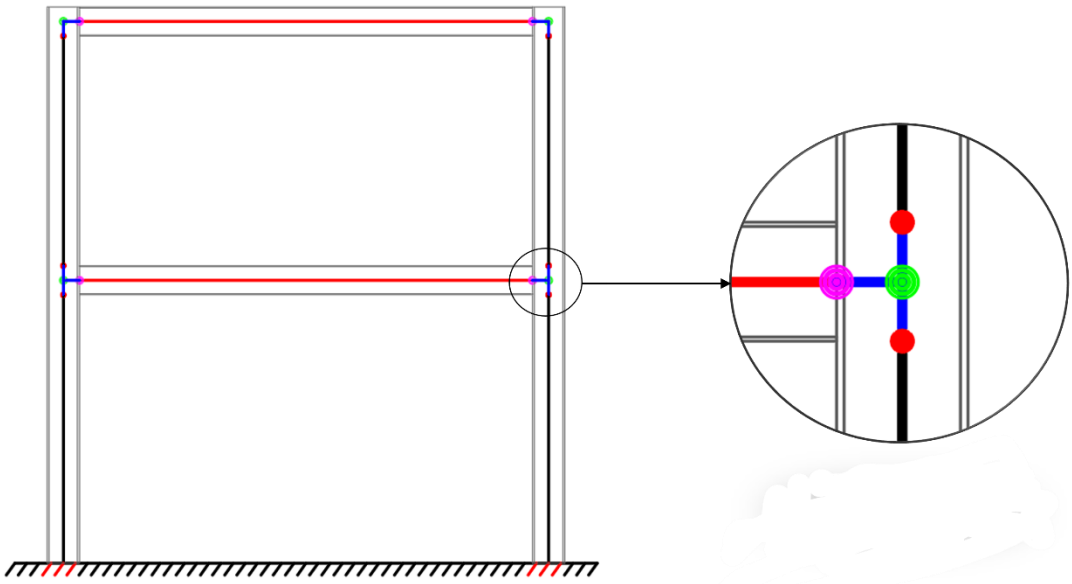

Figure 3.13: Openseespy Moment Resisting Frame model

In the model, geometry is initially defined through the nodes of the frame. Successively, the section profiles are defined and assigned, together with the material, to create elements composing the whole system.

3.2.1.1. Elastic Beam-Column

First and roof floor beams (IPE360) are defined through elastic beam-column. The material assigned to these elements follows an elastic constitutive law, E is equal to 210000000 KN/m^2 and the steel used is s235.

3.2.1.2. Non-Linear Beam-Column: Fiber Section

Inelastic structural components can be modelled in several ways to take into account their plasticity. The main strategies consist in concentrating plasticity in a non-linear spring or plastic hinge, otherwise distributing it along the element length through fiber sections [16]. The columns (HEB400) are modelled as fiber elements. Uniaxial material “steel 01” (Figure 3.14) has been assigned to these elements to capture non-linear hysteretic behavior.

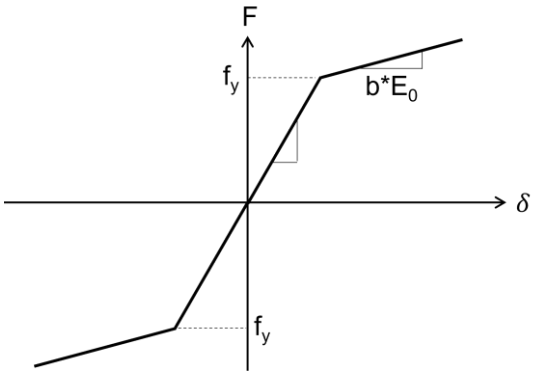

Figure 3.14: Openseespy uniaxial material "steel01" elastic-plastic behavior with hardening

This distributed plasticity model allows a comprehensive evaluation of loss in strength through the section and along the member such flanges degradation or non-linear interaction between flexural and shear [16].

3.2.1.3. Lignos Model

Whereas it’s convenient to choose a distributed model for the columns, for the end beam element it is preferable to choose a model such as inelastic spring with hysteretic properties. This is the simplest non-linear model that concentrates the inelastic deformation and develop moment-rotation parameters capturing degrading response [16]. For this purpose, a zero-length element is assigned and modelled based on the backbone relationship (Figure 3.15) presented by Lignos and Krawinkler [17].

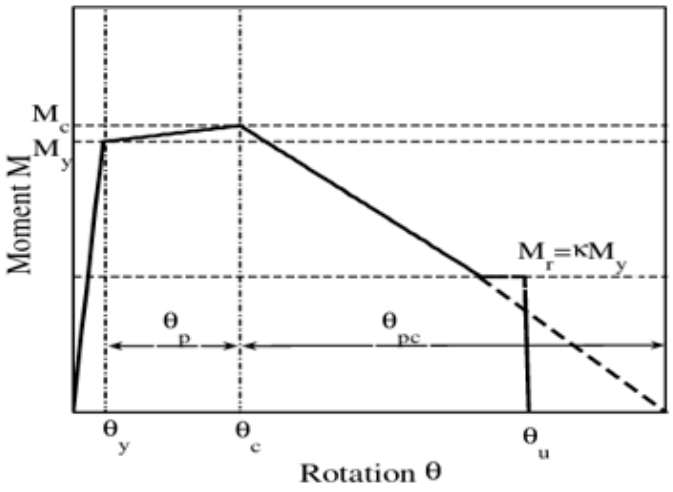

Figure 3.15: deterioration model: monotonic curve

Cyclic deterioration occurs when element is not subjected to monotonic load but to cyclic envelope. Figure 3.15 parameters are rotation pre and post-capping (θ_p, θ_{pc}), yield, capping and ultimate rotation (θ_y, θ_c, θ_u), yield, capping and residual bending moment (M_y, M_c, M_r). Considering the Moment Resisting Frame under investigation and specifically the beams profiles (IPE360: h=334.6vmm, b_f=170vmm, t_f=12.7vmm, t_w=8vmm, d=360vmm), steel s235, and the span length equal to 6 meters, the deterioration model's parameters is obtained as follows:

$$K = \frac{6 * E * I}{L} = 402682.5 KNm / rad \quad (3.34)$$

$$M_y = f_y * W_{pl,y} * \gamma = 263.412 KNm \quad (3.35)$$

$$\theta_y = \frac{M_y}{K} = 0.00065 rad \quad (3.36)$$

$$\theta_p = 0.0865 * (\frac{h}{t_w})^{-0.365} * (\frac{b_f}{2 * t_f})^{-0.140} * (\frac{L}{d})^{0.340} * (\frac{c^1_{unit} * d}{533})^{-0.721} * (\frac{c^2_{unit} * f_y}{355})^{-0.230} = 0.0518 rad \quad (3.37)$$

$$\theta_c = \theta_p + \theta_y = 0.052 \quad (3.38)$$

$$M_c = 0.4 * M_y = 105.365 KNm \quad (3.39)$$

$$\theta_{pc} = 5.63 * (\frac{h}{t_w})^{-0.565} * (\frac{b_f}{2 * t_f})^{-0.800} * (\frac{c^1_{unit} * d}{533})^{-0.280} * (\frac{c^2_{unit} * f_y}{355})^{-0.430} = 0.212 rad \quad (3.40)$$

$$\theta_u = 0.4 \quad (3.41)$$

The yielding rotation (θ_y) of the zero-length element calculated in equation (3.36) is not the value considered during the analysis to set damage states and thresholds limits of the plastic hinge, whereas it's only the value considered as input in the model. Equation (3.36) yield rotation is obtained considered a 10 times bigger stiffness than the actual one, to avoid numerical convergence's problem in Openseespy: before the yielding occurs, the rotation is distributed between elements according to the relative stiffness. Stiffening the non-linear spring (plastic hinge), the beam initially deforms more, taking most of the initial rotation. After yielding, instead, non-linear spring starts to accumulate plastic rotation since the beam, modelled as elastic, doesn't reach any yield. In order to guarantee the beam absorbs a greater amount of the initial rotation, its stiffness must be lower than the inelastic spring one, avoiding the deformation concentrate in the plastic hinge from the beginning. Thus, in the analysis, the actual yielding rotation is considered as 10 times the equation (3.36) one. The ultimate rotation (θ_u) is considered equal to 0.4 in the model for ductile behavior of steel and to avoid numerical convergence's problem in Openseespy but, regarding the actual ultimate rotation, Lignos and Krawinkler suggest a value of 0.06 rad, while EC8 recommend a minimum value of 0.04 rad. In this work the ultimate rotation is considered as 8 times the actual value of the yield rotation, as suggested by EC8. Thus, the ultimate rotation is equal to 0.052 rad. Figure 3.16 represents the monotonic deterioration model for the Moment Resisting Frame's end beam plastic hinge:

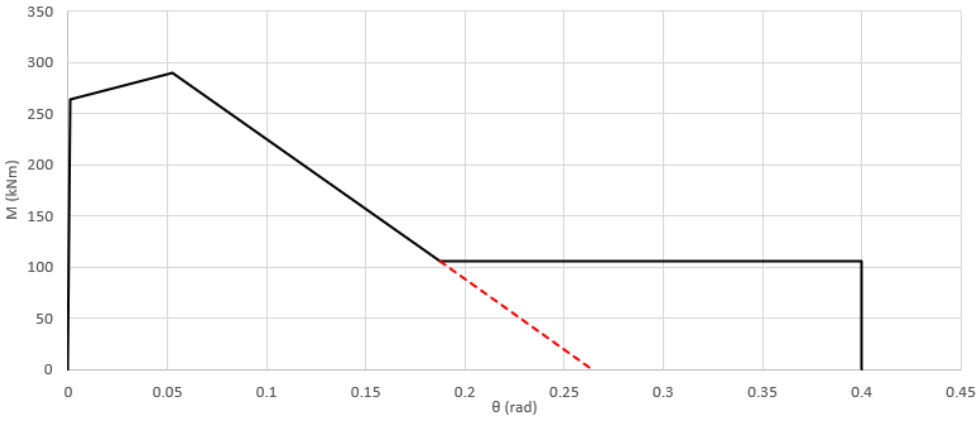

Figure 3.16: Moment Resisting Frame's end beam deterioration model

3.2.2. Static Analysis

Non-linear static analysis is a useful tool for checking the model and deeply understanding the structure response and yielding overall mechanism. In the non-linear static analysis, an incremental lateral load is applied on the structure. The shape distribution of the applied load represents the actual inertia force expected during ground shaking. The load is increased and applied until the structure reaches a target parameter, which could be a floor displacement or

an element rotation. The total gravity load is considered during the analysis as well, to account for the second order effects [16]. In this work the roof end beam non-linear spring is chosen as target parameter, and its rotation is monitored during the non-linear static analysis. The analysis is stopped reaching the ultimate rotation acceptable for the plastic hinge defined in "Lignos Model" (θ_u=0.052 rad). Figure 3.17 shows the triangular forces distribution adopted in the analysis. It's been used as a displacement control integrator a 0.00015m step, while the rotation of the roof plastic hinge is checked too.

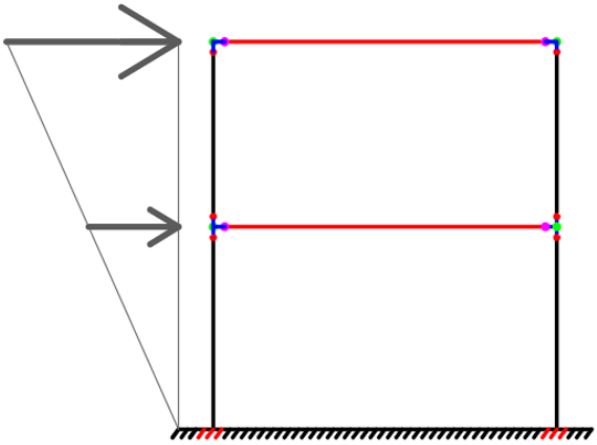

Figure 3.17: pushover triangular forces distribution on the Moment Resisting Frame

3.2.2.1. Element Rotation Capacity

During the analysis several force-deformation diagrams are computed: each plastic hinge has been checked, both for the end beams and base columns. Figure 3.18 gives an illustration of the rotation capacity of the base column (blue curve) and left roof plastic hinge (pink curve):

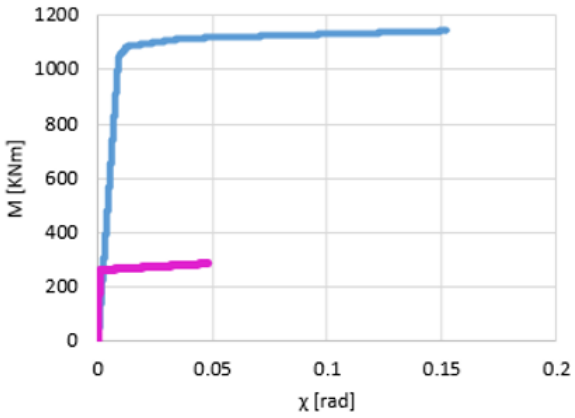

Figure 3.18: Moment Resisting Frame's base column (pink curve) and roof plastic hinge (blue curve) rotation capacity

It should be noticed that the roof plastic hinge (pink curve) behaves with the expected yielding at a rotation of about 0.006 rad and sustains inelastic deformation till the ultimate defined rotation capacity around 0.05 rad. As discussed in "Lignos Model" the initial segment of

the plastic hinge curve shows a steeper branch than the column one, reflecting the choice to assign initial rotation to the other structural elements.

3.2.2.2. Pushover

With the pushover, the global structural behavior is analyzed and represented reflecting the formation of the plastic hinges, as shown in Figure 3.19:

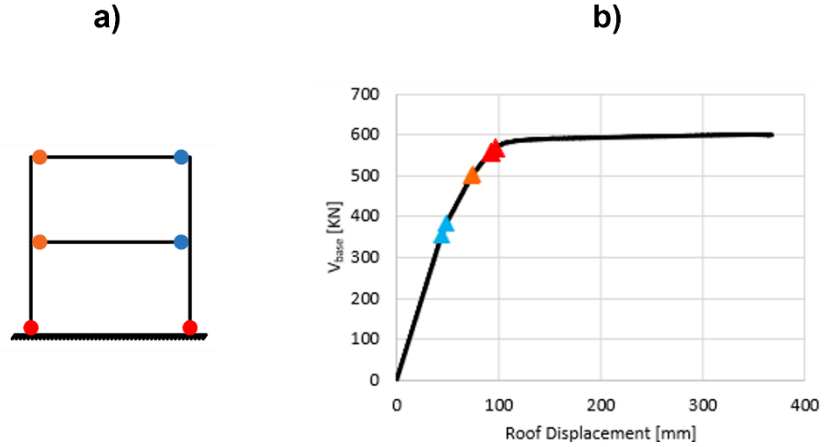

Figure 3.19: pushover a) Moment Resisting Frame's plastic hinges b) base shear (KN) versus roof displacement (mm)

Each plastic hinge formation modifies the global response with a loss of stiffness; indeed, the pushover curve shows a noticeable slope decrease at every formation point. It's also shown in Figure 3.19 that the base column plastic hinges are the last to appear as capacity design ("Structure Ductility") requires.

3.2.3. Dynamic Analysis

Differently from the non-linear static approach, the dynamic procedure provides a more accurate and reliable representation of the structural behavior, since it incorporates inelastic member response under cyclic loading. Indeed, non-linear dynamic analysis simulates directly energy dissipation. The accuracy depends on the quality of the model. Inertia mass must be included with self-weight and gravity loads, so that it results in more reliable force-deformation demand and second order effect [16].

3.2.3.1. Ground Motion Selection and Scaling

Input ground motion should be selected and scaled to represent accurately the site seismic hazard and the target response spectrum defined above "Response Spectrum Analysis", reflecting the features of the dominant earthquake source. Standards typically require many ground motion inputs, usually at least 7 pairs [16]. For this purpose, the engineering strong motion database (ESM) has been used selecting the ground motion record with REXELweb [18],

[19], Figure 3.20 illustrates a suite of 15 ground motion's spectra fitting the target response spectrum derived for L'Aquila, Italy:

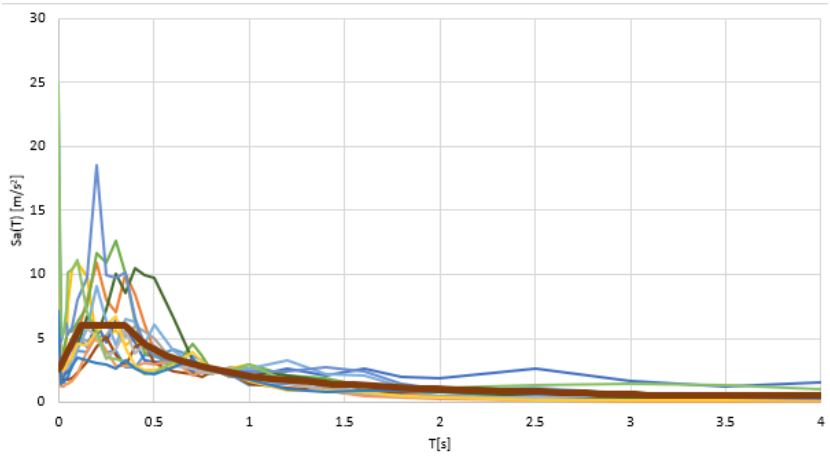

Figure 3.20: ground motion selected and scaled for the dynamic non-linear analysis matching L'Aquila target response spectrum

The ground motion's spectra are scaled to the target spectral acceleration related to the fundamental building period $S_a(T_1)$, derived from L'Aquila spectrum "Figure 3.5". This procedure consists of dividing each component of the accelerogram by $S_a(T_1)_{\text{ground motion}}$ and multiplying it for $S_a(T_1)_{\text{target}}$.

3.2.3.2. Drift Check: Code-Based vs NLTHA

During the elastic design has been attended the drift limitation based on EC8. Equation (3.26) defines the first and second floor threshold, equal respectively to 35 mm and 32 mm. The drift provided by Non-Linear Time History Analysis (NLTHA, Figure 3.21 red points), obtained applying the suite of ground motion derived in "Ground Motion Selection and Scaling", shows a close behavior, as expected, to the drift obtained in the design (Figure 3.21 dotted line, elastic displacement multiplied by the behavior factor):

$$d_{r(\delta_e * q)} * \upsilon \cong d_{r(NLTHA)} * \upsilon \leq 0.01 * h \qquad (3.42)$$

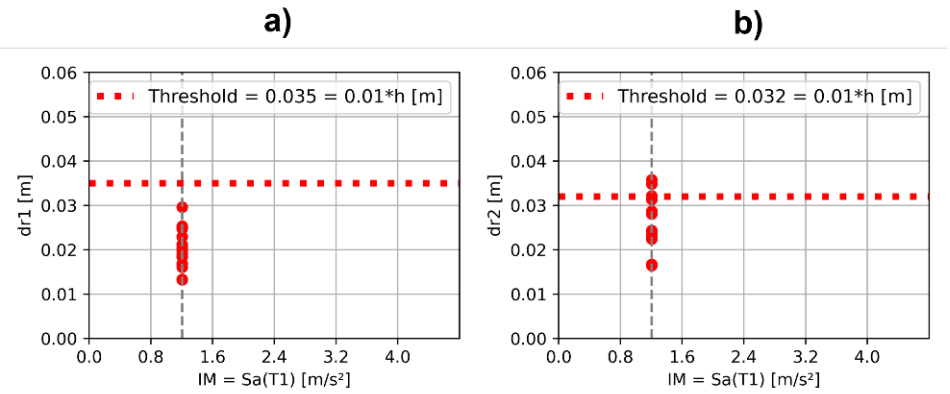

Figure 3.21: NLTHA drift compared with EC8 threeshold a) first story b) second story

From EC8 elastic analysis the drift was around 22 mm for the first story and 28 mm for the second story, as seen in equation (3.26). It should be noticed that for both the first and second stories the mean value of the drift obtained by the 15-ground motion analysis is close to the EC8 result. The small dispersion in NLTHA results, showed in "Figure 3.21", confirms the consistency of the non-linear model.

3.2.3.3. Roof Plastic Hinge Moment-Curvature

As the roof plastic hinge is the key parameter in this work to control the overall structural response and will be taken as local parameter to develop global fragility, it's useful to plot its behavior increasing the seismic intensity level step by step. It's necessary to define some strategies to find numerical convergence during the analysis integration step. Different methods have been implemented. The script inputs a tolerance equal to 0.000001 and 7500 iterations for each step. Since the strategy fails, the script jumps automatically to the other strategies defined, reducing the tolerance and increasing the iteration. Newton and Broyden test are chosen for the energy increment. Finally, to register structure response during analysis has been used "recorder" command. "Figure 3.22" illustrates the roof plastic hinge cyclic response, represented here by moment-curvature diagrams (blue curves), increasing the seismic intensity level (i.e. the set of 15 ground motion derived above in "Ground Motion Selection and Scaling"). The pink curve otherwise represents the plastic hinge capacity defined above (Figure 3.18):

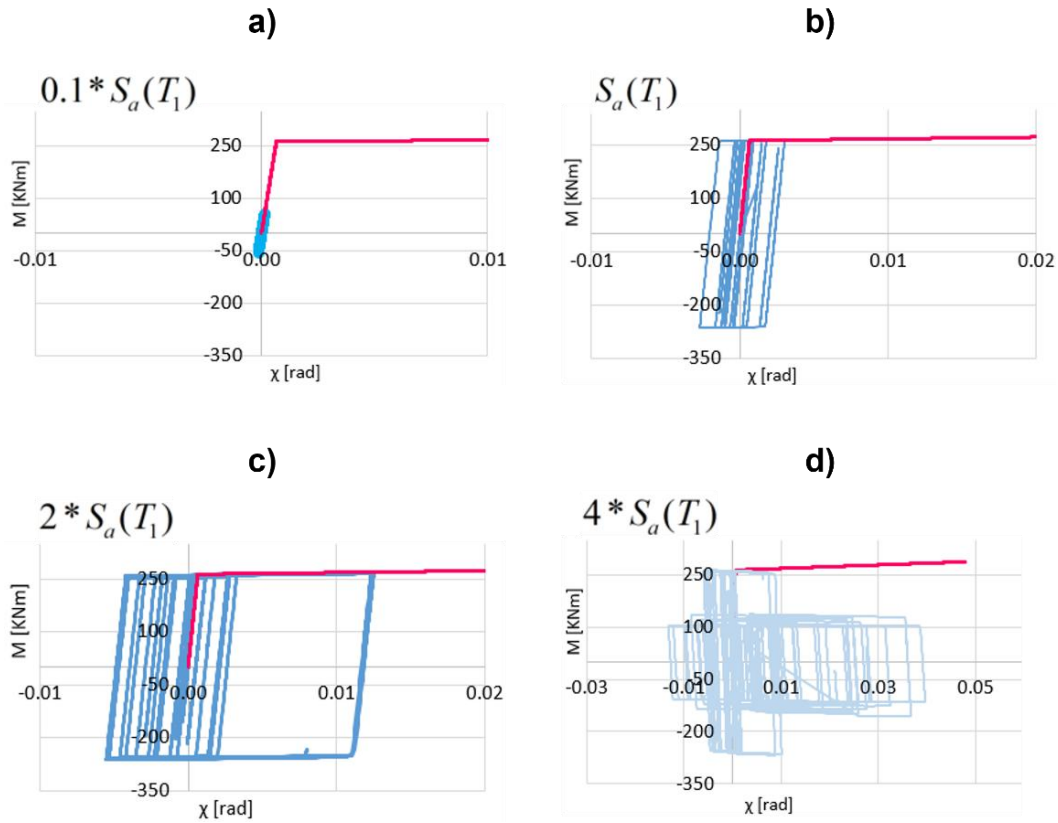

Figure 3.22: roof plastic hinge moment-curvature diagrams under cyclic loading

Each diagram represents a specific behavior under the earthquake cyclic loading. Intensity level is shown here in terms of the target spectral acceleration $S_a(T_1)$.

- a) $S_a(T_1)$ is multiplied by 0.1. Low seismic level produces a purely elastic response of the structure.
- b) The target acceleration is exactly equal to $S_a(T_1)$, the one used in EC8 design. It's noticeable the first plasticization of the hinge.
- c) 2* $S_a(T_1)$: this diagram presents a larger plastic deformation, increasing the hysteresis cycles and energy dissipation
- d) when the target acceleration is 4 times the design one, it's noticeable a pronounced stiffness and strength deterioration, as discussed in "Lignos Model". This degradation behavior is just seen in Figure 3.15.

3.2.4. Incremental Dynamic Analysis (IDA)

Incremental Dynamic Analysis (IDA) is a parametric analysis that allows to estimate structural performance through a suite of ground motions each scaled to different levels of intensity, producing curves having an EDP as ordinates and the intensity level in the abscissa. The growth in computer processing power gives the possibility to perform several runs with

the objectives to better understanding range of demands, structural implications on severe ground motion levels, strength degradation and global structural system response[13].

3.2.4.1. Principles

During IDA, seismic records are scaled by means of a scale-factor to represent all the seismic intensity level. In this work, the suite of ground motion is scaled to obtain the target spectral acceleration $S_a(T_1)$ equal to 1, as shown in Figure 3.23. Structural response is defined by a chosen EDP, such as plastic hinge rotation or interstory drift. IDA consist, thus, of a set of non-linear dynamic analysis performed with different seismic record on the same target intensity level (i.e. the spectral acceleration), scaling step by step the records using the scale factor (Figure 3.24), describing the overall behavior from the elastic range to the collapse.

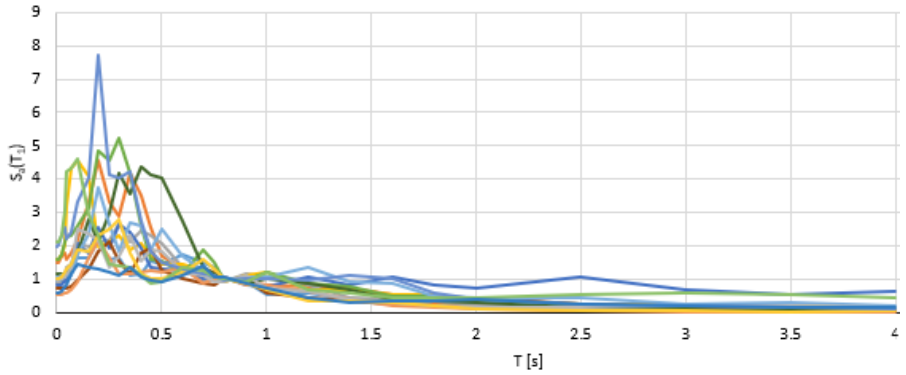

Figure 3.23: ground motion's spectra scaled to $S_a(T_1)$ =1

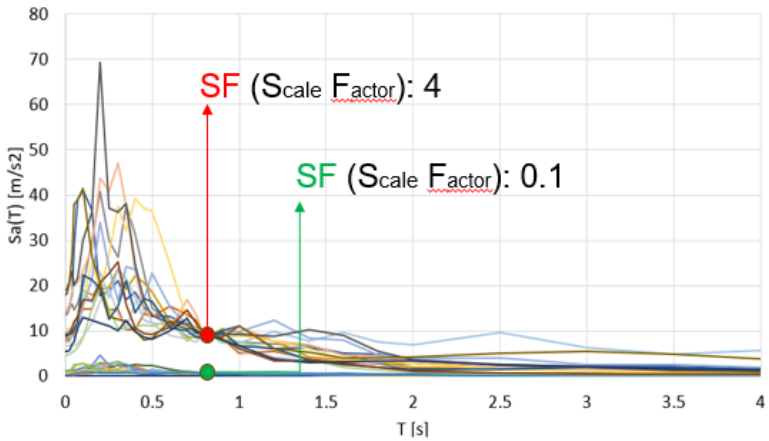

Figure 3.24: ground motion's spectra scaling

Figure 3.24 can be analyzed concurrently Figure 3.22. When the scale factor is 0.1 the roof plastic hinge response is still elastic, instead with a scale factor value of 4, the deterioration and loss of strength occur.

3.2.4.2. EC8 Damage State Threshold

As discussed in the previous section, IDA is a subsequential result, increasing the seismic intensity level, of single non-linear dynamic analysis on a structural model. When a suite of ground motion is employed and performed with cycle iteration, each intensity level presents a set of EDP values, corresponding to each scaled ground motion input. It's useful to define some thresholds to assess which record, during the IDA, results in exceeding these defined damage states. In this work the analyzed EDPs are the roof plastic hinge rotation and interstory drift ratio, to evaluate both local and global EDPs. The EC8 rotation thresholds are related to yielding, large plastic deformation and collapse and are assumed respectively equal to θ_y, 6* θ_y, 8* θ_y. Regarding the interstory drift, the chosen thresholds are 0.7% for damage state 1, 2.5% and 5% for damage state 2 and collapse [20]. During the analysis, some ground motion, especially for high intensity seismic level, could result in numerical convergence problems. A fallback strategy has been implemented in the Openseespy's script to solve this issue, and the corresponding record considered as resulting in structural collapse.

3.2.4.3. Local EDP: Roof Plastic Hinge Rotation

Figure 3.25 gives an illustration of the IDA results for the local plastic hinge rotation EDP:

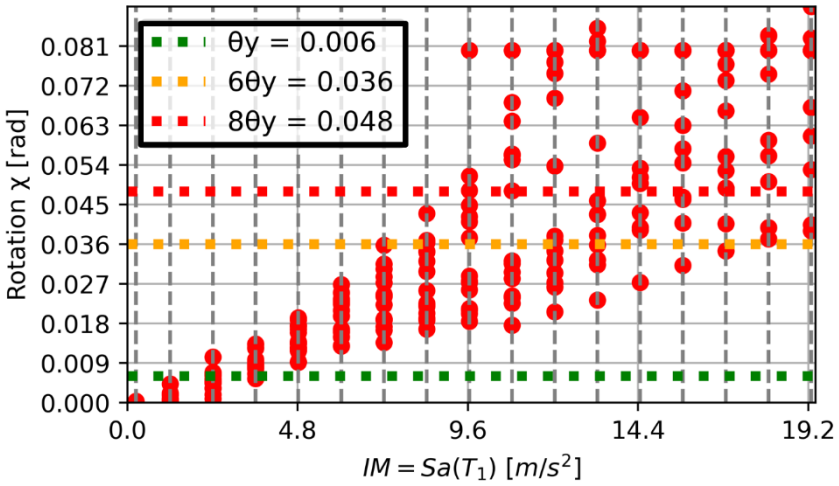

Figure 3.25: IDA result, roof plastic hinge EDP

Each red point represents the result in structural response of a single record (i.e. each vertical dotted grey line contains 15 points corresponding to the 15-ground motion set used). The horizontal green, orange and red dotted lines represent instead the damage state defined in the previous section "EC8 Damage State Threshold".

3.2.4.4. Global EDP: Interstory Drift Ratio (IDR)

As described for the roof plastic hinge EDP (Figure 3.25), the global EDP'S IDA (Figure 3.26) is presented:

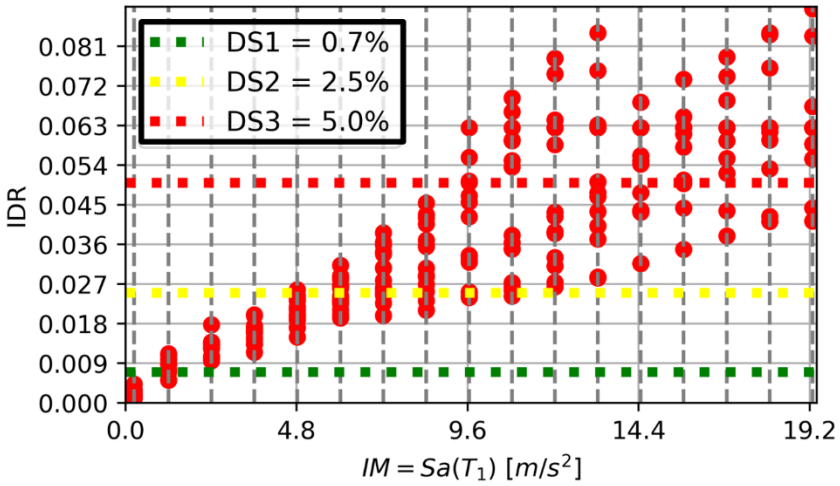

Figure 3.26: IDA result, interstory drift EDP

3.2.5. Fragilities Curves

Since IDA for local and global EDP is performed, it's possible to convert this result into curves which describe the probability a certain damage state would be exceeded depending on the seismic intensity level: these are the so-called fragilities curves. The procedure to obtain fragility curve consists in measuring the number of ground motion, exceeding a certain damage state, within the total set, referring to a certain intensity level, and compute the probability such damage state would be exceeded (e.g. Figure 3.26 damage state 2 has 100% of probability to be exceeded when the intensity level reach 14.4 m/s^2). Then repeat the process for all the intensity level covered in the IDA analysis. In the current work, fragilities curves are obtained as for the IDA curves with Openseespy, using the methodology just described. The equation summarizing this process is reported in the following equation (3.43-3.45):

$$\forall SF : P(D > DS) = \frac{n_{exceeding}}{n_{tot}} \tag{3.43}$$

$$\theta = \lambda_{i-1} + [\frac{0.5 - p_{i-1}}{p_i - p_{i-1}} * (\lambda_i - \lambda_{i-1})] \tag{3.44}$$

$$\beta = \frac{\ln(\lambda_{84\%}) - \ln(\lambda_{16\%})}{2} \tag{3.45}$$

Where θ and β is the median and dispersion of the resulting fragilities.

3.2.5.1. Local EDP: Roof Plastic Hinge Rotation

Figure 3.27 shows the resulting fragilities referring to the roof plastic hinge. Each damage state corresponds to the previously defined ("EC8 Damage State Threshold") rotation limits of θ_y, 6* θ_y, 8* θ_y.

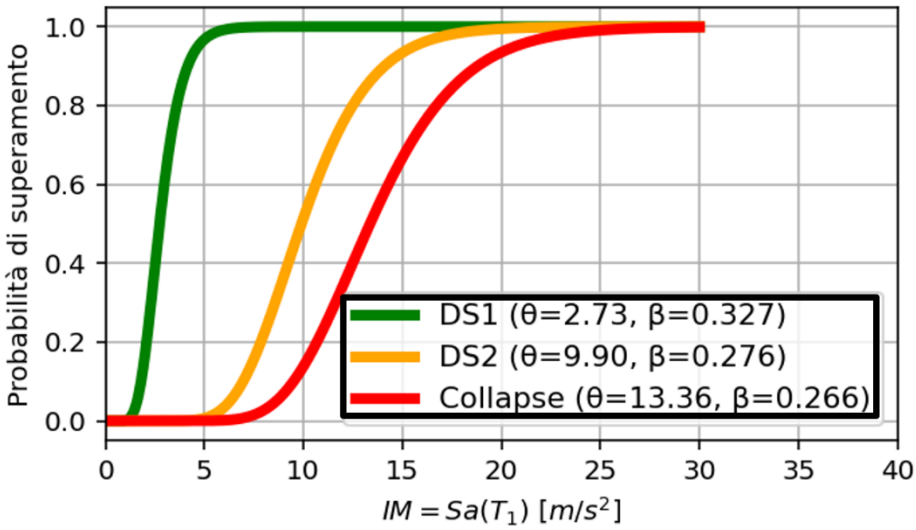

Figure 3.27: local EDP fragility: roof plastic hinge

The box contained in Figure 3.27 presents the actual values of median and dispersion of each curve, corresponding respectively to the yielding, huge plastic deformation occurring and collapse.

3.2.5.2. Global EDP: Interstory Drift Ratio (IDR)

As for the roof plastic hinge fragilities, the global EDP fragilities are obtained as well in Figure 3.28, referring to the damage thresholds of "EC8 Damage State Threshold", where the interstory drift limits are 0.7%, 2.5% and 5%.

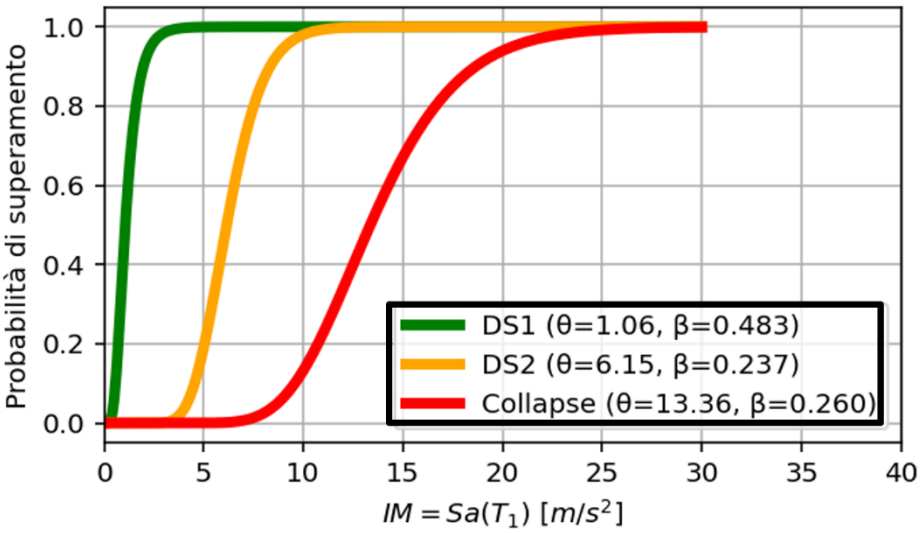

Figure 3.28: global EDP fragility: interstory drift

Again, the box contains each damage state's median and dispersion values corresponding to the 3 curves. The collapse fragility is the same both for the local and the global EDP fragility curve, thus the median collapse spectral acceleration computed is equal to 13.3 m/s^2. This value is going to be used during the development of the FEMA P-58 framework as defined in "Building Fragilities".

3.3. PACT Losses Analysis

Since non-linear structural analysis is carried out, the overall structural behavior depicted and the building collapse fragility defined, it's possible to going on with the implementation of the FEMA P-58 framework. The implementation requires basic building data and building vulnerability information, such as structural and non-structural fragilities. Successively, the various non-linear analysis results are imported in PACT to develop the demand set required for the Montecarlo procedure, as discussed in "Demand Set Developing: Monte Carlo Simulation" [21].

3.3.1. Building Data

What's been implemented in applying the methodology is site, structural model, occupancy category, structural and non-structural fragilities. The main data inserted in the tool is reported in the following Figure 3.29, Figure 3.30:

Main building data	Description
story number, height	2, 11.5 ft (first story), 10.5 ft (second story)
floor area	3487.50 sq. Ft
total replacement cost, time	1673998 $, 350 days
core and shell replacement cost	585900 $
carbon emission, emodied energy replacement	693000 kg, 9560334 MJ
population model	see next figure

Figure 3.29: main PACT building data

hour	weekdays	weekend
12:00	0%	0%
01:00	0%	0%
02:00	0%	0%
03:00	0%	0%
04:00	0%	0%
05:00	0%	0%
06:00	0%	0%
07:00	25%	0%
08:00	50%	5%
09:00	75%	5%
10:00	100%	5%
11:00	100%	5%
12:00	50%	5%
01:00	50%	5%
02:00	100%	5%
03:00	100%	5%
04:00	75%	5%
05:00	50%	5%
06:00	25%	0%
07:00	0%	0%
08:00	0%	0%
09:00	0%	0%
10:00	0%	0%
11:00	0%	0%

Figure 3.30: PACT building population model

As discussed previously “Demand Set Developing: Monte Carlo Simulation”, when Monte Carlo process a statistically obtained realization, it assigns a day and hour too, in order to evaluate how many people is present in the building and allows losses calculation regard casualties and injuries. Structural and non-structural components are chosen based on the Moment Resisting Frame model and on FEMA P-58 Volume 3 which provides electronics products to support in seismic performance assessment. The excel workbook “normative quantity estimation tool” assist in estimating non-structural component quantity by means of typical components present in buildings of a given category and gross square feet area [22]. The Moment Resisting Frame building is designed as office building. Figure 3.31 shows the computed structural and non-structural quantities derived from both an overview of the building and the normative excel tool, related to the “direction 1”. “Direction 2” quantities are assumed to be the same, given the symmetry in the structure design. Non-directional components quantities are presented successively in Figure 3.32. Each quantities table refers to a single floor. Quantity items on the other floors does not change. PACT requires the quantities to be computed referring to the units of measurement defined by FEMA P-58

methodology [3]. As discussed in “Building Fragilities”, unit of measurement divides the actual component quantity before to be inserted in PACT. A fragility data folder is provided, containing fragility and consequence specifications. This database is useful to derive fragility information related to the chosen component. Particularly, units of measurements referred to a specific fragility component/group are defined in this folder. Units of measurements are EA (each), SF (square feet), LF (lineal feet).

direction 1, floor 1			
fragility code	**component type**	**quantities**	**unit of measurement**
B1031.001	Bolted shear tab gravity connections	16	EA
B1035.021	Post-Northridge welded steel moment connection other than RBS, beam one side, beam depth <= W27	4	EA
B2022.001	Curtain Walls - Generic Midrise Stick-Built Curtain wall, Config: Monolithic, Lamination: Unknown, Glass Type: Unknown, Details: Aspect ratio = 6:5, Other details Unknown	12	30 SF
C1011.001a	Wall Partition, Type: Gypsum with metal studs, Full Height, Fixed Below, Fixed Above	3.5	100 LF
C2011.001b	Prefabricated steel stair with steel treads and landings with no seismic joint.	1	EA

Figure 3.31: PACT directional component's quantities

Non directional, floor 1			
fragility code	**component type**	**quantities**	**unit of measurement**
C3032.003a	Suspended Ceiling, SDC D,E (Ip=1.0), Area (A): A < 250, Vert & Lat support	5	600 SF
C3034.002	Independent Pendant Lighting - seismically rated	52	EA
D1014.011	Traction Elevator – Applies to most California Installations 1976 or later, most western states installations 1982 or later and most other U.S installations 1998 or later.	1	EA
D2021.013a	Cold or Hot Potable - Small Diameter Threaded Steel - (2.5 inches in diameter or less), SDC D, E, or F, PIPING FRAGILITY	0.15	1000 LF
D3041.011b	HVAC Galvanized Sheet Metal Ducting less than 6 sq. ft in cross sectional area, SDC C	0.26	1000 LF
D3041.031b	HVAC Drops / Diffusers in suspended ceilings - No independent safety wires, SDC C	3.08	10 EA
D3041.041b	Variable Air Volume (VAV) box with in-line coil, SDC C	1.71	10 EA
D4011.033a	Fire Sprinkler Drop Standard Threaded Steel - Dropping into unbraced lay-in tile SOFT ceiling - 6 ft. long drop maximum, SDC D, E, or F	0.69	100 EA

Figure 3.32: PACT non-directional component's quantities

Once the building data is implemented in PACT, the several analyses proposed by FEMA P-58 can be developed. There are 3 analyses available for the performance assessment: intensity-based, scenario-based and time-based.

3.3.2. Intensity-Based Analysis

In the current work, Intensity-based analysis is developed to assess seismic performance with respect to the seismic intensity level adopted during EC8 design. As introduced in "Probabilistic Hazard Consistent Spectrum (EC8 & PACT Intensity-Based Spectrum)", FEMA P-58 requires for this type of analysis a target acceleration code-based response spectrum[3]. The procedure consists of:

- Select a code-based target response spectrum consistent with site topography
- Select a suite of ground motion spectrum consistent with the reference spectrum
- Amplitude/scale each ground motion pair to the target spectral acceleration $S_a(T_1)$

3.3.2.1. Earthquake Hazard

The response spectrum and the suite of ground motion selected for the intensity-based analysis are those adopted in the EC8 design and during non-linear dynamic analysis, as shown in Figure 3.33:

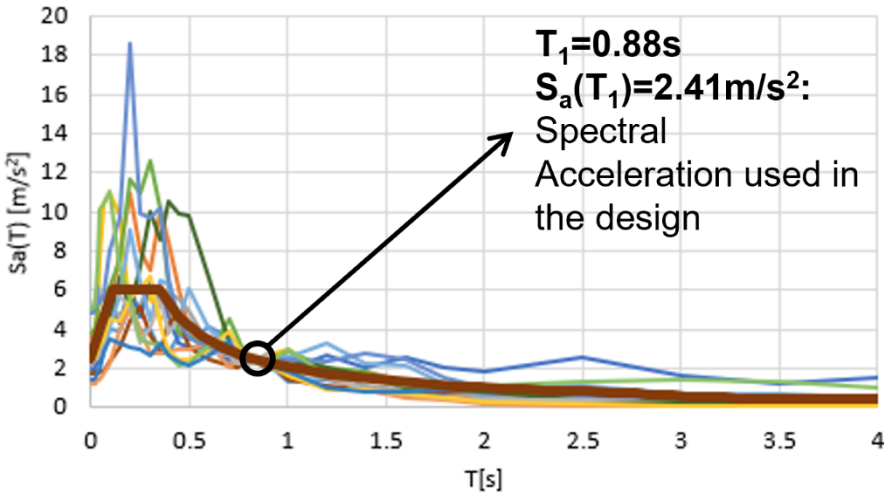

Figure 3.33: PACT intensity-based response spectrum and selected/scaled ground motion suite

Defined the spectrum and the suite of ground motion, several non-linear analyses are carried out using Openseespy and the results are imported in PACT. Monte Carlo procedure is then applied by PACT, and loss analysis is made. PACT results consist in a set of global fragilities which describes the probability the repair time and repair cost would exceed a certain value. Each component defined in PACT's building model gives a major or lower contribution to the global fragilities. There are loss realizations diagrams which include the whole set of realizations with

each single result in terms of repair time or repair cost. Global fragility is thus derived by enveloping each realization's result.

3.3.2.2. Global Repair Cost Fragility

As discussed in the previous section, the global repair cost fragility (cumulative density function) referred to such damage occurred during the intensity-based earthquake target spectral acceleration, is derived (Figure 3.34). The x-axis represents total repair cost whereas the y-axis the probability that the correspondent cost would be exceeded, depending on the contributions of each damaged component. The median cost is defined as such repair cost where earthquake's event gives a central estimate expected loss.

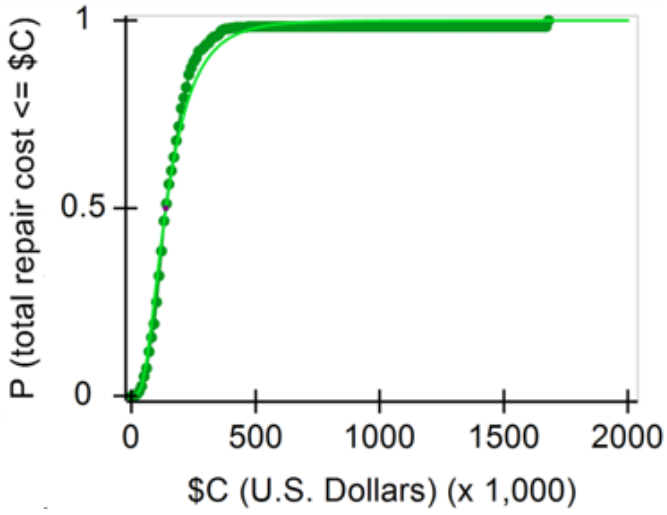

Figure 3.34: intensity-based repair cost fragility

The median cost that may be incurred during the intensity-based analysis is equal to 137000 $. The next figure shows how the damaging components affect the median repair cost realization (Figure 3.35):

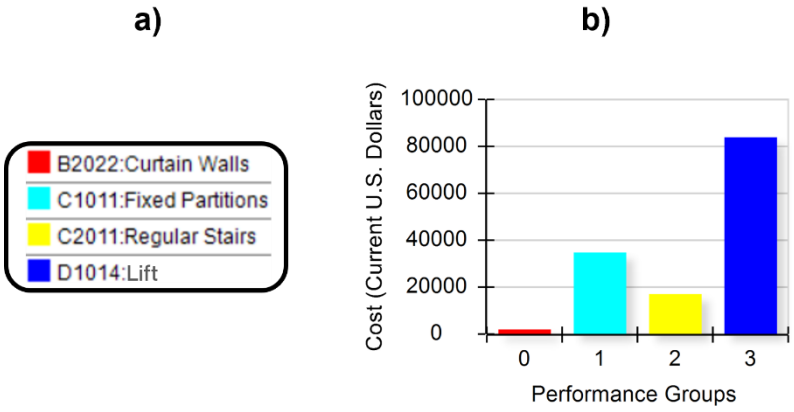

Figure 3.35: intensity-based component's influence on the median repair cost a) legend of considered components b) total realization's repair cost contribution

3.3.2.3. Global Repair Time Fragility

Similarly as what's been derived from the repair cost fragilities, the global repair time fragility is shown successively (Figure 3.36), including its median value as well. Repair time (i.e. Downtime, such time required to plan, finance, and complete repair facilities damaged by seismic events or others) is thus computed and reported [23], [24]. Global repair time fragility's x-axis represents total repair time while the y-axis represents the same probability discussed for "Global Repair Cost Fragility".

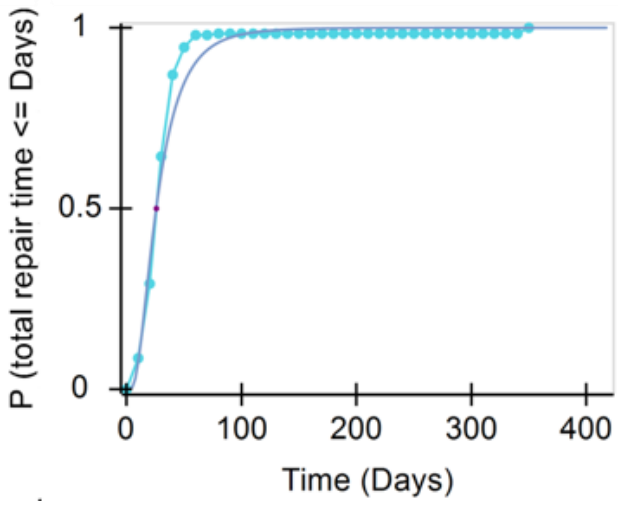

Figure 3.36: intensity-based repair time fragility

The median downtime expected to be incurred in the current intensity-based analysis is equal to 25 days. The next figure illustrates how damaging components affect the median repair time realization (Figure 3.37):

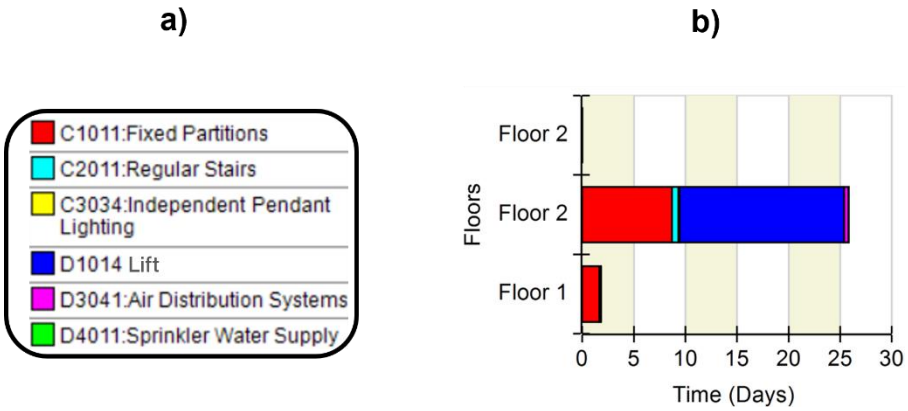

Figure 3.37: intensity-based component's influence on the median repair time a) legend of considered components b) total realization's repair time contribution

The downtime is currently computed considering parallel repair time actions (i.e. repair conducted contemporary for both the first and second floor).

3.3.3. Scenario-Based Analysis

Scenario-based analysis is developed to assess the building performance against L'Aquila earthquake that occurred in April 2009, at 03:32 am. As previously discussed in the section "Deterministic Spectrum (PACT Scenario-Based Spectrum)", scenario-based analysis requires a deterministic spectrum as target response spectrum, developed by means of attenuation relationship. The procedure consists in selecting an appropriate magnitude and site-to-source distance and creating, with the selected ground motion prediction equation, the median spectrum. Then select and scale a suite of ground motion to the target spectral acceleration $S_a(T_1)$ as for the intensity-based analysis [3].

3.3.3.1. Earthquake Hazard

As discussed in "Attenuation Relationship", equation (3.46) is implemented for the current case study:

$$\log_{10} Y = e_1 + F_D(R,M) + F_M(M) + F_S + F_{Sof} \tag{3.46}$$

The equation is solved by means of coefficient described in "Attenuation Relationship" for several periods to compute the spectral acceleration ($\log_{10}$Y) and develop the deterministic spectrum. L'Aquila earthquake (normal fault) magnitude is considered equal to 6.4, the Joyner-Bore distance R_{jb} equal to 0 km and the rupture distance R_{rup} equal to 5.4 km. The following figures (Figure 3.38, Figure 3.39) summarize the coefficient adopted and each spectral acceleration computed ($\log_{10}$Y):

T[s]	e1	c1	c2	h	c3	b1	b2	sA	sB	sC	sD	sE	f1	f2	f3	f4
PGA VALUE	3.672	-1.94	0.413	10.322	0.000134	-0.262	-0.0707	0	0.162	0.24	0.105	0.57	-0.0503	0.105	-0.0544	0
0.04	3.725	-1.976	0.422	9.445	0.00027	-0.315	-0.0787	0	0.161	0.24	0.06	0.614	-0.0442	0.106	-0.0615	0
0.1	3.796	-1.794	0.415	9.5	0.00255	-0.29	-0.0651	0	0.178	0.247	0.037	0.599	-0.0656	0.111	-0.0451	0
0.15	3.799	-1.521	0.32	9.163	0.00372	-0.0987	-0.0574	0	0.174	0.24	0.148	0.74	-0.0755	0.123	-0.0477	0
0.2	3.75	-1.379	0.28	8.502	0.00384	0.0094	-0.0517	0	0.156	0.234	0.115	0.556	-0.0733	0.106	-0.0328	0
0.25	3.699	-1.34	0.254	7.912	0.00326	0.086	-0.0457	0	0.182	0.243	0.14	0.254	-0.0568	0.102	-0.0314	0
0.3	3.753	-1.414	0.255	8.215	0.00219	0.124	-0.0435	0	0.201	0.244	0.213	0.301	-0.0564	0.0877	-0.0313	0
0.35	3.6	-1.32	0.253	7.507	0.00232	0.154	-0.0437	0	0.22	0.257	0.243	0.235	-0.0523	0.0905	-0.0382	0
0.4	3.549	-1.262	0.233	6.76	0.00219	0.225	-0.0406	0	0.229	0.243	0.235	0.235	-0.0532	0.0927	-0.0363	0
0.45	3.55	-1.261	0.223	6.775	0.00176	0.292	-0.0306	0	0.226	0.271	0.237	0.181	-0.0597	0.0886	-0.0289	0
0.5	3.526	-1.181	0.184	5.992	0.00186	0.384	-0.025	0	0.218	0.28	0.263	0.168	-0.0599	0.0802	-0.0252	0
0.6	3.561	-1.23	0.178	6.382	0.00114	0.436	-0.0227	0	0.212	0.296	0.219	0.145	-0.0599	0.079	-0.0239	0
0.7	3.485	-1.172	0.154	5.574	0.000942	0.529	-0.0185	0	0.21	0.303	0.496	0.134	-0.0461	0.0896	-0.0435	0
0.8	3.325	-1.115	0.163	4.998	0.000909	0.545	-0.0215	0	0.21	0.304	0.621	0.15	-0.0457	0.0795	-0.0328	0
0.9	3.318	-1.137	0.154	5.231	0.000483	0.563	-0.0263	0	0.212	0.315	0.68	0.154	-0.0315	0.0715	-0.0364	0
1	3.264	-1.114	0.14	5.002	0.000254	0.599	-0.027	0	0.221	0.332	0.707	0.152	-0.0298	0.066	-0.0362	0
1.25	2.896	-0.986	0.173	4.34	0.000783	0.579	-0.0336	0	0.244	0.365	0.717	0.183	-0.0207	0.0614	-0.0292	0
1.5	2.675	-0.96	0.192	4.117	0.000802	0.575	-0.0353	0	0.251	0.375	0.667	0.203	-0.014	0.0505	-0.0365	0
1.75	2.584	-1.006	0.205	4.505	0.000427	0.574	-0.0371	0	0.252	0.357	0.593	0.22	0.00154	0.037	-0.0385	0
2	2.537	-1.009	0.193	4.373	0.000164	0.597	-0.0367	0	0.245	0.352	0.54	0.226	0.00512	0.035	-0.0401	0

Figure 3.38: L'Aquila deterministic spectrum attenuation relationship coefficients by Bindi et al

sigmaB	sigmaW	BETAgm	FD(R,M)	FM(M)	FS	FSOF	log10Y	T[s]	Sa(Ti) [cm/s2]	
0.172	0.29	0.337	-1.381792765	0.08303925	0.162	-0.0503	2.484946485	0	305.4544698	
0.154	0.307	0.343	-1.353129908	0.10060925	0.161	-0.0442	2.589279342	0.04	388.4001079	
0.154	0.328	0.363	-1.207653733	0.09352525	0.178	-0.0755	2.794271517	0.1	622.689463	
0.179	0.318	0.365	-1.062632798	0.0275135	0.174	-0.0733	2.862380702	0.15	728.4180556	
0.209	0.32	0.382	-0.946245006	-0.00962325	0.156	-0.0568	2.876831744	0.2	753.0637519	
0.21	0.328	0.343	-0.906806133	-0.03569825	0.182	-0.0564	2.881695617	0.25	761.5450812	
0.218	0.29	0.363	-0.982541049	-0.04872875	0.201	-0.0523	2.866330201	0.3	735.0725429	
0.221	0.283	0.359	-0.860621704	-0.05925325	0.22	-0.0532	2.847825046	0.35	704.4092423	
0.21	0.279	0.349	-0.789278518	-0.0837235	0.229	-0.0597	2.851797982	0.4	710.8827598	
0.204	0.284	0.35	-0.798530743	-0.1059485	0.226	-0.0599	2.811820757	0.45	648.3667823	
0.203	0.283	0.349	-0.727294924	-0.1374625	0.218	-0.0599	2.819342576	0.5	659.6940629	
0.203	0.283	0.348	-0.795637109	-0.15538075	0.212	-0.0461	2.762082141	0.6	578.2053965	
0.203	0.283	0.354	-0.717942793	-0.18741625	0.21	-0.0457	2.743540957	0.7	554.0397916	**Sa(T1) [cm/s^2]:**
0.213	0.284	0.353	-0.623326698	-0.19338375	0.21	-0.0315	2.672589552	0.8	470.5324199	438.5917909
0.214	0.286	0.357	-0.664147534	-0.20027175	0.212	-0.0298	2.634080716	0.9	430.6066336	
0.222	0.283	0.36	-0.642830413	-0.2129575	0.221	-0.0207	2.599412087	1	397.5686096	
0.227	0.29	0.368	-0.476780081	-0.206766	0.244	-0.014	2.435753919	1.25	272.7431922	
0.218	0.303	0.373	-0.427298129	-0.20557425	0.251	0.00154	2.279127621	1.5	190.1637008	
0.219	0.305	0.376	-0.471503193	-0.20544475	0.252	0.00512	2.160592057	1.75	144.7411628	
0.211	0.308	0.373	-0.47396105	-0.21344575	0.245		2.0997132	2	125.8094316	
		0.35825								

Figure 3.39: L'Aquila deterministic spectrum attenuation relationship coefficients by Bindi et al

The spectral median acceleration has thus been computed. The last value contained in the column "BETAgm" of Figure 3.39 represents the dispersion of the deterministic spectrum mean acceleration value, equal to 0.35. The spectrum is then determined by interpolating the various $S_a(T_i)$ values, as illustrated in Figure 3.40:

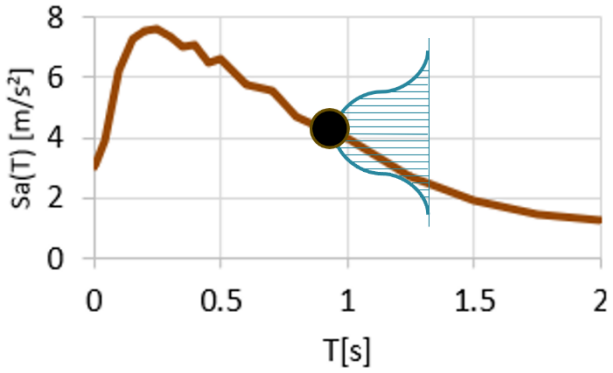

Figure 3.40: L'Aquila deterministic median response spectrum

As for the intensity-based analysis, a suite of ground motion is first selected using REXELweb [19], then scaled to the deterministic spectrum's target spectral acceleration. Finally, Figure 3.41 shows the scenario-based spectrum and the selected/scaled records:

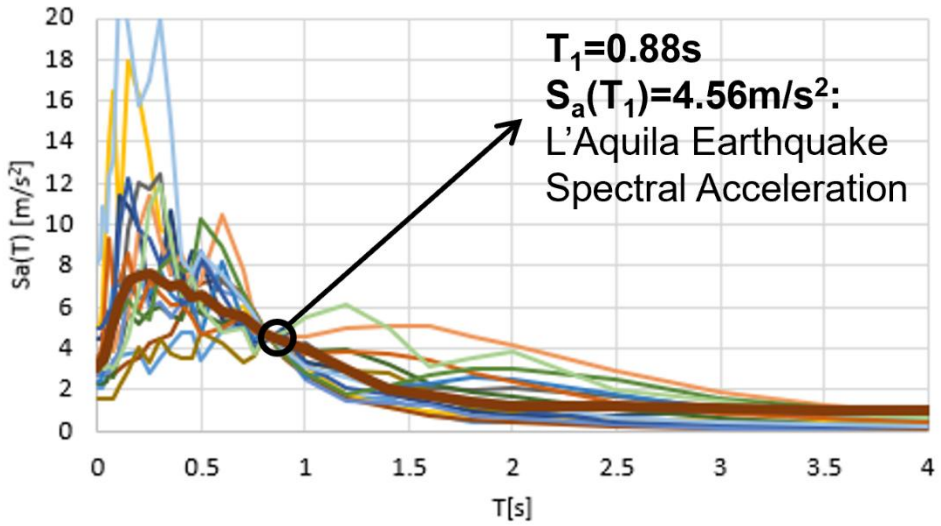

Figure 3.41: PACT intensity-based response spectrum and selected/scaled ground motion suite

Defined the spectrum and the suite of ground motion, several non-linear analyses are carried out using Openseespy and the results is imported in PACT. Monte Carlo procedure is then applied by PACT, and loss analysis is made. PACT results consist in a set of global fragilities which describes the probability the repair time and repair cost would exceed a certain value. Each component defined in PACT's building model gives a major or lower contribution to the global fragilities. There are loss realizations diagrams which include the whole set of realizations with each single result in terms of repair time or repair cost. Global fragility is thus derived by enveloping each realization's result.

3.3.3.2. Global Repair Cost Fragility

The global repair cost fragility (cumulative density function) is again computed for the scenario-based analysis in a similar manner to what's done in the previous sections "Global Repair Cost Fragility". Repair time fragility is shown in (Figure 3.42). The x-axis represents total repair cost whereas the y-axis the probability that the correspondent cost would be exceeded, depending on the contributions of each damaged component. The median cost is defined as such repair cost where earthquake's event gives a central estimate expected loss.

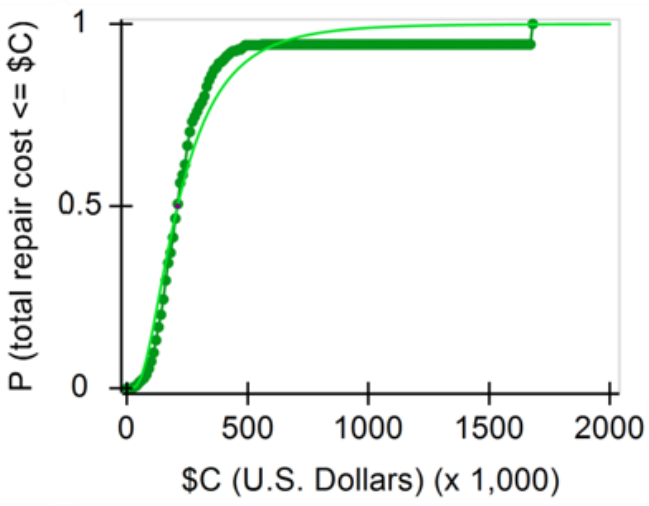

Figure 3.42: scenario-based repair cost fragility

The median cost that may be incurred during the intensity-based analysis is equal to 208100 $. The following figure shows how the damaging components affect the median repair cost realization (Figure 3.43):

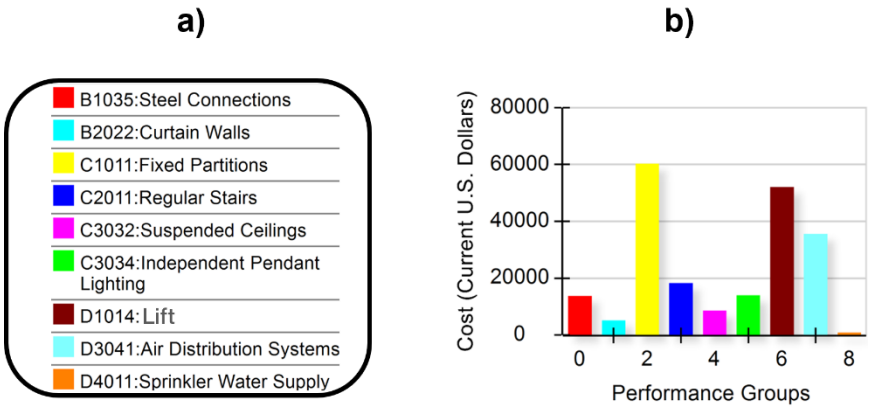

Figure 3.43: scenario-based component's influence on the median repair cost a) legend of considered components b) total realization's repair cost contribution

3.3.3.3. Global Repair Time Fragility

The global repair time fragility is computed as well and shown in (Figure 3.44). Repair time fragility's x-axis represents total repair time while the y-axis represents the same probability discussed for "Global Repair Cost Fragility".

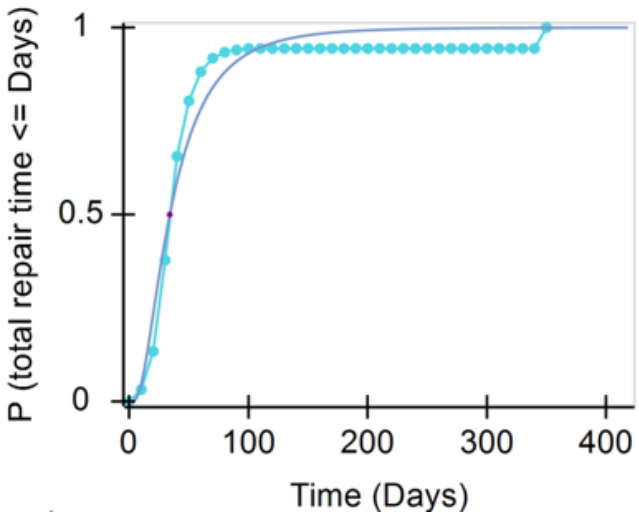

Figure 3.44: scenario-based repair time fragility

The median downtime expected to be incurred in the current intensity-based analysis is equal to 34 days. The next figure (Figure 3.45) illustrates how damaging components affect the median repair time realization:

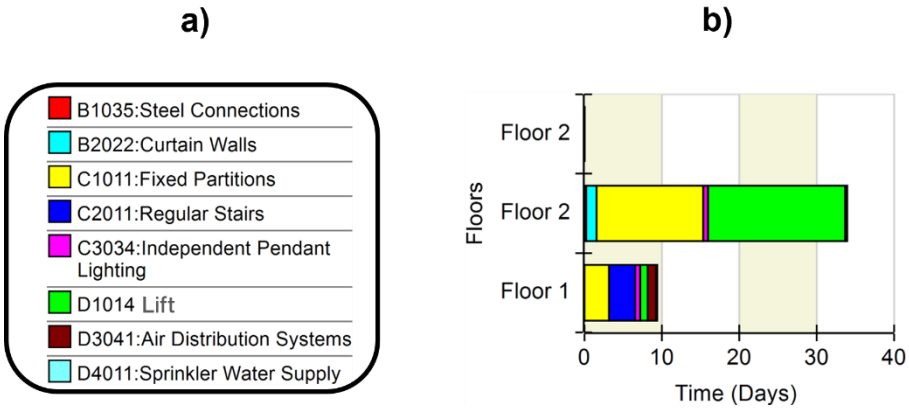

Figure 3.45: scenario-based component's influence on the median repair time a) legend of considered components b) total realization's repair cost contribution

3.3.4. Time-Based Analysis

Time-based analysis is developed to analyze building behavior within a certain increasing seismic intensity level over the life period of the building. It's necessary to develop a seismic hazard curve as described in "MAFE Curve (PACT Time-Based hazard)". An appropriate response-spectrum is defined to match the hazard represented by the MAFE curve. Then a suite of ground motion is selected and scaled as described for the intensity and scenario-based analysis [3]. Hazard EFEHR web platform provides interactive tools such as seismic hazard models [25]. This online platform has been adopted to develop such curves described in chapter "MAFE Curve (PACT Time-Based hazard)". Both the probability of exceedance over 50 years

curve (Figure 3.48) and MAFE hazard curve (Figure 3.49) is reported below, developed accurately for the Moment Resisting Frame building under analysis:

- T_1=0.88s
- Latitude: 42.34985, longitude: 13.39950
- European Seismic Hazard 2020 (ESHM20)
- Rock_vs30_800ms

Equation (3.47) has been used to compute the MAFE values starting from the probability over 50 years. The whole data set computed to develop such curves is reported as well (Figure 3.46, Figure 3.47):

$$P(Y^* > y^*) = 1 - e^{-\lambda T} \quad (3.47)$$

Probability of Exceedance in 50 years					
S_a(T=1s)	P(Y*>y*|50anni)	S_a(T=0.75s)	P(Y*>y*|50anni)	Sa(T=0.75s)	P(Y*>y*|50anni)
0.005	0.999999	0.005	0.999999	0.005	0.999999
0.010323	0.999997	0.010573	0.999997	0.010453	0.999997
0.021313	0.99998	0.02236	0.999997	0.02185744	0.99998884
0.044005	0.998717	0.047287	0.999629	0.04571164	0.99919124
0.090856	0.978321	0.1	0.989816		0.9842984
0.187585	0.863053	0.211474	0.910501	0.20000728	0.88772596
0.387298	0.60155	0.447213	0.677519	0.4184538	0.64105388
0.799634	0.315902	0.945741	0.375188	0.87560964	0.34673072
1.650963	0.12937	2	0.158349	1.83246224	0.14443908
3.408658	0.041615	4.229485	0.052191	3.83548804	0.04711452
7	0.009504	8.944271	0.012248	8.02910588	0.01093088
14.530324	0.001259	18.914832	0.001621	16.81026816	0.00144724
30	0.000066	40	0.000078	35.2	0.00007224

Figure 3.46: probability of exceedance in 50 years data set, Moment Resisting Frame building (T_1=0.88s), L'Aquila

Mean Annual Frequency of Exceedance					
Sa(T=1s)	MAFE	Sa(T=0.75s)	MAFE	Sa(T=0.88s)	MAFE
0.005	0.276310211	0.005	0.276310211	0.005	0.276310211
0.010323	0.254337965	0.010573	0.254337965	0.010453	0.254337965
0.021313	0.216395566	0.02236	0.254337965	0.02185744	0.228063492
0.044005	0.133171084	0.047287	0.15798617	0.04571164	0.142400167
0.090856	0.076628225	0.1	0.091738748	0.09561088	0.083079853
0.187585	0.039763226	0.211474	0.048270557	0.20000728	0.043736252
0.387298	0.018403465	0.447213	0.022634221	0.4184538	0.02049166
0.799634	0.007593082	0.945741	0.009406089	0.87560964	0.008515317
1.650963	0.002770764	2	0.003447797	1.83246224	0.00311996
3.408658	0.000850114	4.229485	0.001072045	3.83548804	0.000965211
7.037677	0.000190989	8.944271	0.000246472	8.02910588	0.000219821
14.530324	2.51959E-05	18.914832	3.24463E-05	16.81026816	2.89658E-05
30	1.32004E-06	40	1.56006E-06	35.2	1.44485E-06

Figure 3.47: Mean Annual Frequency of Exceedance data set, Moment Resisting Frame building (T_1=0.88s), L'Aquila

The hazard curves:

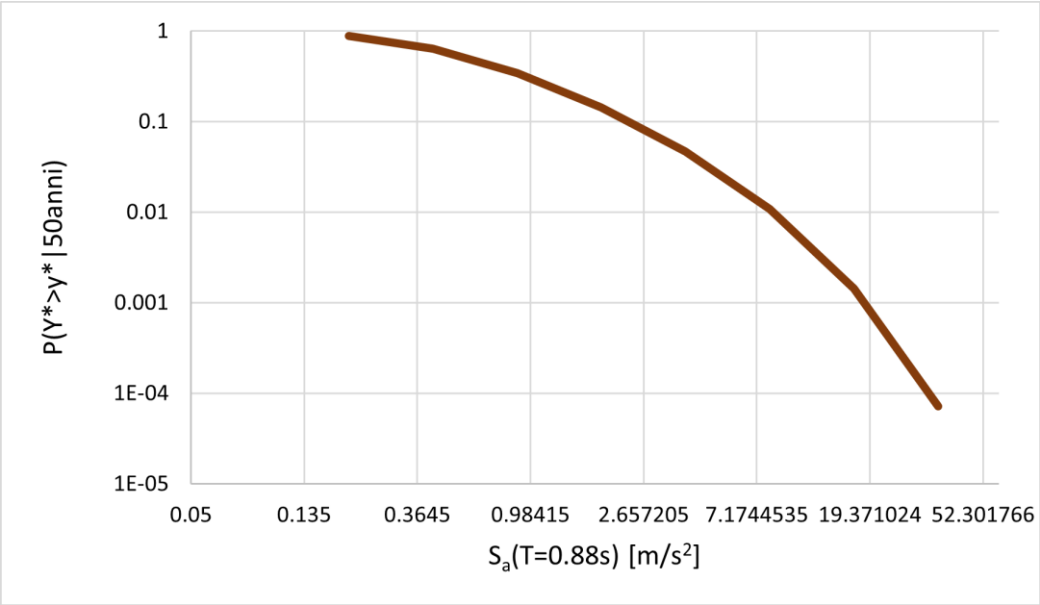

Figure 3.48: probability of exceedance in 50 years versus $S_a(T_1=0.88s)$ hazard curve; Moment Resisting Frame building, L'Aquila

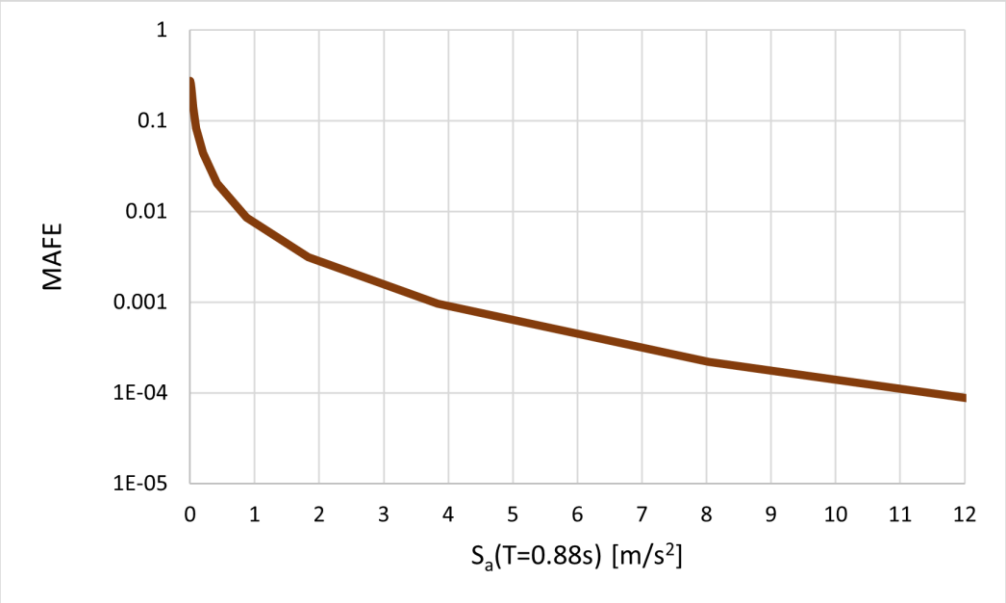

Figure 3.49: MAFE versus $S_a(T_1=0.88s)$ hazard curve; Moment Resisting Frame building, L'Aquila

FEMA P-58 imposes spectral acceleration limits to assess the building in a reliable site hazard acceleration range. Equation (3.48) defines these limits:

$$S_a(T_1)_{\min} = \frac{0.05}{T_1} \cong \frac{0.05}{0.88} \cong 0.05 m/s^2$$
$$S_a(T_1)_{\max} = \left\{ \begin{array}{c} 2 * S_a(T_1) \mid \lambda = 0.0004 \\ \theta_{collapse}(mediancollapsefragility) \end{array} \right\} \quad (3.48)$$

Since the minimum value between the maximum allowed spectral accelerations is represented by the median collapse fragility, such value is chosen as limit. Moment Resisting

Frame's collapse fragility defined in "Fragilities Curves" is equal to 12.5 m/s^2. Is necessary to divide the MAFE hazard curve into a set of "n" segments to develop the various intensity analysis conducted during Time-based assessment. The median spectral acceleration of each segment is taken and will be used as target spectral acceleration for loss assessment. In the current work the hazard curve is divided into 8 segments: 8 loss assessments referred to 8 different target spectral accelerations (1.25 m/s^2, 2.75 m/s^2, 4.25 m/s^2, 5.75 m/s^2, 7.25 m/s^2, 8.75 m/s^2, 10.25 m/s^2, 11.75 m/s^2) is carried out. "Figure 3.50" shows the segmented MAFE hazard curve:

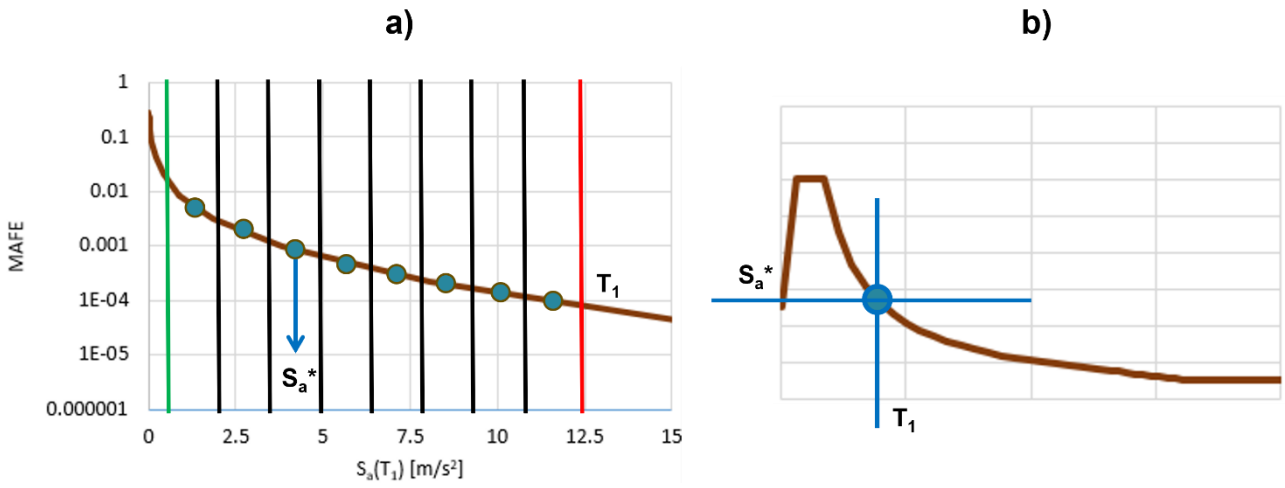

Figure 3.50: time-based hazard curve a) segmented MAFE curve b) target spectral acceleration of the "" segment*

The spectrum used during EC8 design and intensity-based analysis is adopted in this chapter as well, amplitude/scaled to each of the "n" segment's target spectral acceleration. MAFE curve is divided into n=8 segments and thus 8 set of non-linear analyses are carried out using Openseespy. The results are imported in PACT and Monte Carlo procedures are applied for each of the 8 set of assessments. PACT time-based results consist, as for intensity and scenario-based assessments, in a set of global curves which describe the probability the repair time and repair cost would exceed a certain value. On the other hand, in the time-based assessment there is not a fragility curve describing this probability. 2-dimension and 3-dimension diagrams illustrate the probability of exceeding a certain cost/time by summing the contribution of each of the 8 intensities. Each component defined in PACT's building model gives a major or lower contribution to the intensity-assessment and thus, to the global curves. There are loss realizations diagrams which include the whole set of realizations with each single result in terms of repair time or repair cost. Global curves are derived by enveloping each realization's result. Whereas others PACT analysis carries out 1 assessment related to a single target spectral acceleration, time-based assessment develops "n" assessment as many as the "n" hazard segment defined. It's possible to go beyond each "n" performance assessment considering it as

an intensity-based analysis. On the other hand, it can read the overall computation referred to the global set of analyses: annualized probabilities are computed by PACT, such unsafe placards, complete loss due to residual drift and collapse probability. Time-based results give also curves describing the annual repair cost/time, showing different probability of exceeding a certain loss level, including the contribution of each of the "n" analysis. Thus, differently from the fragility's curves derived in intensity and scenario-based, time-based performance assessment illustrates how each intensity contributes to the overall exceedance probability. The next Figure 3.51 illustrates the legend for the 8 intensities adopted in the time-based performance assessment:

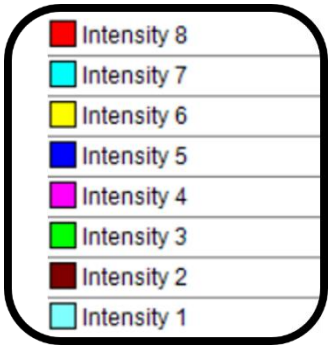

Figure 3.51: time-based intensity of earthquake's target spectral acceleration

Intensity 1 is the lower and the corresponding spectral acceleration is equal to 1.25 m/s^2. The 8 one corresponds to the strongest earthquake occurring and the considered spectral acceleration is equal to 11.75 m/s^2.

3.3.4.1. Global Repair Cost Curves

As discussed above, the global repair cost curve, showing the influence of each intensity analyzed, is presented in the following Figure 3.52. The x-axis represents, as in the intensity and scenario-based analyses, the total repair cost. The y-axis differs from the others PACT's analysis, showing the annual probability that such cost would be exceeded, depending on the contributions of each intensity. Each intensity contribution refers to Figure 3.51 legend.

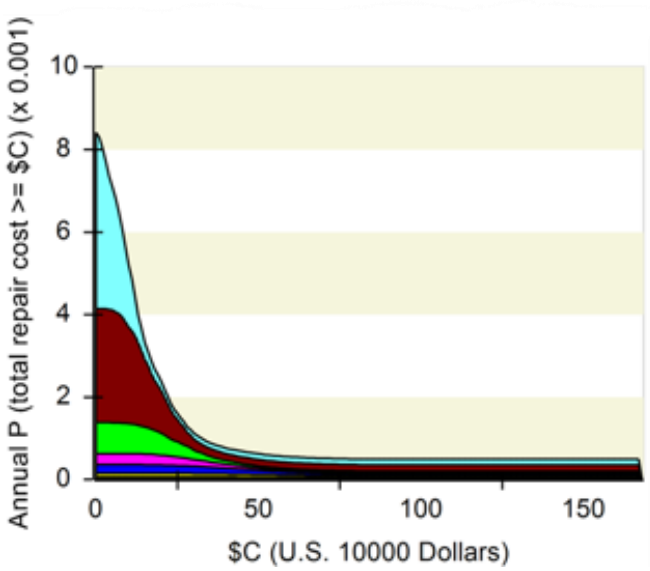

Figure 3.52: time-based repair cost curve 2D

The next Figure 3.53 illustrates the same curve described in Figure 3.52, in a 3-dimensional representation, to easily represent the whole set of intensities:

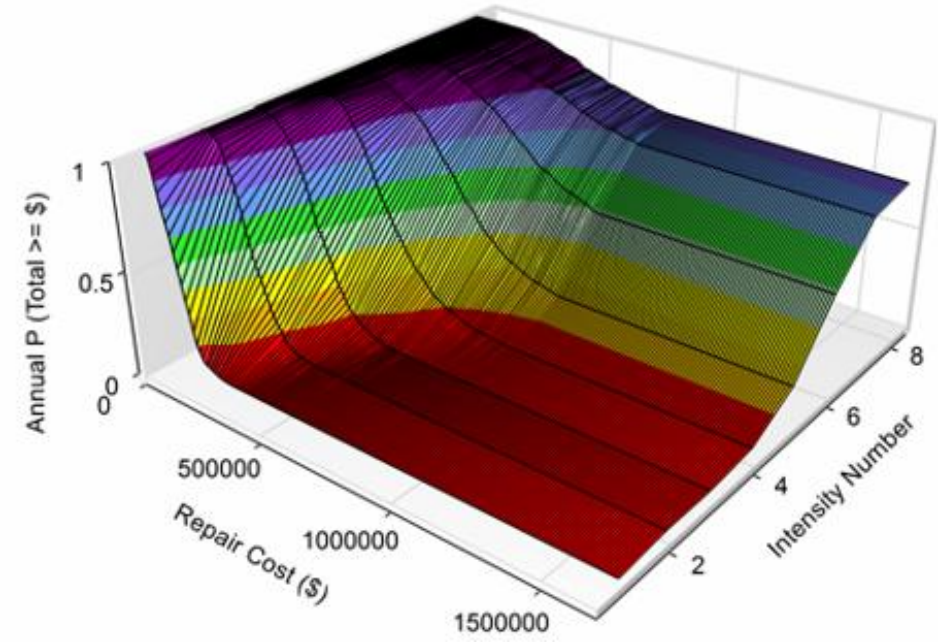

Figure 3.53: time-based repair cost diagram 3D

3.3.4.2. Global Repair Time Curves

Similarly, global repair time curve is derived and presented (Figure 3.54). Also in this case, x-axis represents the total repair cost while y-axis the annual probability to exceed a certain cost.

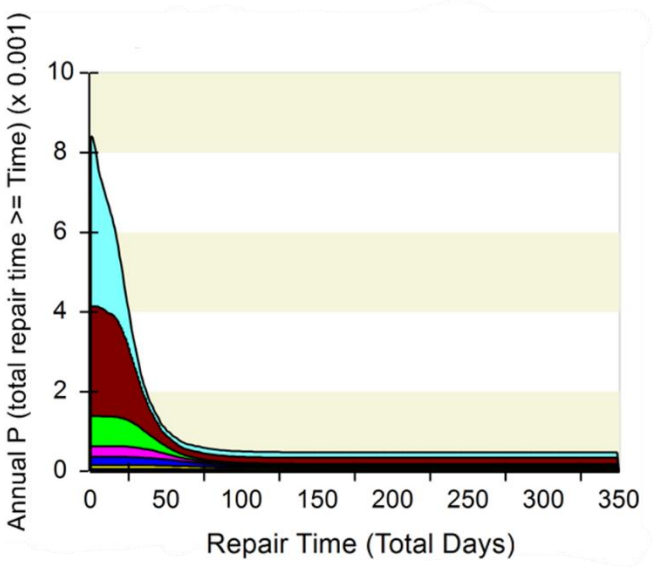

Figure 3.54: time-based repair time curve 2D

Where the repair time is considered parallel: the workers act simultaneously both in the first and second floor of the Moment Resisting Frame building. Finally, the next Figure 3.55 shows the 3-dimensional representation of the repair time curve.

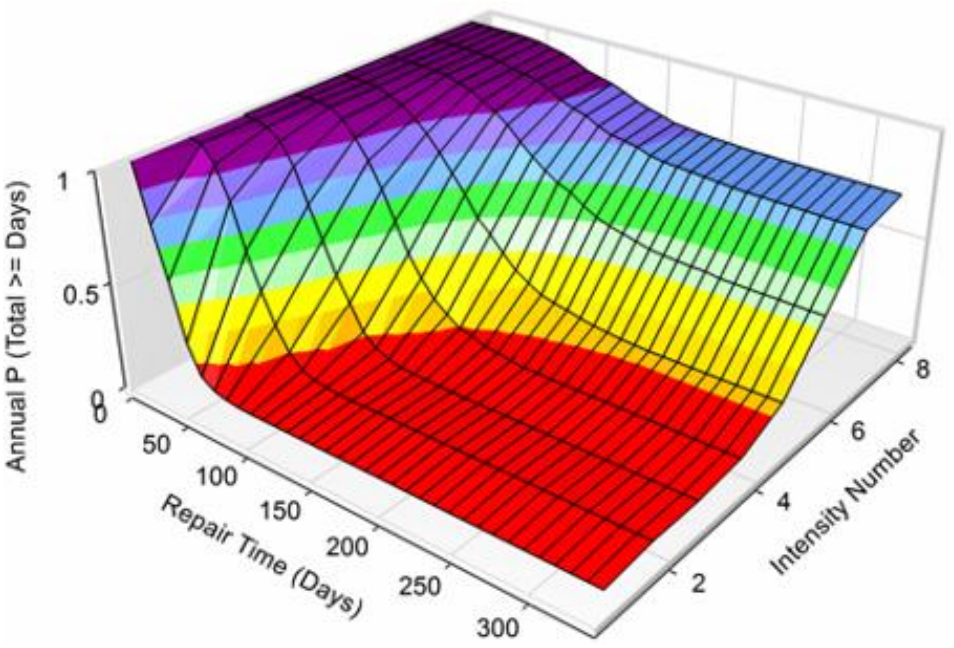

Figure 3.55: time-based repair time diagram 3D

4. RESULTS

PACT results are here discussed to present a comparison between the losses incurred from intensity and scenario-based analyses and to develop a life cycle analysis of the analyzed MRF building. This approach of the Performance-Based Seismic Design aims to reduce economic losses due to post-events repair. Essentially, it promotes more comprehensive risk management, helps designers with practical guidelines and considerations, supports the selection of target performances to be achieved.

4.1. Intensity-Based (Code-Based) vs Scenario-Based (L'Aquila Earthquake, 2009) Losses

The comparison between code-based losses, defined according to L'Aquila design seismic intensity, and the losses occurred in a real situation such as the L'Aquila Earthquake, 2009, is fundamental to deeply understanding how different evaluation methodologies can lead in significant variation, even for the same site, in the expected losses. The code-based analysis relies in a probabilistic spectrum "Earthquake Hazard", whereas the scenario's hazard is obtained by selecting specific magnitude-to-distance pairs and developing specific attenuation relationships "Earthquake Hazard". The discussion is expressed both for the individual components behavior and highlighting overall building's response, reporting the increasing repair costs and times in the scenario-based situation.

4.1.1. Repair Cost Comparison

4.1.1.1. Repair Cost fragilities

The following "Figure 4.1" shows the total repair cost fragilities function, where the median repair cost for both code-based and L'Aquila, 2009, situations are highlighted:

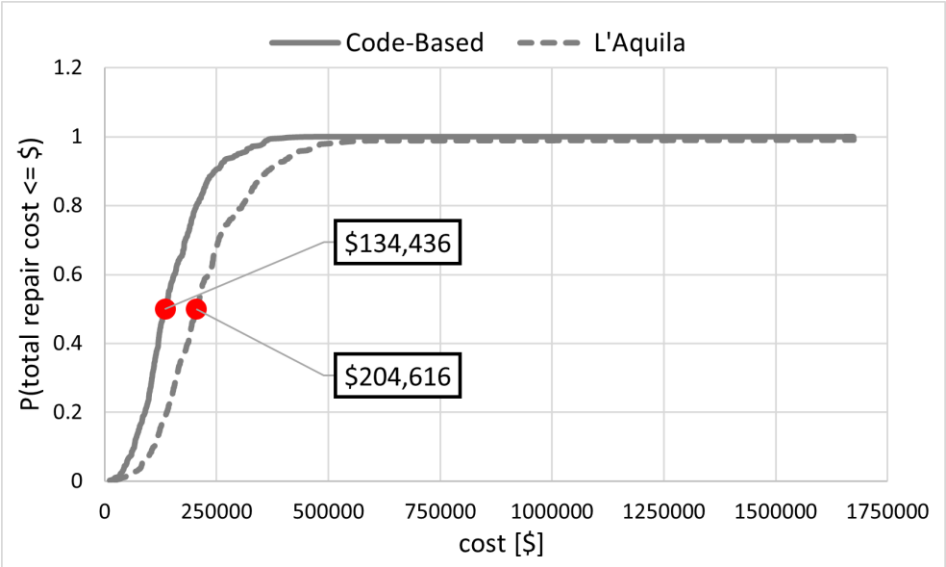

Figure 4.1: total repair cost fragilities comparison: code-based vs L'Aquila, 2009

This overview over the global building's response shows that L'Aquila, 2009 scenario results in 52% higher median repair cost compared to the code-based situation.

4.1.1.2. Components repair cost distribution

In order to better understand the meaning and reason of the 52% increasing on the global median repair cost (Figure 4.1), each component contribution is investigated and compared, as in the previous section, between the code-based an L'Aquila situation. The cost distribution, among the whole 500 realization conducted by PACT, is considered. The whole component's set discussed previously (Figure 3.31, Figure 3.32), is again reported below (Figure 4.2) as a legend, and will be adopted as reference in the following figures of this chapter "Results".

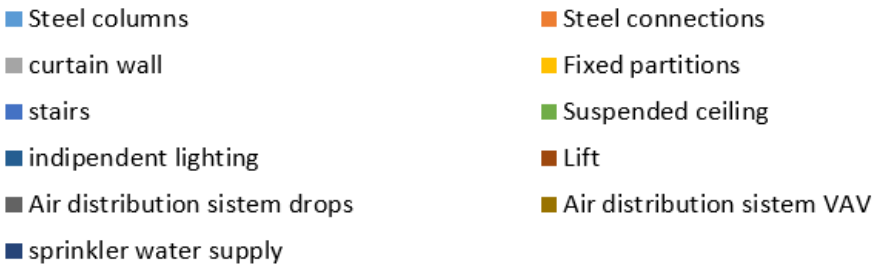

Figure 4.2: PACT's components legenda

Steel connections are concerned with the bolted connection adopted in the gravity frame and, on the other hand, steel columns deal with the post-Northridge welded steel moment connection. The next "Figure 4.3" illustrates the behavior of each main component, chosen referring to their amount on the global median repair cost, over the realizations set:

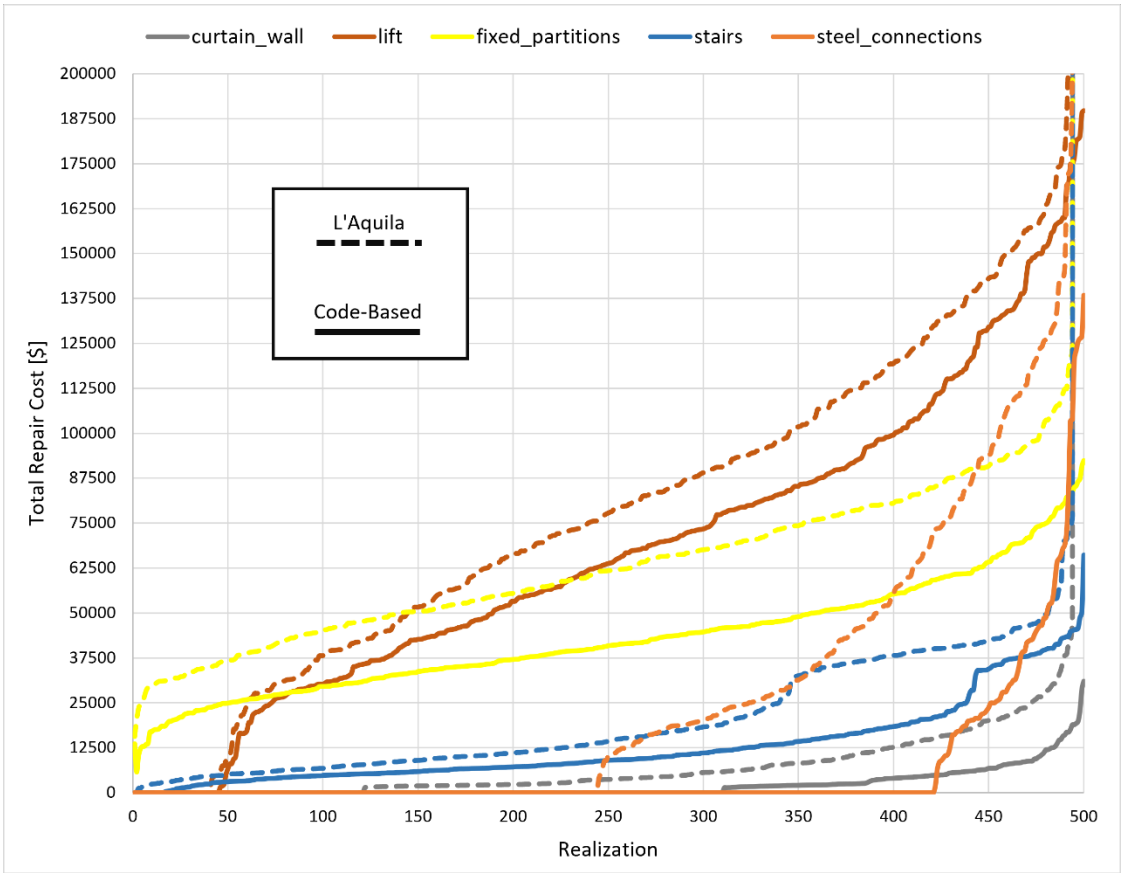

Figure 4.3: components cost distribution comparison: code-based vs L'Aquila, 2009

To quantify the contribution of each component in the overall increase of the median repair cost, in the next "Figure 4.4" are illustrated the absolute and percentual differences from code-based to L'Aquila, 2009 results. Components whose contribution in code-based situation is 0, are considered with the absolute difference:

MEDIAN REPAIR COST COMPARISON (CODE-BASED VS L'AQUILA 2009)				
	Code Based Median Cost [$]	L'Aquila, 2009 Median Cost [$]	Difference [$]	Increase [%]
Curtain Wall	0	3752	3752	No Cost At Median
Lift	63918	78937	15019	23
Fixed Partitions	40926	61812	20886	51
Stairs	9123	14711	5589	61
Steel Connection	0	11132	11132	No Cost At Median

Figure 4.4: main components cost increase: code-based vs L'Aquila, 2009

4.1.2. Repair Time Comparison

The subsequent section repeats the same calculation with the approach of "Repair Cost Comparison", considering repair time instead of the cost.

4.1.2.1. Repair Time Fragilities

"Figure 4.5" illustrates the global repair time fragilities function and the increase on the median repair time:

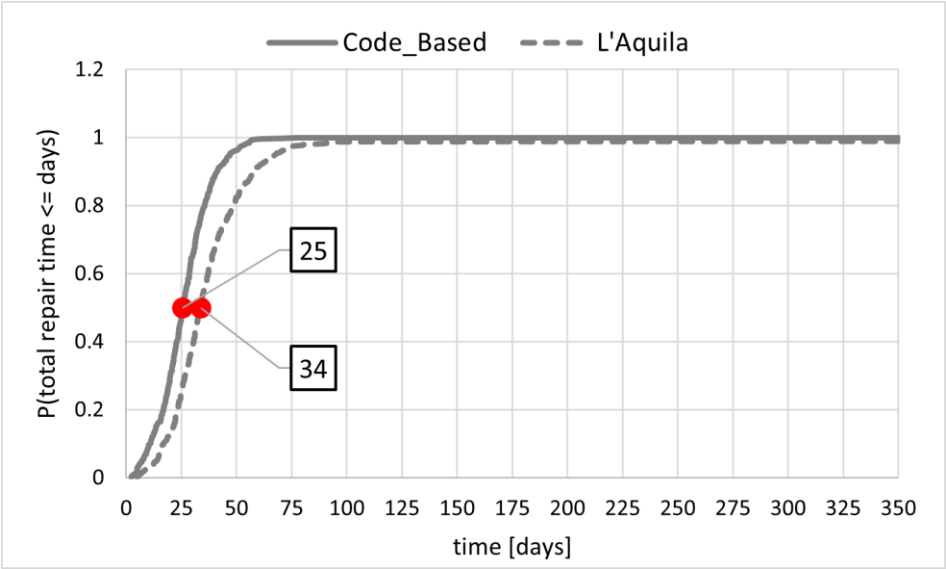

Figure 4.5: total repair time fragilities comparison: code-based vs L'Aquila, 2009

4.1.2.2. Components repair time distribution

The behavior of each component over the realization set (Figure 4.6):

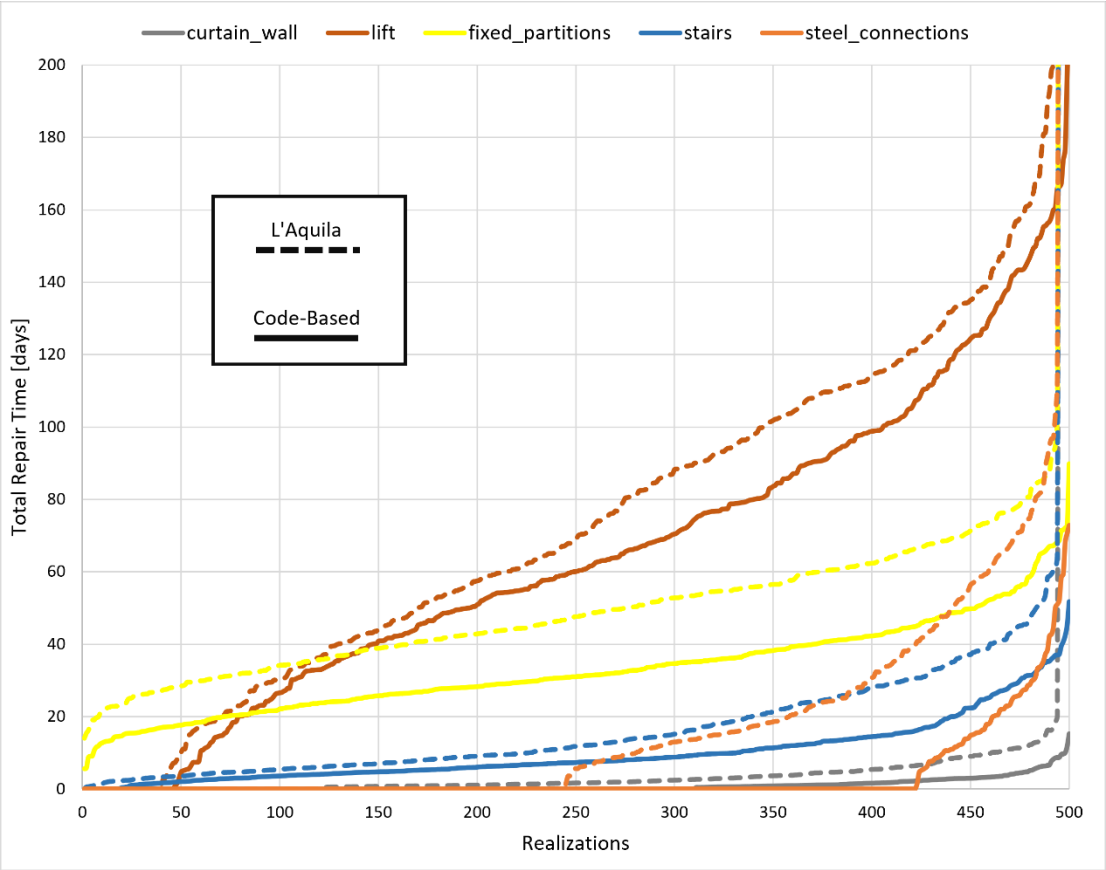

Figure 4.6: components time distribution comparison: code-based vs L'Aquila, 2009

Finally, the absolute and percentual differences are:

MEDIAN REPAIR TIME COMPARISON (CODE-BASED VS L'AQUILA 2009)				
	Code Based Median Time [days]	L'Aquila, 2009 Median Time [days]	Difference [days]	Increase [%]
curtain wall	0	0	0	No Time At Median
lift	16	17	1	7
fixed partitions	6	9	3	49
stairs	1	3	1	72
steel connection	0	2	2	No Time At Median

Figure 4.7: main components time increase: code-based vs L'Aquila, 2009

4.2. Time-Based Losses

After comparing the global and component-level repair losses between code-based and L'Aquila earthquake, 2009, it's useful to evaluate the losses evolution with respect to gradual increasing of the seismic intensity. Time-based analysis allows to highlight how repair cost and

times progressively vary with the seismic demand. Each analyzed intensity correspond to a specific ground motion scaling throughout the entire range defined in "Time-Based Analysis", considering all the possible intensity level that may occur during the Moment Resisting Frame building's lifetime. The analysis is carried out by means of both repair costs and time, considering 8 fragilities functions and the incremental losses variations across the mentioned intensities level.

4.2.1. Repair Cost: Variation with Intensity

4.2.1.1. Repair Cost Fragilities

"Figure 4.8" shows the global fragilities function corresponding to each intensity level, defined in "Time-Based Analysis". It illustrates the progressive evolution of the median repair cost from the lower intensity (0.125 g), where the median cost is equal to 70829$, to the maximum (1.175 g) one, where the median cost is assumed as the total replacement cost (i.e. equal to 1673998$).

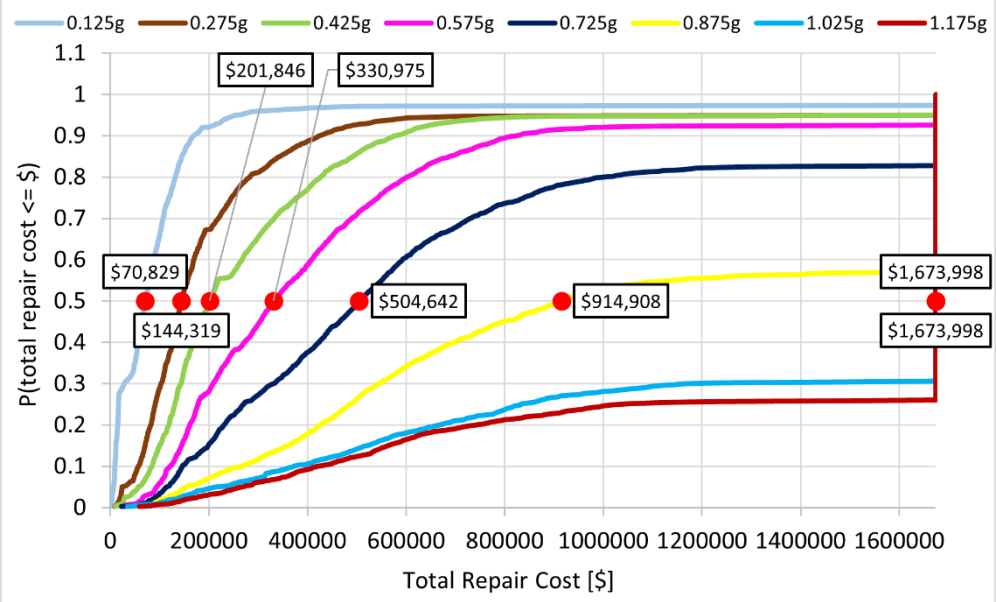

Figure 4.8: time-based fragilities function: median repair cost evolution

In order to better understand how the median repair cost increases across the various intensity, "Figure 4.9" summarizes the information of "Figure 4.8" by plotting only the median repair cost of each fragility. Red markers correspond to the defined intensities. Repair costs increase clearly non-linearly with the seismic demand. From intensity 2 (0.275 g) to intensity 3 (0.425 g), for example, the increasing is around 40%, while from 0.725 g to 0.875 g is approximately 82%. This percentage goes to increase in each subsequent step.

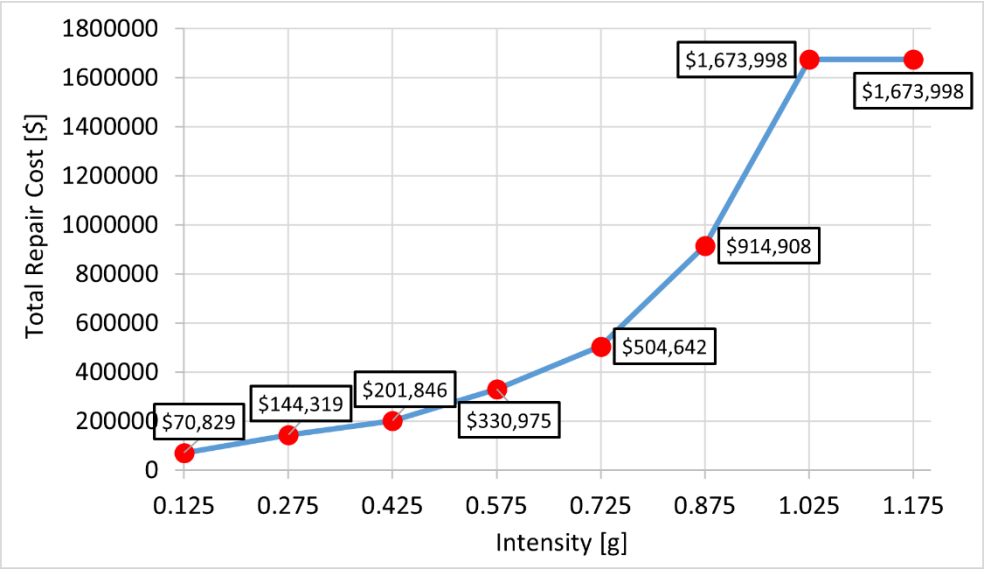

Figure 4.9: median repair cost evolution

4.2.1.2. Incremental Component Repair Cost Distribution

Since the previous section has given an overview of the global building's response, it's interesting to go beyond each single analysis and depict the contribution of each component. "Figure 4.11" illustrates the total median repair cost of each carried analysis. Each component follows the legenda defined previously (Figure 4.2), and the cost contribution is presented in the stacked column. This chart allows to evaluate the actual cost of each element and thus define the main drivers in terms of local contribution. "Figure 4.12" support what's defined in the first graph (Figure 4.11) and gives an easy illustration of the progressive increase/decrease of each component influence. For example, lift is the component which contribution is dominant in the lowest intensity (63% of the total median repair cost), while at higher intensities its contribution is not such relevant with respect to structural component as steel connections (e.g. 17% contribution of the lift against 40% global steel connection contribution). Similarly, fixed partitions play a fundamental role (29%) for low intensities, but their trend decreases to 13% at higher intensities. Components are also divided by their category (Figure 4.10): steel columns, connections and curtain walls are considered as shell parts. Fixed partitions, stairs, suspended ceiling and independent lighting are interiors elements. In the end, the other components such as lift, air distribution system and sprinkler are considered as services. This additional subdivision provides an alternative way to compute element contribution. For example, when intensity reaches 0.875 g, 47% of the total median repair cost is given by shell (8%+32%+7%), while interiors and services contribute respectively with 28% and 25%. Overall, when the seismic level achieves intensities 7 (1.025 g) and 8 (1.175 g), the median

repair cost is given by the total replacement, which means that more than a half of the realizations resulted in a collapse state (i.e. collapse occurred or residual drift limit is exceeded).

Figure 4.10: PACT's components legenda: main categories

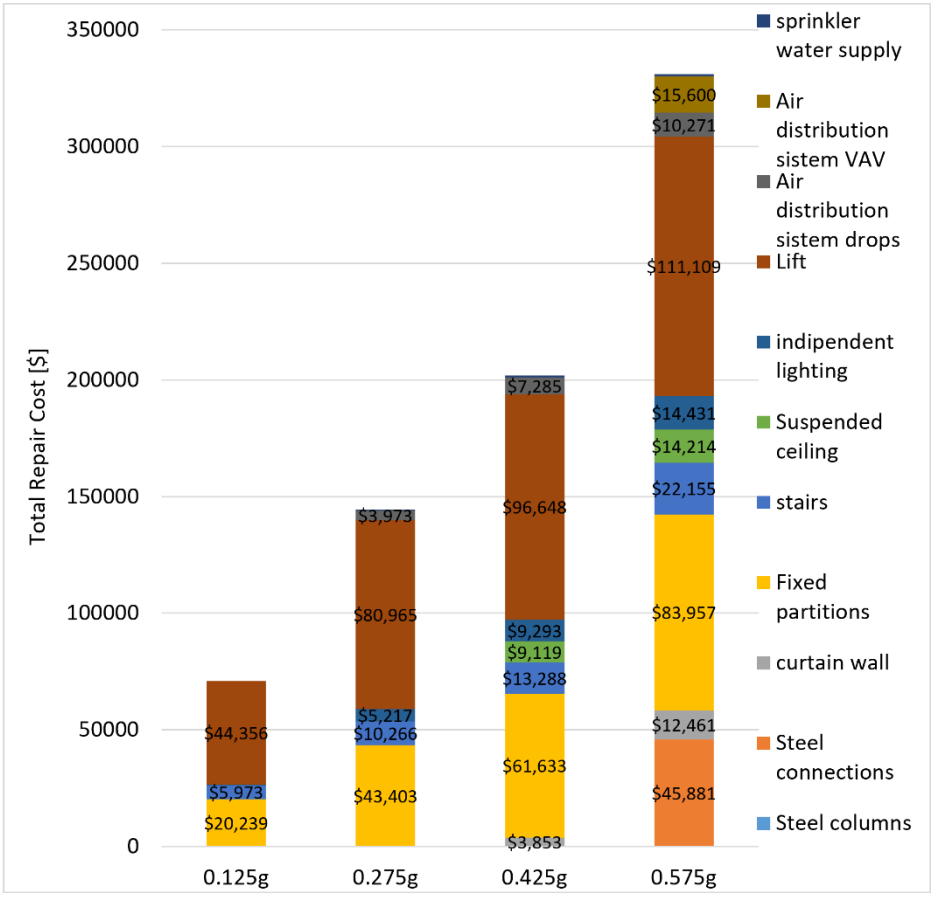

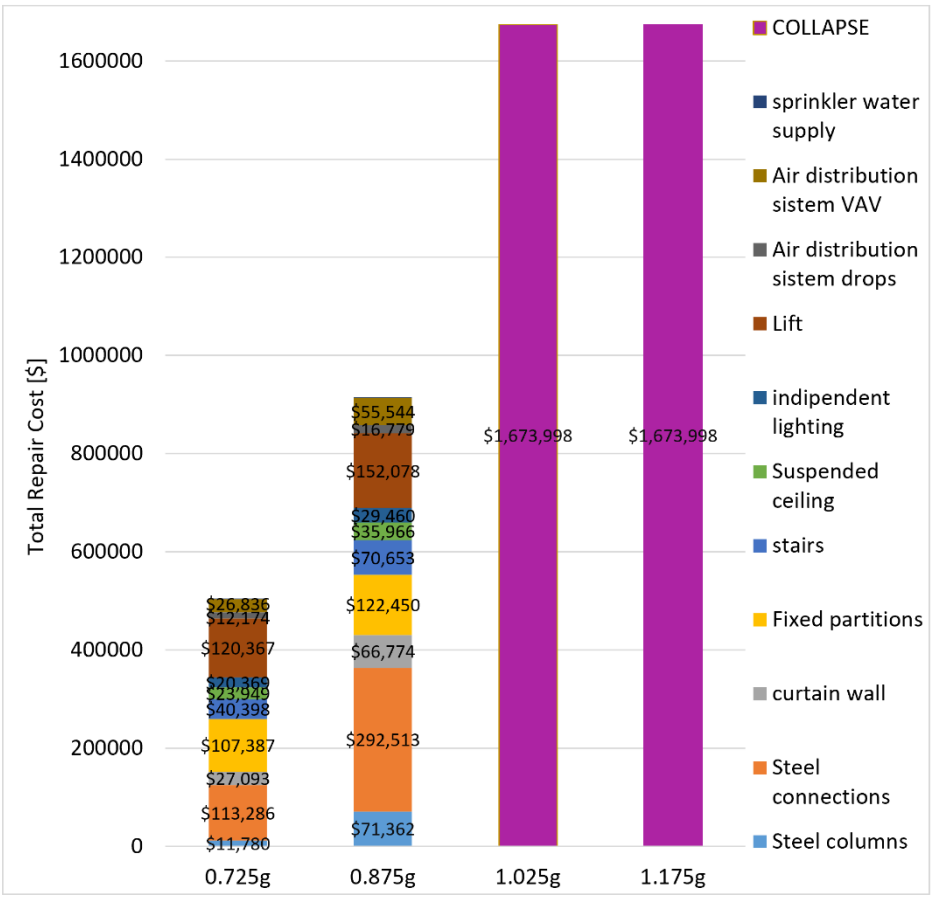

Figure 4.11: component contribution to median repair cost: 0..125 g - 1.175 g

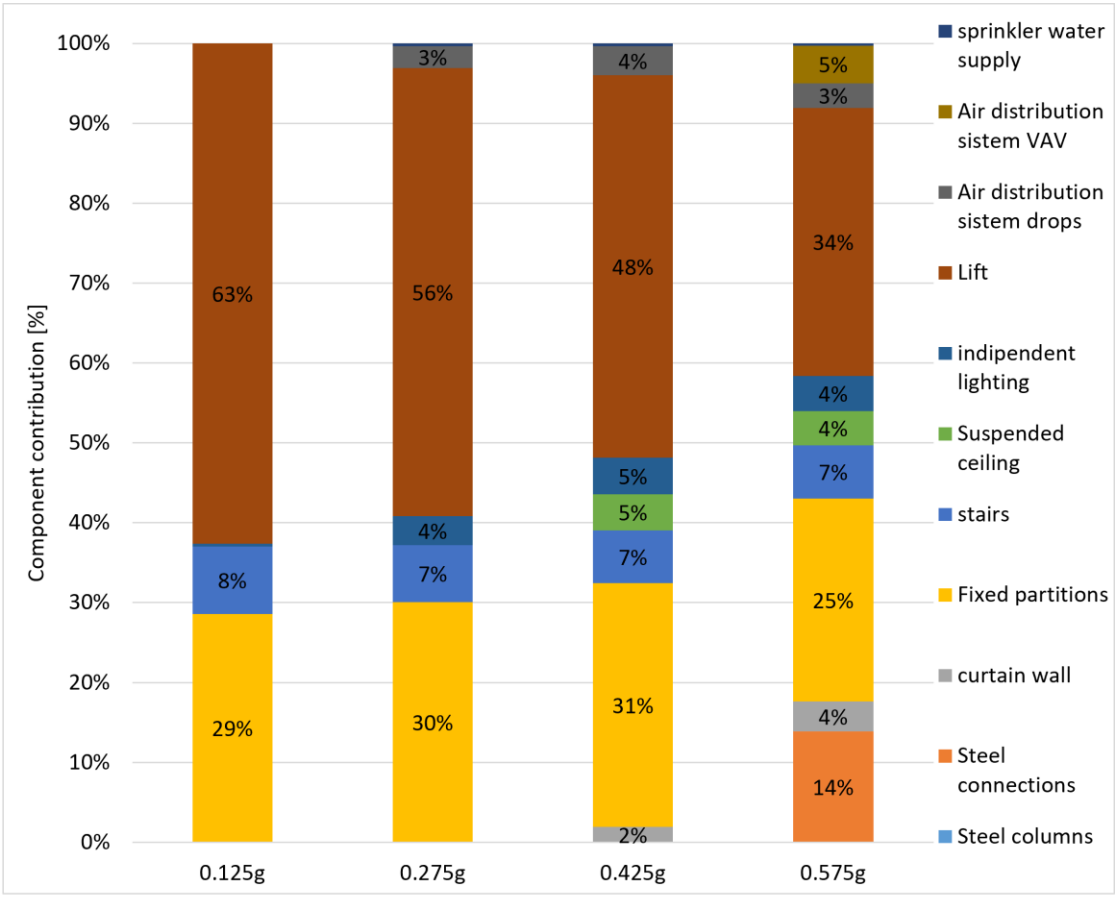

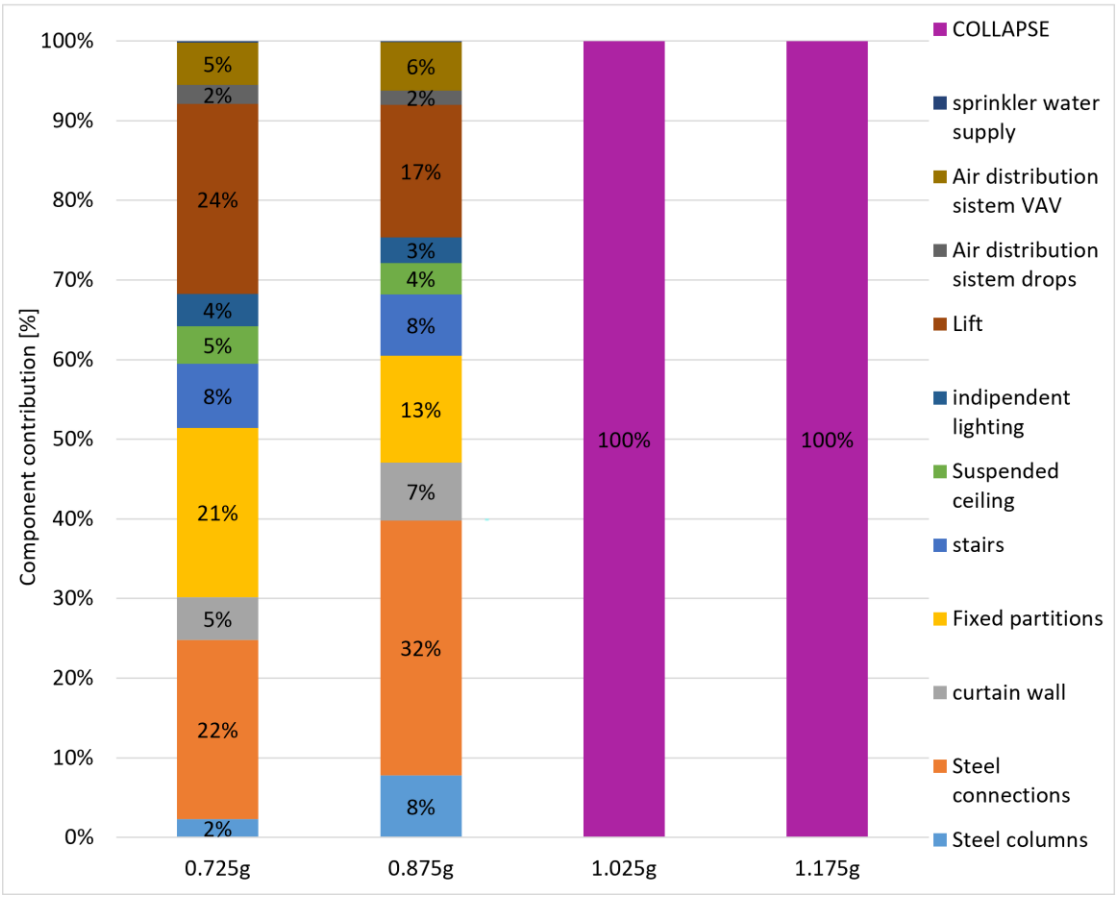

Figure 4.12: percentage component contribution to median repair cost: 0.125 g - 1.175 g

4.2.2. Repair Time: Variation with Intensity

The subsequent section presents the same approach discussed previously (Repair Cost: Variation with Intensity), in terms of repair time. The total repair time have been computed considering parallel time (i.e. repair first and second floor simultaneously) and 0.01 as number of workers for m^2.

4.2.2.1. Repair Time Fragilities

(Figure 4.13) shows the global median repair time fragilities presented for the 8 intensity level used: the lower intensity result in 16 days repair time whereas the higher one in 350 days, that's the total replacement time.

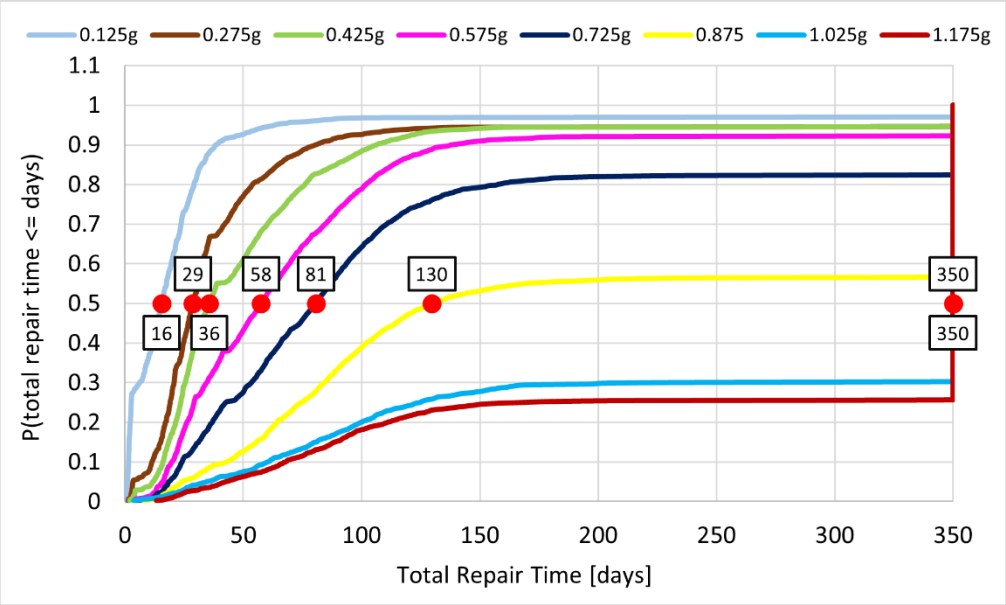

Figure 4.13: time-based fragilities function: median repair cost evolution

As before, "Figure 4.14" condenses "Figure 4.13" marking only the median point and highlighting their non-linear increasing path: modest increasing at low intensities level begins sharp rise around 0.725 g. indeed, for example, while between 0.275 g and 0.425 g there's a 24% increasing of repair time, approximately 170% increase characterize the last step (0.875 g – 1.025 g) before collapse state occurs. Highest intensity achieves the total replacement time.

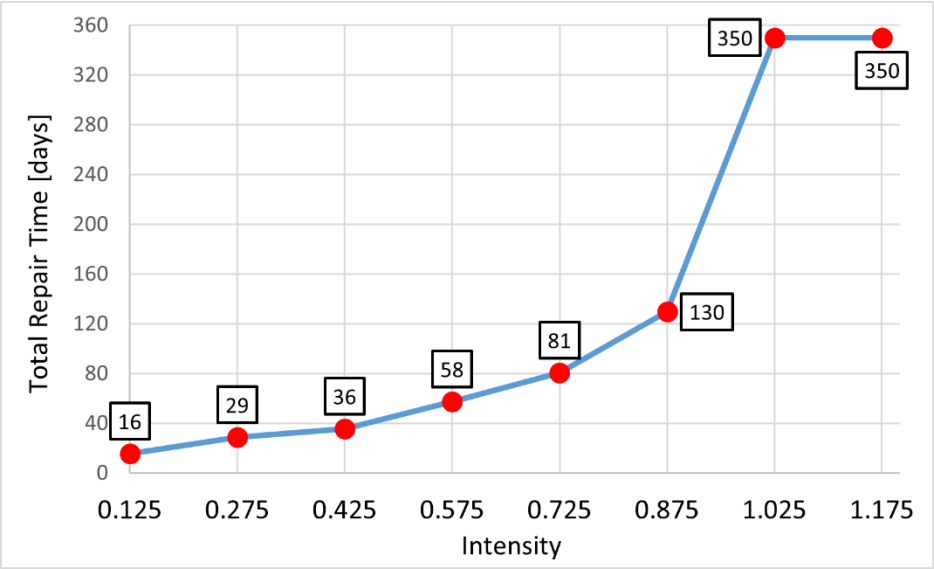

Figure 4.14: median repair cost evolution

4.2.2.2. Incremental Component Repair Time Distribution

"Figure 4.15" reports the median repair time at each intensity as stacked column and illustrates the component's local influence, as previously done for the repair cost (Incremental Component Repair Cost Distribution). On the other hand, "Figure 4.16" shows the percentage composition. Again, low seismic demand is dominated by services like lift and fixed partitions, respectively with 73% and 19% influence on the global repair cost. High intensity level is mainly influenced by structural elements such as steel connections: 34% of the total repair cost is given by the contribution of both the welded and bolted steel connections, while lift and fixed partitions contribute with 21% and 11%. When the seismic level exceeds 1.025 g, the number of realizations resulting in a collapse state is more than the non-collapse situations. Median repair time is then considered, for intensities 7 and 8 (i.e. 1.025 g – 1.175 g), as the total replacement cost.

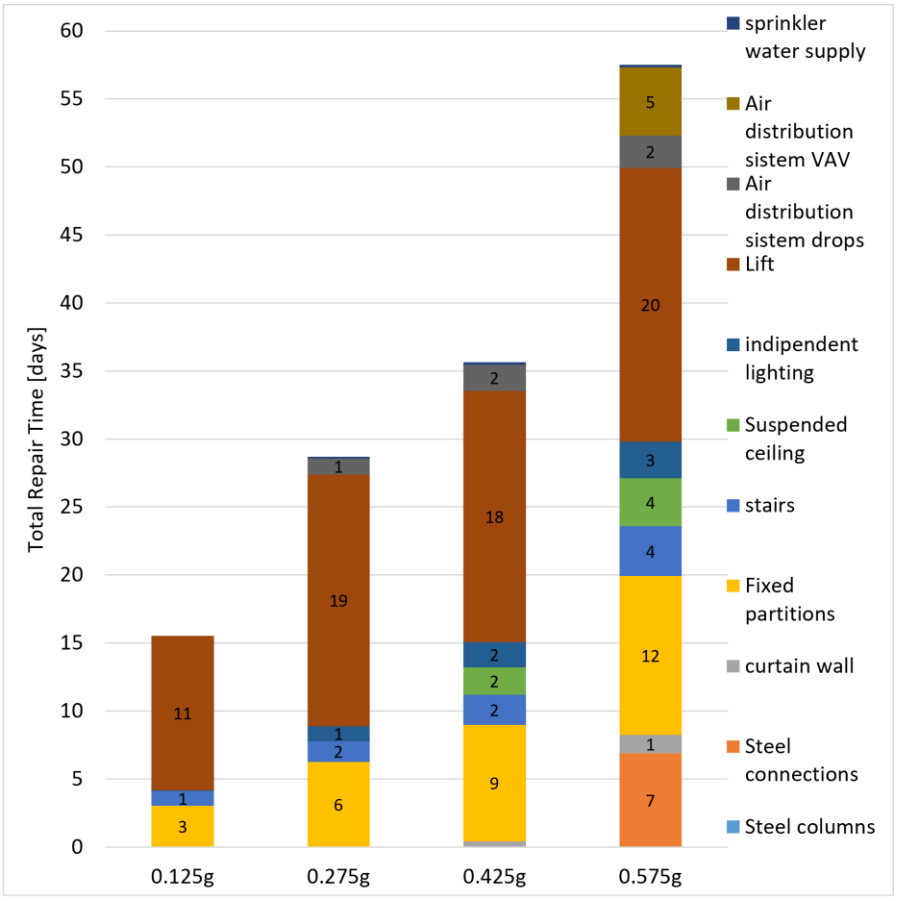

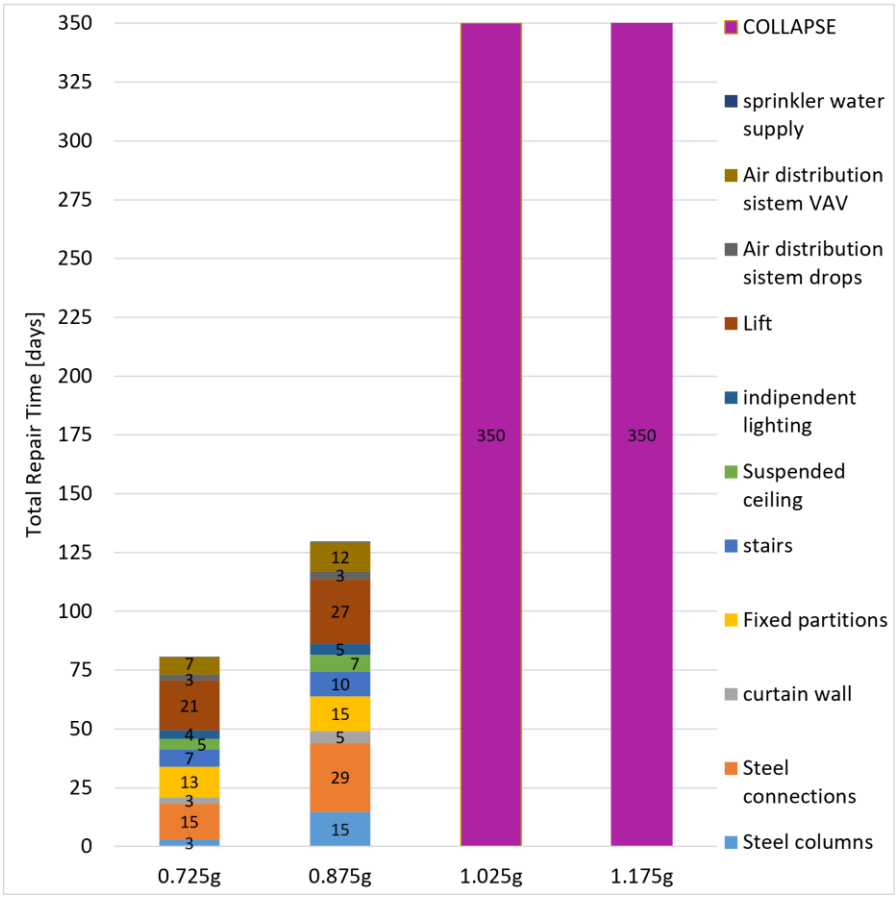

Figure 4.15: component contribution to median repair time: 0..125 g - 1.175 g

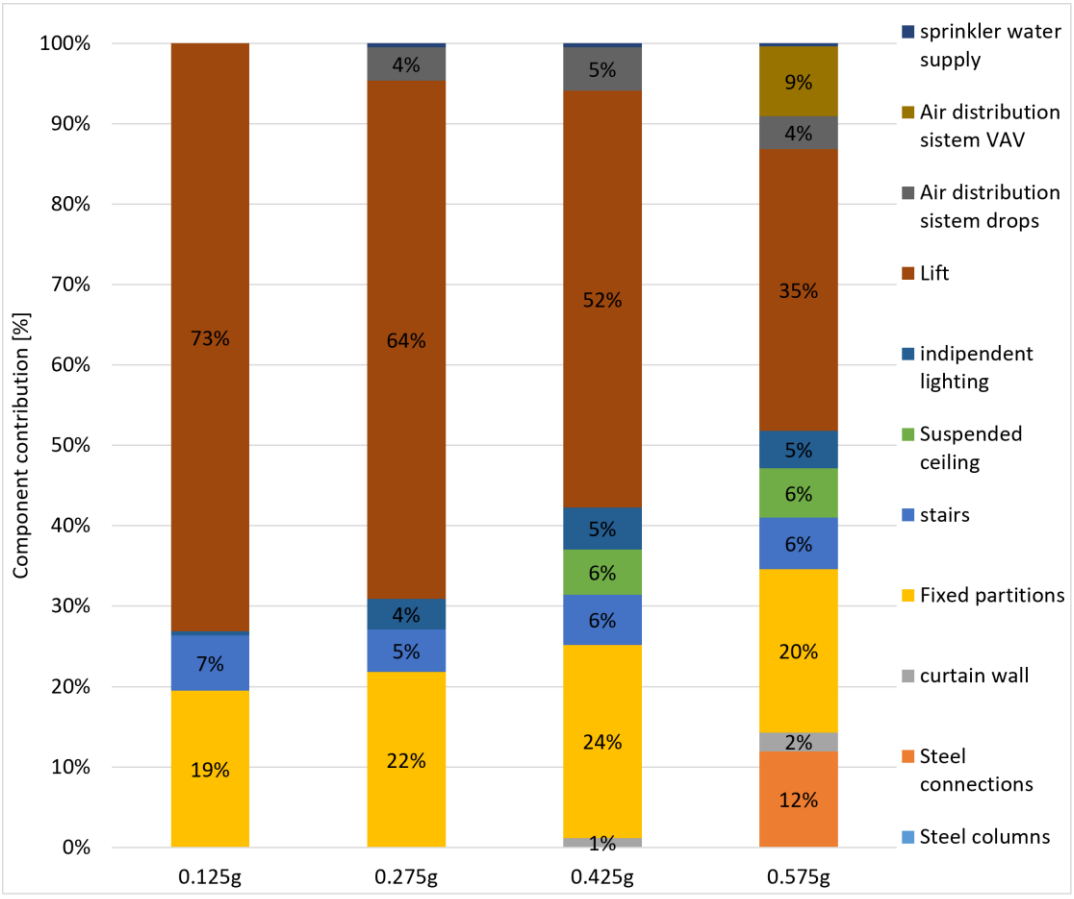

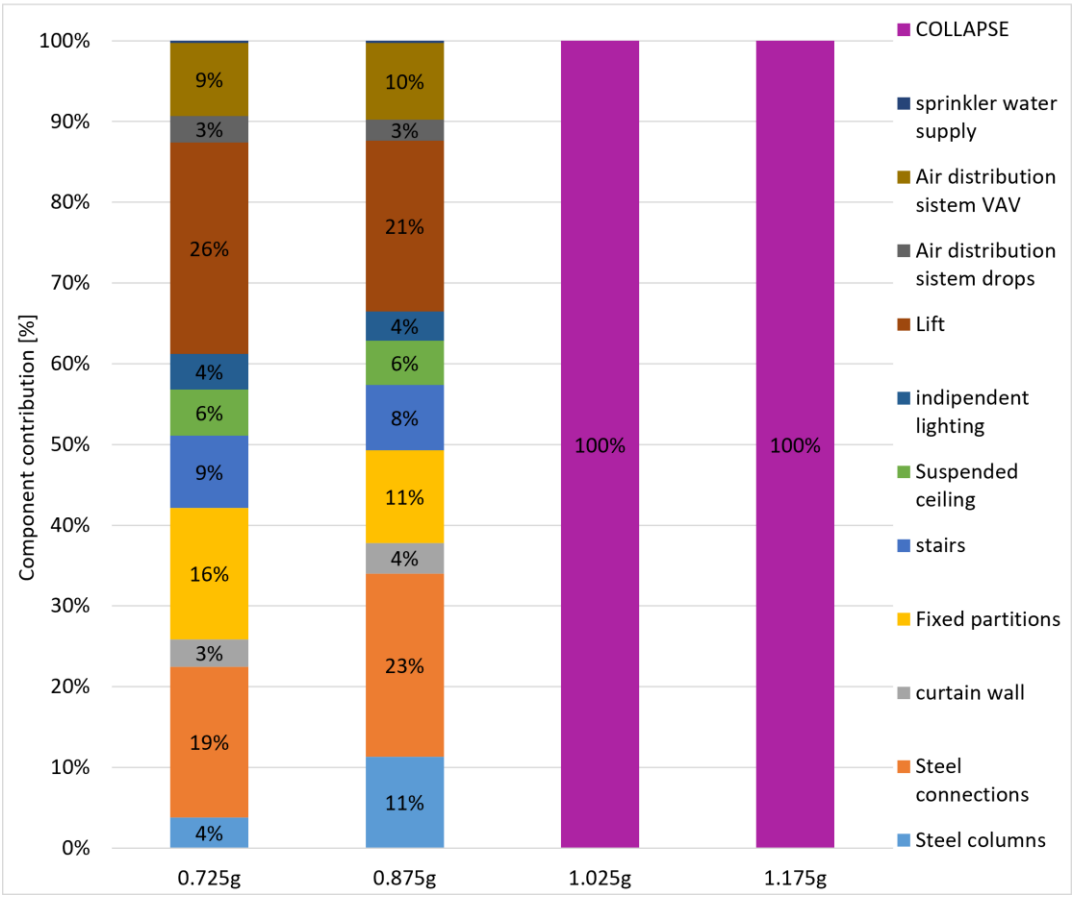

Figure 4.16: percentage component contribution to median repair time: 0.125 g - 1.175 g

4.2.3. Annualized Probabilities

Since in the previous chapter the Moment Resisting Frame building's response is evaluated focusing on each defined intensity, the last step to carry out consist of extending the assessment towards annualized losses. This PACT's evaluation combines the site seismic hazard with the computed fragilities. The hazard curve is computed (Figure 3.49) and divided into 8 chosen segments (Figure 3.50). Each segment is represented by a spectral acceleration and defines the number of analyses that PACT will execute. The resulting fragility representing the building losses of each analyzed segment can be associated with a specific MAFE and, thus, with a specific annualized hazard. Subsequently, all the obtained fragilities are combined, considering that lower intensity measures are more likely to be exceeded and thus their contribution is heavier, even though they result in lower repair costs and time with respect to stronger and rarer events. The final annualized functions describe the yearly probability to exceed a given repair cost and time.

4.2.3.1. Annualized Repair Cost

The annualized repair cost function represents the combination of the whole set of fragility obtained in the time-based analysis (Figure 4.8), considering their probability of occurrence. The result expresses the probability a given repair cost would be exceeded. "Figure 4.17" shows the stacked chart where each intensity contribution to the total probability is illustrated. The intensity legenda is that defined previously (Figure 3.51), where intensity 1 corresponds to the lowest one (0.125 g) and intensity 8 to the highest (1.175 g). "Figure 4.18" represents the total line chart.

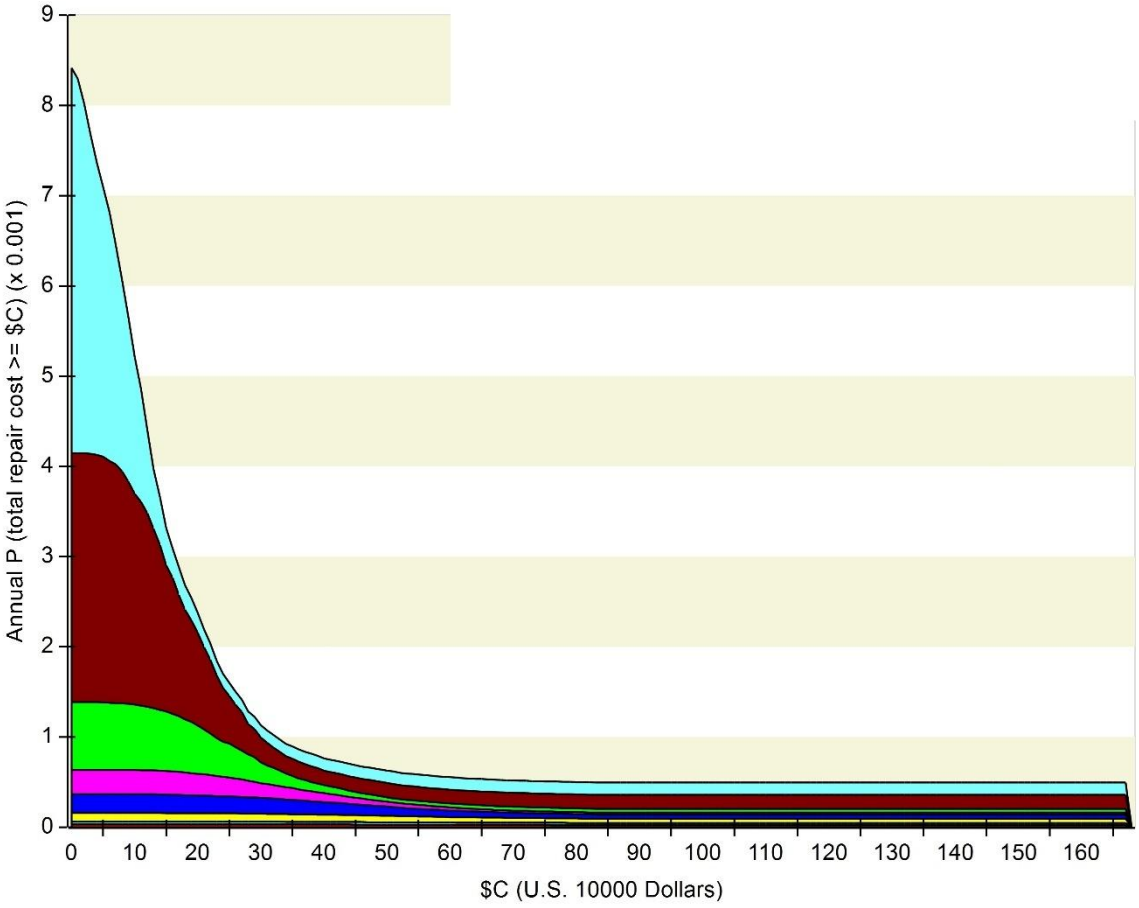

Figure 4.17: annualized repair cost: stacked chart

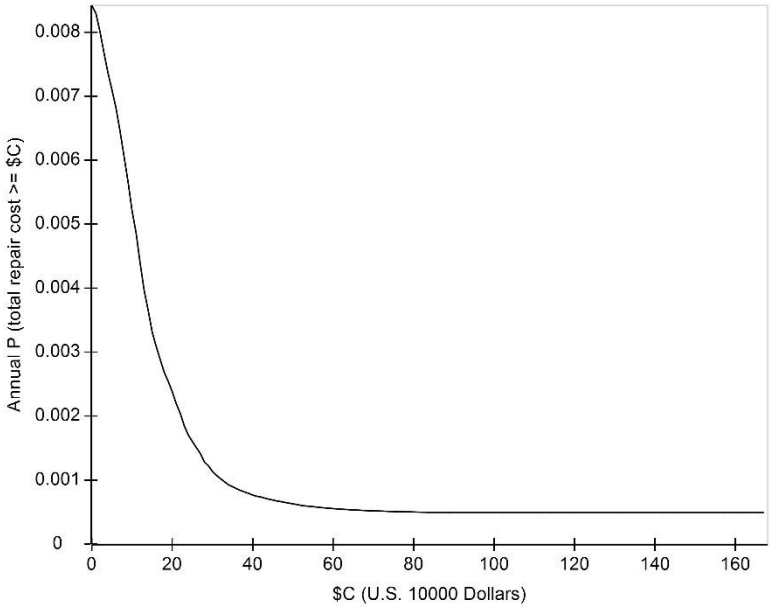

Figure 4.18: annualized repair cost: total line

The cumulative trend of these curves (Figure 4.17, Figure 4.18) shows the expected behavior. Low intensity events dominate the annual probability, and the repair costs are respectively moderate. On the other hand, extremely expensive repair scenarios are much less likely to occur.

4.2.3.2. Annualized Repair Time

Similarly to the previous case (Annualized Repair Cost), annualized repair time functions have been computed. “Figure 4.19” represent the annualized repair time stacked curve, while “Figure 4.20” the total line.

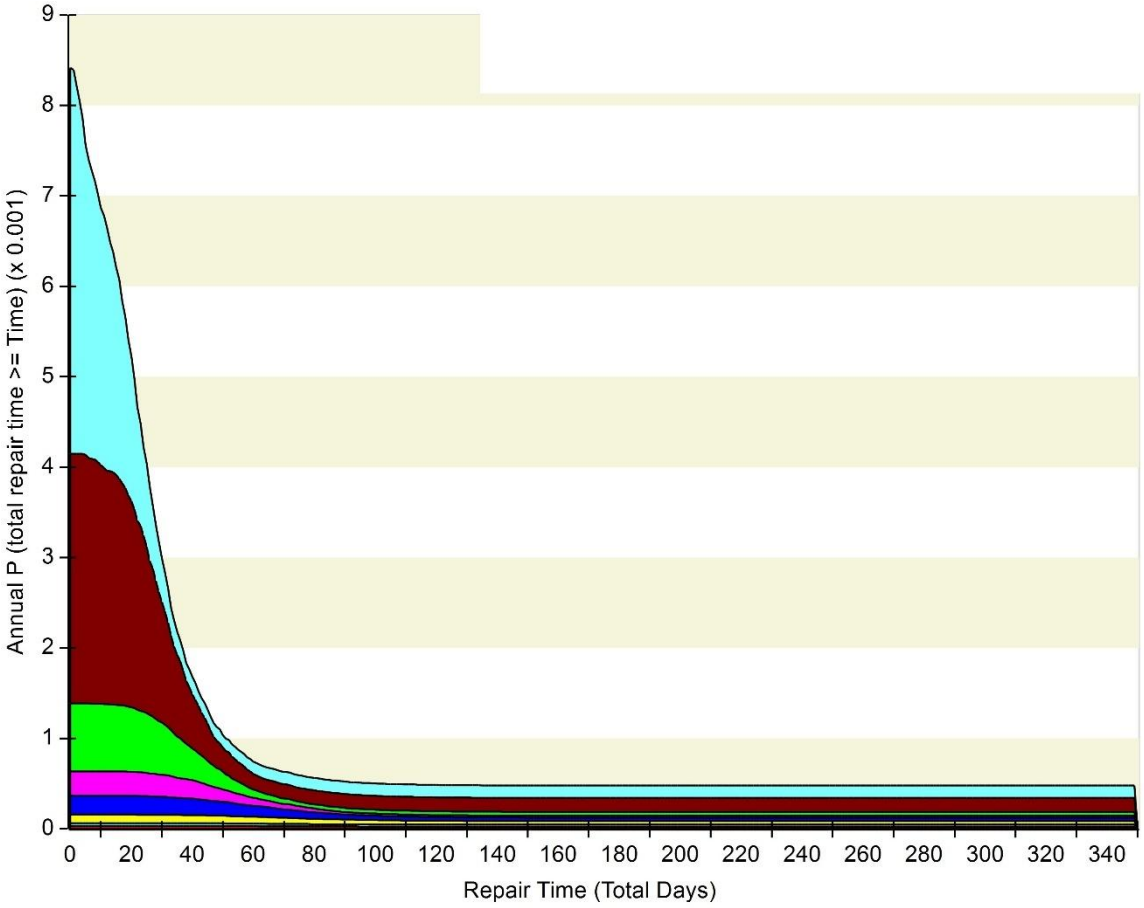

Figure 4.19: annualized repair time: stacked chart

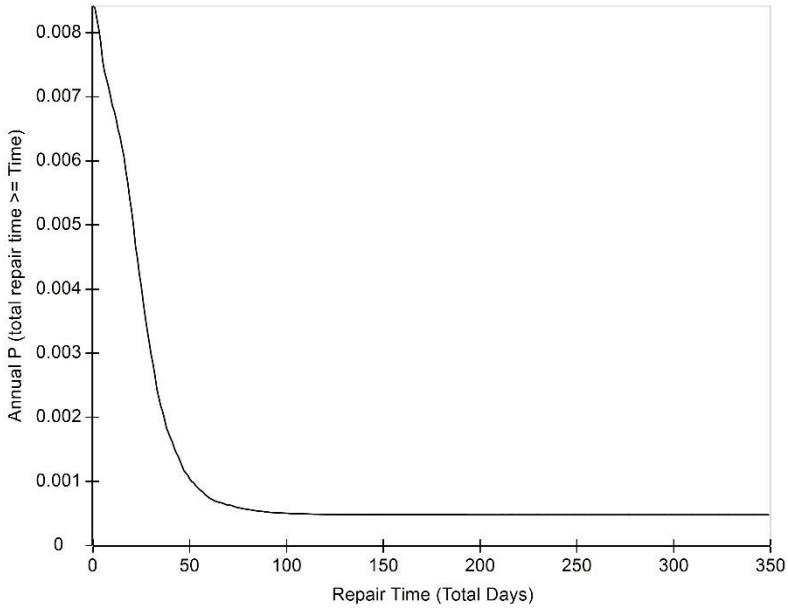

Figure 4.20: annualized repair time: total line

4.2.3.3. Annualized Probability of Collapse, Residual Drift Exceedance and Unsafe Placards

To conclude the assessment of the Moment Resisting Frame building, PACT provides 3 additional information regarding the probability of exceedance of specific limit states. Indeed, in addition to the annual repair cost and time curves, "Figure 4.21" illustrates the annualized probability of collapse, of achieving unsafe placards and, lastly, the yearly probability of complete loss due to residual drift.

LIMIT STATE	ANNUALIZED PROBABILITY [%]
Unsafe Placards	0.06
Complete Loss Due To Residual Drift	0.03
Collapse	0.002

Figure 4.21: annualized limit states exceedance probability

4.3. Time-Based Losses: Infills Integration

Previous sections evaluated seismic losses considering, during the Openseespy modelling phase, the moment resisting system as a bare frame. However, most of the existing steel office buildings have infills panels and these elements, even considered their non-structural meaning, can modify the behavior of the building. Infills panel increase global stiffness and then provide an additional support on the seismic resistance of the frame [26]. To quantify the inflills influence, time-based analysis is carried out again. The previous PACT results are compared

with the new one, obtained by integrating the masonry panels in the Openseespy model and repeating the whole time-based assessment.

4.3.1. Openseespy Infill Modelling

The infills modelling is carried out by adding an equivalent strut to the steel moment resisting frame analyzed in the previous section (Openseespy Model). The chosen approach is the one proposed by Panagiotakos and Fardis, developed to take into account the masonry panel behavior [26]. In the current model, described by "Figure 4.22", each panel is composed by 2 pair of diagonal equivalent strut.

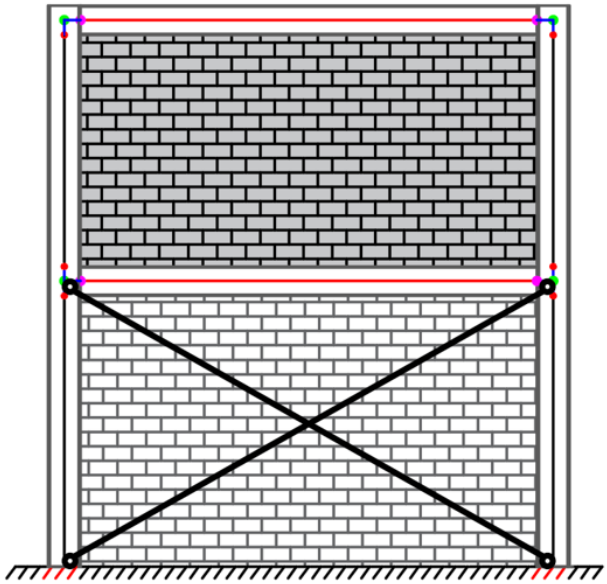

Figure 4.22: Openseespy infills representation

Each diagonal element is modelled as "corotTruss" Openseespy defined element, which hysteretic non-linear behavior is currently assigned to the "Pinching4" material. This material shows the stiffness reduction of the masonry panels and their strength cyclic degradation as illustrated in the following "Figure 4.23". The blue line represents the backbone of the "corotTruss" element, while the orange one is the cyclic degradation of the material when subjected to a seismic excitation.

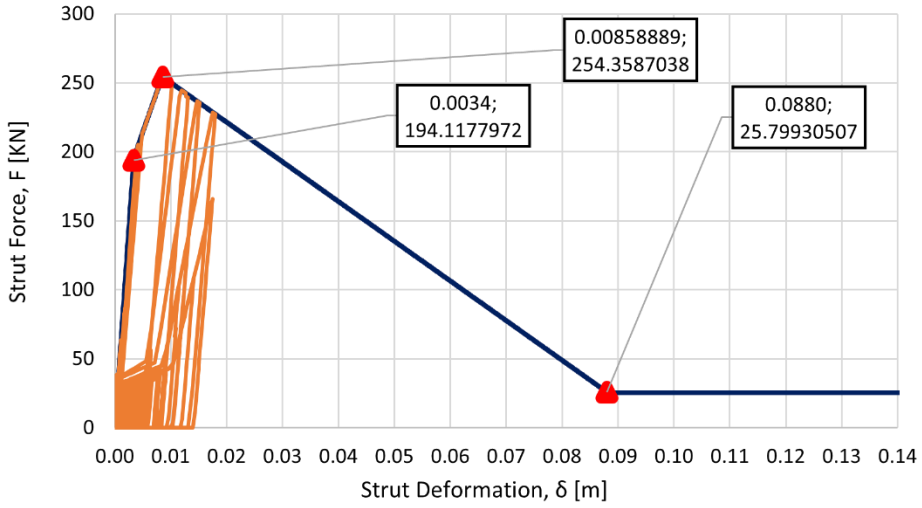

Figure 4.23: masonry panel (Openseespy "corotTruss" element) behavior

There are showed the main values describing the backbone as well. The yielding, maximum and residual forces in the diagonal strut are, respectively 194, 254, 25 KN. Are reported also the correspondent deformation of the strut. "Figure 4.24" shows a better plotting to deeply understand the pinched behavior of the cycles:

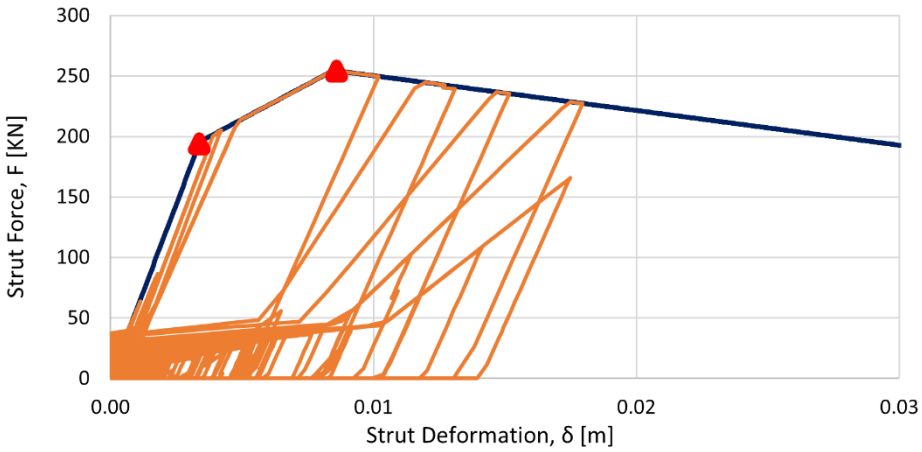

Figure 4.24: masonry panel, pinching illustration

4.3.2. Repair Cost: Variation with Intensity (With/Without Infills)

As developed in the time-based assessment of the bare frame, a losses analysis is carried out by means of FEMA P-58 framework to quantify the infills influence on the global median repair cost. The infills interaction with the moment resisting frame gives a reduction of the global losses and this section aims to evaluate this additional element contribution. "Figure 4.25" illustrates the median repair cost path both for the bare and filled frame.

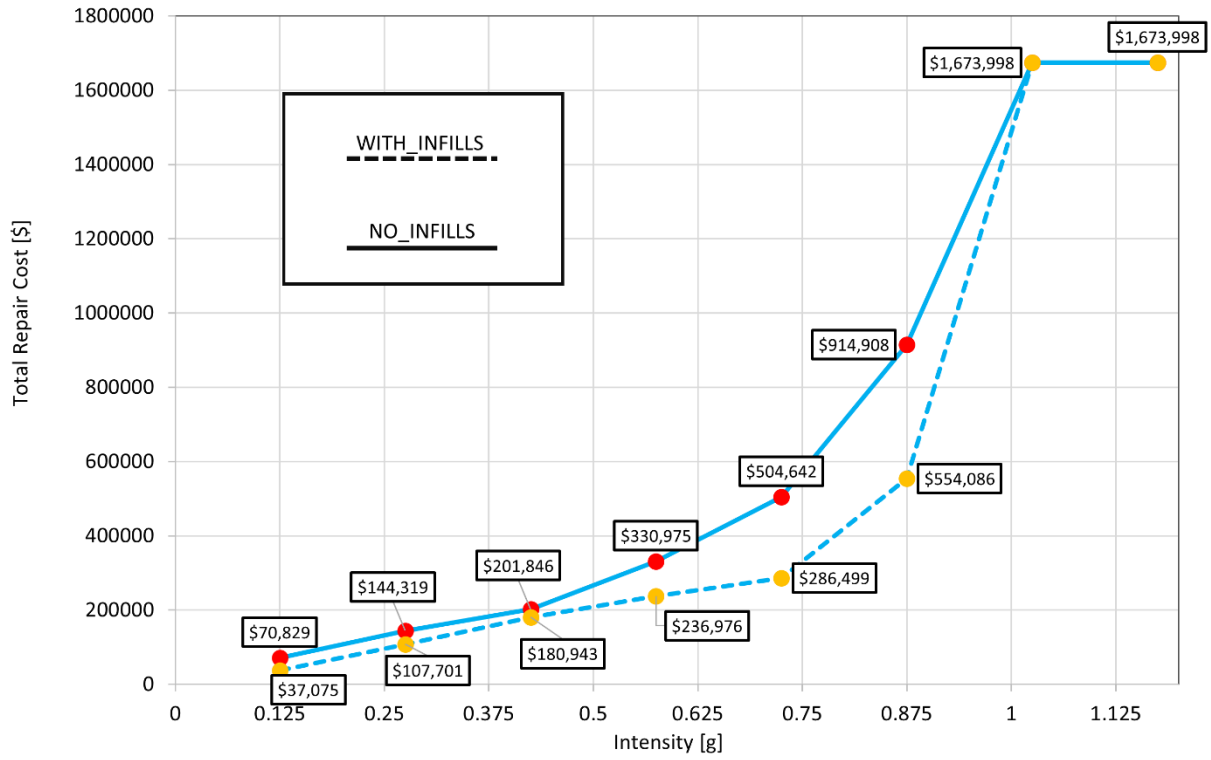

Figure 4.25: median repair cost evolution (with/without infills)

This trend is resumed and explained in the following tables "Figure 4.26". The global cost decrease for the intensity range 0.125g-0.875g, whereas the infill influence expires when the intensity approaches the median collapse level: that's because the infill interaction with the bare frame is considered negligible when the seismic excitation reaches high intensities.

MEDIAN REPAIR COST VARIATION	
0.125g	-48%
0.275g	-25%
0.425g	-10%
0.575g	-28%
0.725g	-43%
0.875g	-39%
1.025g	NO INFLUENCE
1.175g	NO INFLUENCE

Figure 4.26: median repair cost variation [%] (with/without infills)

4.3.2.1. Incremental Component Repair Cost Distribution (With/Without Infills)

The same results obtained in the last table are here reported in "Figure 4.27" with a stacked column chart. Each intensity presents the cost comparison between the bare and infilled

situation (2 stacked column each intensity). Each column represents the total median repair cost occurred in such intensity situation and follows the legenda previously defined (Figure 4.2). Is reported the median repair cost variation (bold value) ahead of each intensity as well. “Figure 4.28” indicates the same results with percentage values.

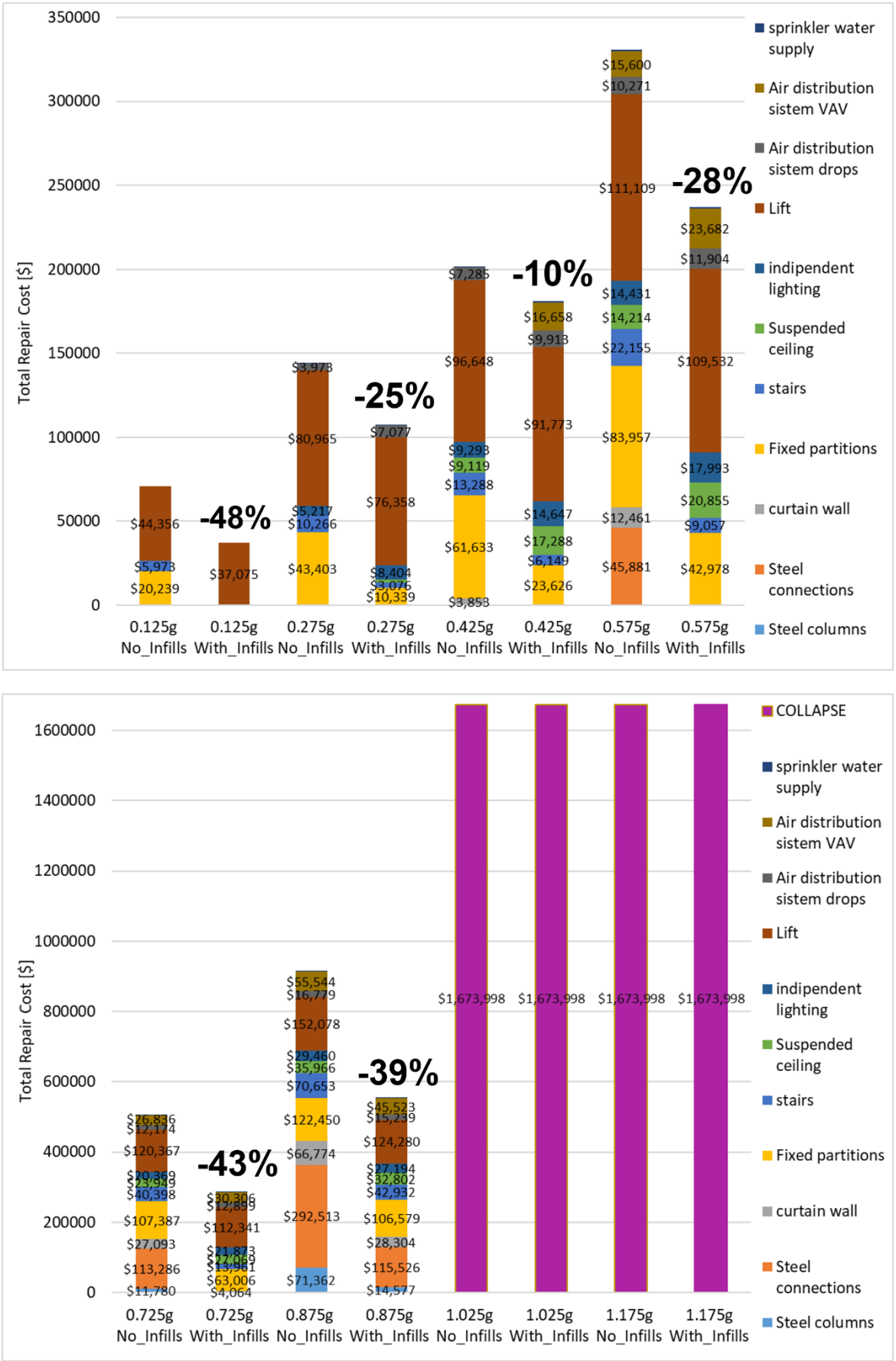

Figure 4.27: component contribution to median repair cost: 0..125 g - 1.175 g (with/without infills)

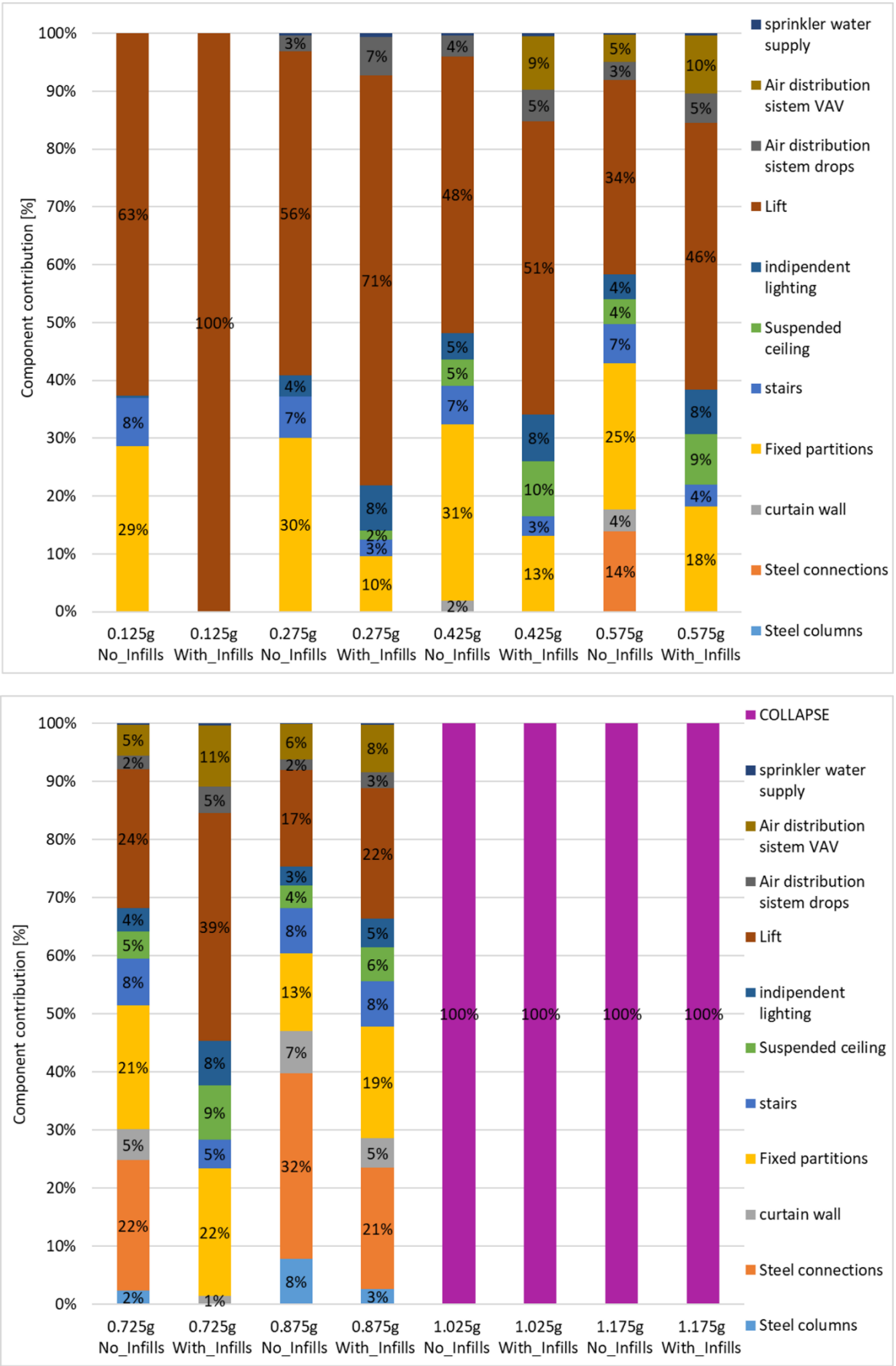

Figure 4.28: percentage component contribution to median repair cost: 0.125 g - 1.175 (with/without infills)

To conclude the losses assessment and deeply understand how each component is influenced by the infill presence, the following step consists into analyze the whole seismic range (0.125g-1.175g) as before, highlighting each single component cost. Indeed, while previous section analyzed the global median repair cost, each component category (shell, interiors, services) is here discussed alone. Infill modelling modifies not only the global median repair cost but the path of each single component. The following figures "Figure 4.29, Figure 4.31, Figure 4.33" illustrate the direct comparison with/without infills, and the subsequent tables "Figure 4.30, Figure 4.32, Figure 4.34" report the average median cost variation. Firstly, is illustrated the shell components cost variation:

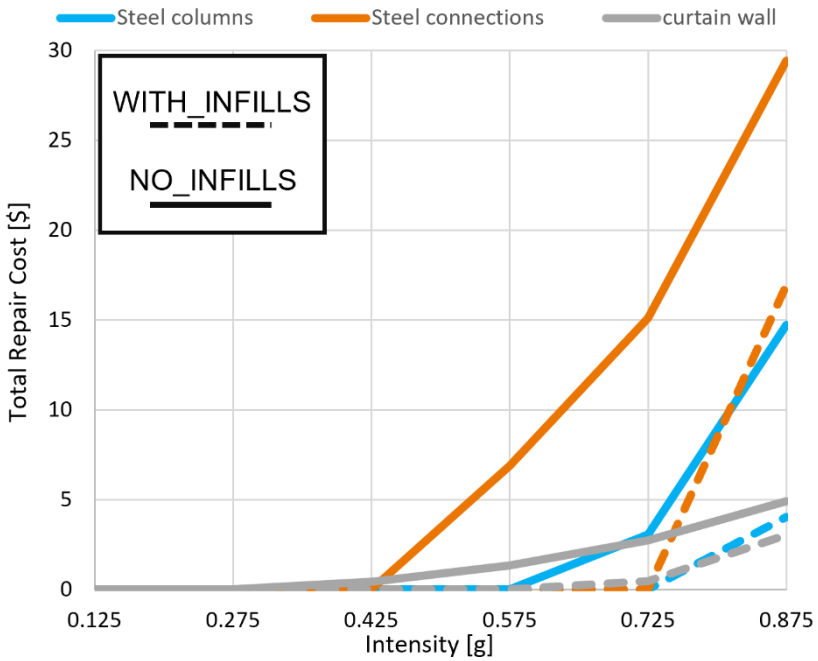

Figure 4.29: shell components cost comparison (with/without infills)

The average cost variation is also reported in the following table:

SHELL COMPONENT AVERAGE COST VARIATION	
Steel Columns	-82%
Steel Connections	-74%
Curtain Wall	-72%

Figure 4.30: shell components average cost variation

Shell component is largely influenced by the infill modelling as the average percentage demonstrates. The drift reduction due to the increased lateral stiffness provided by the masonry panels allows a strong reduction of the average cost. The interiors components cost variation:

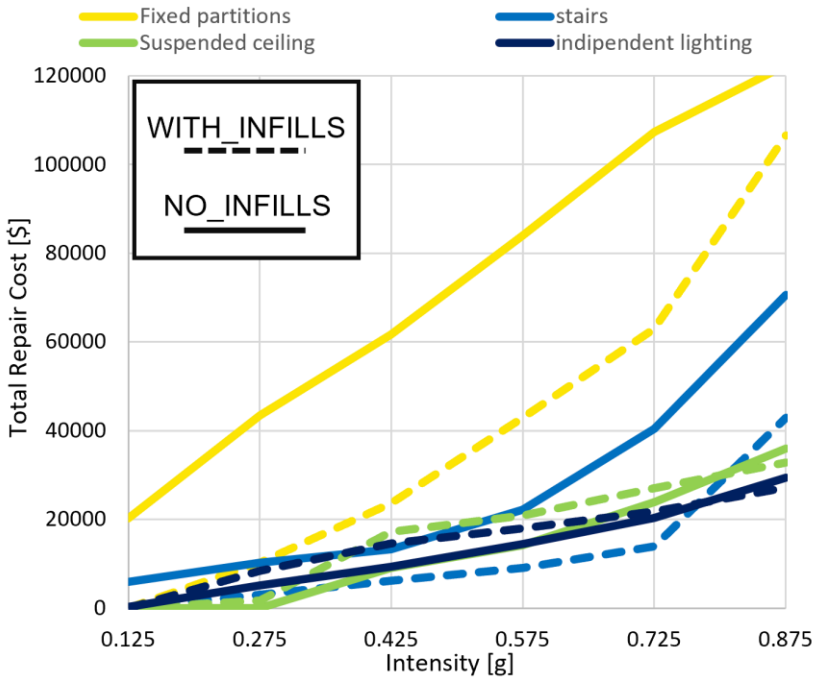

Figure 4.31: interiors components cost comparison (with/without infills)

The average cost variation is then reported:

INTERIOR COMPONENT AVERAGE COST VARIATION	
Fixed Partitions	-44%
Stairs	-54%
Suspended Ceiling	+20%
Indipendent Lighting	+14%

Figure 4.32: interiors components average cost variation

While fixed partitions elements and stairs have benefits from the drift decreasing, elements which are subjected to floor acceleration may incur higher damage such as suspended ceiling and independent lighting. The consequently, mass increasing results in a lower building period and, consequently, higher acceleration (increased stiffness leads elements to attract larger forces/accelerations). Finally, the services elements cost variation:

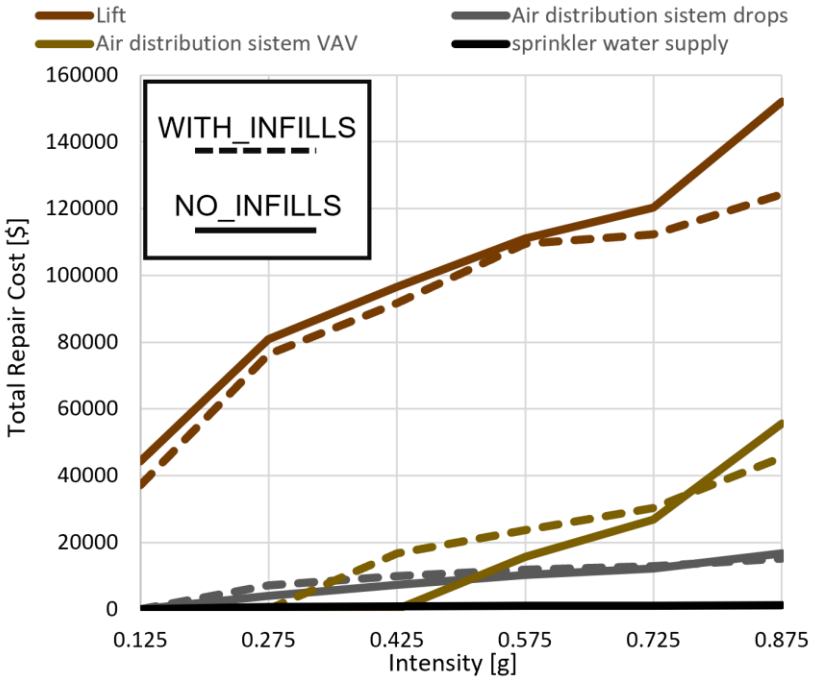

Figure 4.33: services components cost comparison (with/without infills)

And the average cost variation:

SERVICES COMPONENT AVERAGE COST VARIATION	
Lift	-9%
Air Distribution System Drops	+13%
Air Distribution System VAV	+19%
Sprinkler Water Supply	+5%

Figure 4.34: services components average cost variation

Except for the lift, the whole set of services acceleration sensitive components result in increasing in the average median repair cost. Overall, repair cost analysis confirms that the infills inclusion modifies the distribution of the seismic losses: drift-sensitive elements experience lower damage and then occur in lower repair cost, whereas acceleration-sensitive components tend to show an opposite trend. The largest variation is observed for the shell components, then in the interior's components and finally for services elements.

4.3.3. Repair Time: Variation with Intensity (With/Without Infills)

As developed for the repair cost, the same procedure is carried out for repair time as well. The goal is again to compute the actual influence of the infills' presence. "Figure 4.35" shows the global median repair time path for both the bare and filled frame:

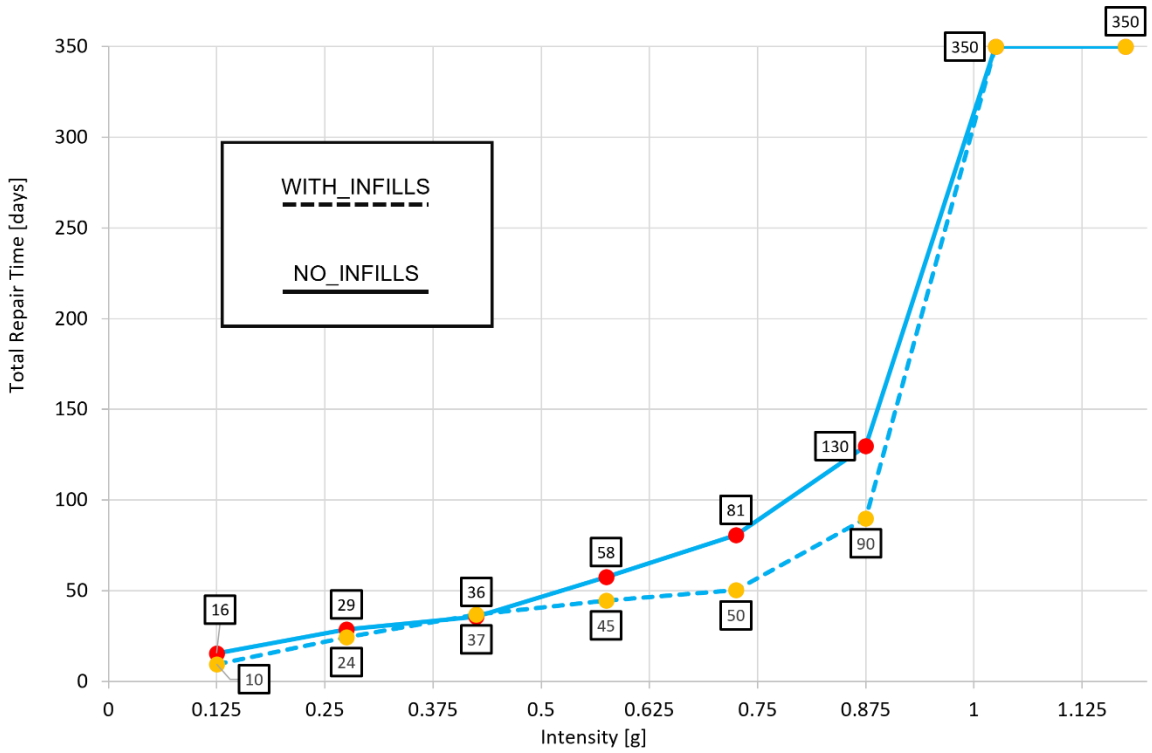

Figure 4.35: median repair time evolution (with/without infills)

This trend is confirmed and resumed in the following "Figure 4.36". The infills presence globally reduces median repair time (except for 0.425 g) and expires when the seismic intensity achieves 1.025 g.

MEDIAN REPAIR TIME VARIATION	
0.125g	-39%
0.275g	-15%
0.425g	+4%
0.575g	-23%
0.725g	-38%
0.875g	-31%
1.025g	NO INFLUENCE
1.175g	NO INFLUENCE

Figure 4.36: median repair time variation [%] (with/without infills)

4.3.3.1. Incremental Component Repair Time Distribution (With/Without Infills)

"Figure 4.37" and "Figure 4.38" shows the median repair time with stacked column chart, comparing the bare and filled situation.

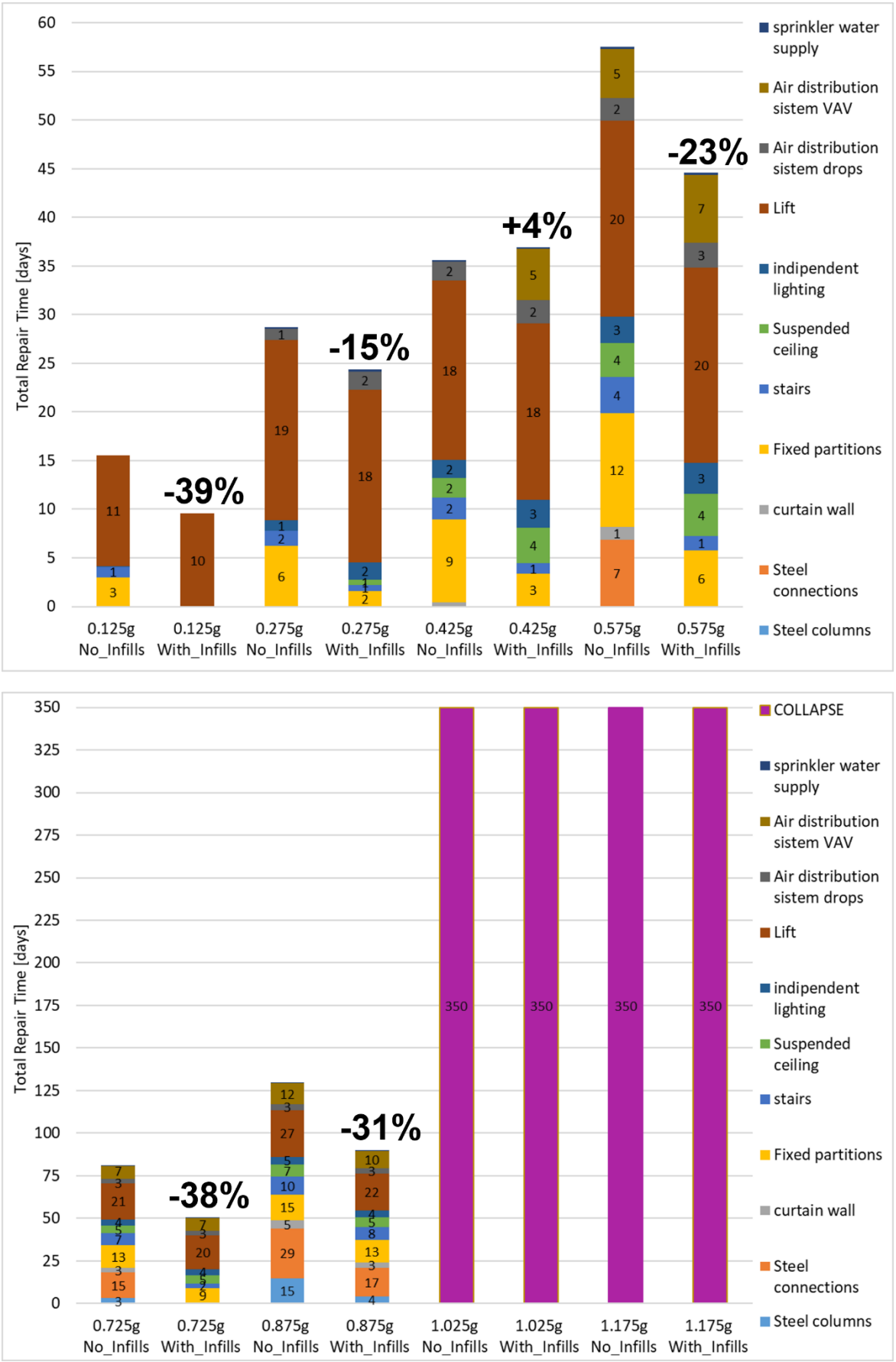

Figure 4.37: component contribution to median repair time: 0..125 g - 1.175 g (with/without infills)

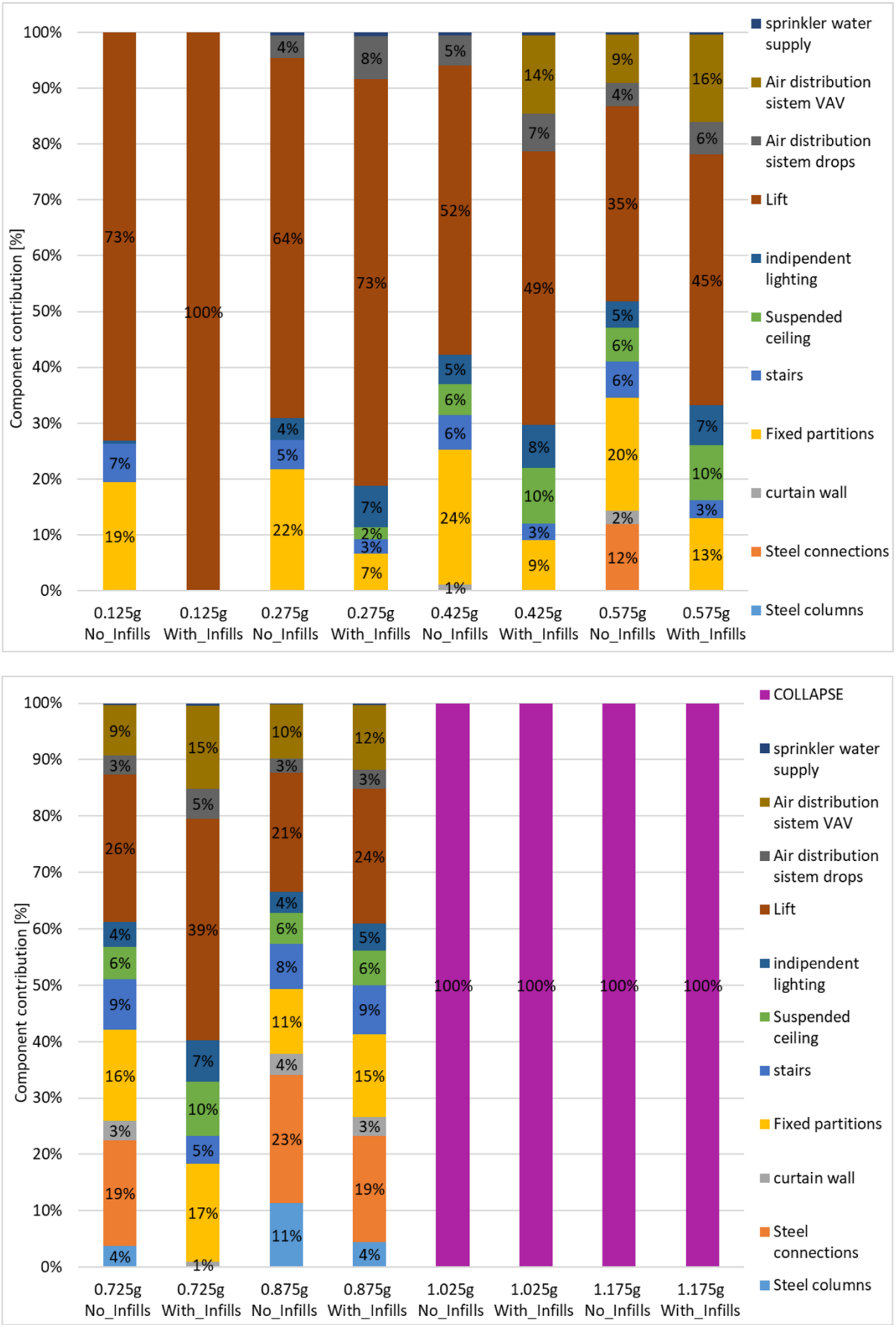

Figure 4.38: percentage component contribution to median repair time: 0.125 g - 1.175 (with/without infills)

To further assess the infills influence, this section evaluates individually the shell, interiors and services component time variation. “Figure 4.39, Figure 4.41, Figure 4.43” compare the with/without infills conditions, while “Figure 4.40, Figure 4.42, Figure 4.44” present the average time variation. The shell time distribution:

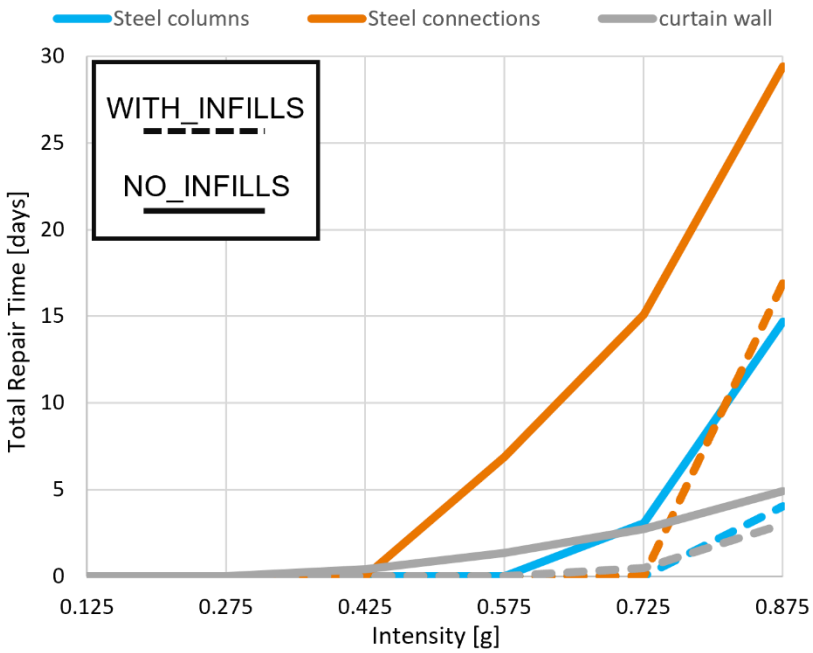

Figure 4.39: shell components time comparison (with/without infills)

And the average time variation:

SHELL COMPONENT AVERAGE TIME VARIATION	
Steel Columns	-77%
Steel Connections	-67%
Curtain Wall	-63%

Figure 4.40: shell components average time variation

Shell component is hugely influenced by infills modelling due to their sensitivity to drift reduction. The interiors time variation:

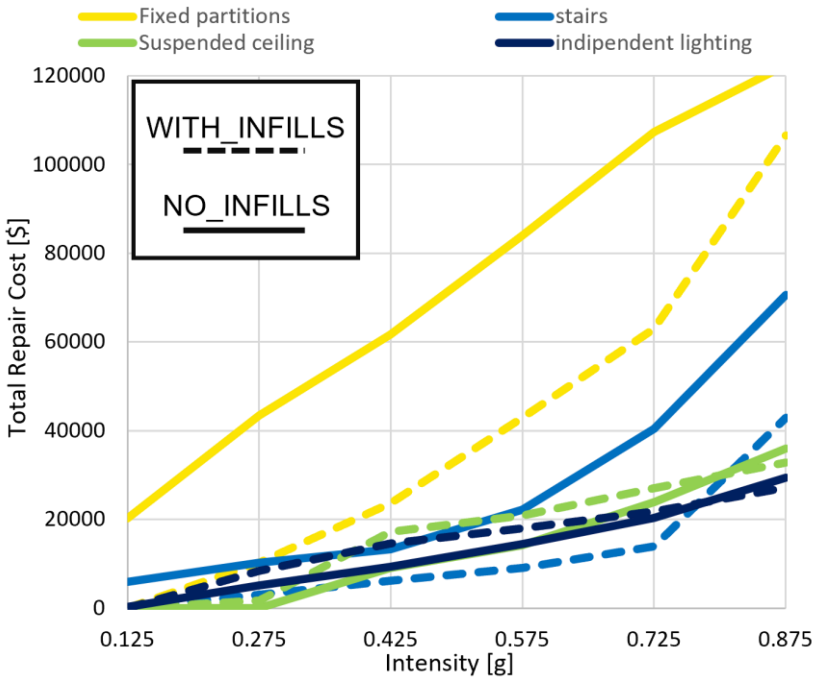

Figure 4.41: interiors components time comparison (with/without infills)

The average time variation is reported as well:

INTERIOR COMPONENT AVERAGE TIME VARIATION	
Fixed Partitions	-43%
Stairs	-49%
Suspended Ceiling	+9%
Indipendent Lighting	+13%

Figure 4.42: interiors components average time variation

Elements such as suspended ceiling and independent lighting, which are subjected to larger floor acceleration, occur in larger repair time. Finally, the services time distribution is subsequent reported:

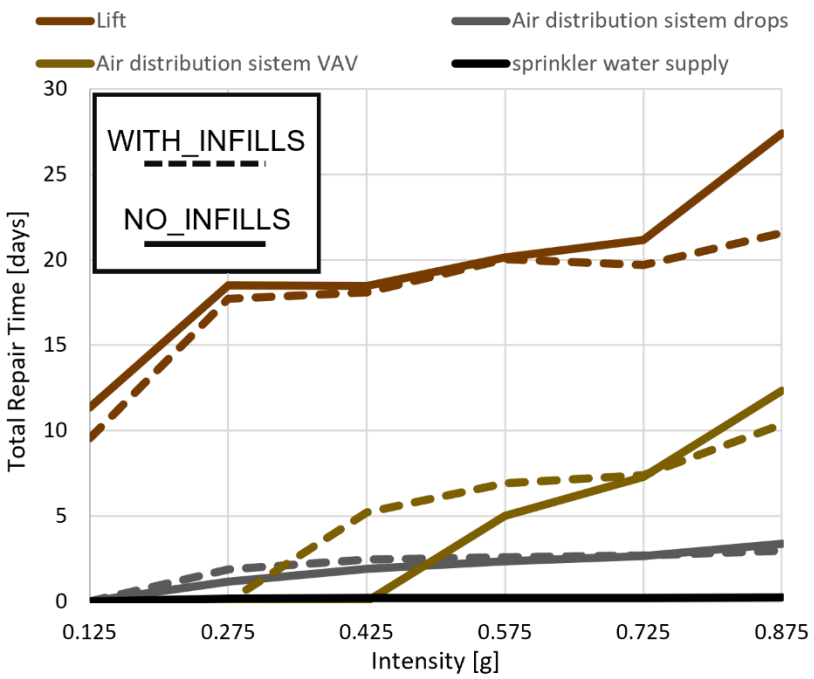

Figure 4.43: services components time comparison (with/without infills)

And the last average time variation:

SERVICES COMPONENT AVERAGE TIME VARIATION	
Lift	-9%
Air Distribution System Drops	+10%
Air Distribution System VAV	+21%
Sprinkler Water Supply	-4%

Figure 4.44: services components average time variation

Overall, the acceleration-sensitive components occur in larger repair time. On the other hand, playing masonry panels a fundamental role in increase of the lateral stiffness, the drift-sensitive elements show a decrease in repair time, due to the decrease in lateral displacement and consequently in the drift demand.

5. CONCLUSIONS

The current work investigated the seismic performance of a steel Moment Resisting Frame office building designed according to EC3, EC8, and located in L'Aquila, Italy. Non-linear analyses using Openseespy are carried out developing pushover, IDAs and fragilities curves. FEMA P-58 methodology is then implemented to quantify building's repair cost and downtime over its lifetime. The structural model is constructed to investigate non-linear behavior of dissipative elements. Plastic hinges were modelled according to Lignos formulation, while columns were defined as fiber-section and beam as elastic, composing together the Moment Resisting Frame system. The main structural performance results are reported as follows (Figure 5.1, Figure 5.2):

PUSHOVER		
	Roof Displacement [mm]	Base Shear [KN]
First Plastic Hinge Couple	50	380
Second Plastic Hinge Couple	80	490
Base Column Plastic Hinges	95	570

Figure 5.1: Moment Resisting Frame building's pushover results

Pushover curve reflect the progressive formation of the plastic hinges in the Moment Resisting Frame's resistant system. Base column hinges are the last one being formed, confirming a good hierarchy of strengths.

FRAGILITIES			
	DS_1 Median Acceleration [m/s^2]	DS_2 Median Acceleration [m/s^2]	Collapse Median Acceleration [m/s^2]
Roof Plastic Hinge Rotation	2.73	9.9	12.5
IDR	1.06	6.15	12.5

Figure 5.2: Moment Resisting Frame building's IDA derived fragilities results

As expected, IDR fragilities result in stronger damages with respect to local EDP one, while maintaining consistent trends. Moreover, the building's response to increasing seismic intensities reflects good ductile behavior. The structural assessment conducted provides the

basis for the subsequent losses computation towards FEMA P-58 framework. PACT comparison between Intensity-Based (code-based) and Scenario-Based (L'Aquila earthquake, 2009), showed a 52% increase of median repair cost and 34% increase of median repair time. Component-level median costs and times increase are illustrated below (Figure 5.3):

MEDIAN LOSSES VARIATION (CODE-BASED VS L'AQUILA 2009)				
	Median Cost Increasing [$]	Median Cost Increasing [%]	Median Time Increasing [days]	Median Time Increasing [%]
Curtain Wall	3752	No Cost At Median	0	No Time At Median
Lift	15019	23	1	7
Fixed Partitions	20886	51	3	49
Stairs	5589	61	1	72
Steel Connection	11132	No Cost At Median	2	No Time At Median

Figure 5.3: component median cost and time increasing from code-based to L'Aquila earthquake, 2009, scenario

Lift and fixed partitions are the most influent drivers, with consistent behavior both for costs and times. The contribution of steel connections becomes relevant during the transition, showing the occurrence of structural damage. Overall, repair times trend reflects quite accurately the cost results. Finally, Time-based analysis extends the losses evaluation over the life-cycle period of the building, combining the hazard curve with each computed fragility. By coupling the fragility with the corresponding mean annual frequency of exceedance, losses are each weighted by its probability of occurring and contribute differently to the global annualized curve. The annualized collapse probability is equal to 0.002%. Similarly, the annualized probabilities of achieving unsafe placards or complete loss due to residual drift are, respectively, 0.06% and 0.03%. The component influence over the entire intensity range is depicted as follows both for costs (Figure 5.4) and times (Figure 5.5):

LOSSES (COST) DISTRIBUTION OVER THE SEISMIC RANGE			
Intensity [g]	Dominant Components (Main categories)	Cost Contribution [%]	Global Median Repair Cost [$]
0.275	Services (Lift) Interiors (Fixed Partitions)	59 (56) 41 (30)	144319
0.575	Services (Lift) Interiors (Fixed Partitions)	42 (34) 40 (25)	330975
0.875	Shell (Steel Connections) Interiors (Fixed Partitions)	47 (40) 28 (13)	914908
1.175	Collapse	Collapse	Collapse (1673998)

Figure 5.4: component contribution to the total median repair cost over the intensities range

LOSSES (TIME) DISTRIBUTION OVER THE SEISMIC RANGE			
Intensity [g]	Dominant Components (Main categories)	Time Contribution [%]	Global Median Repair Time [days]
0.275	Services (Lift) Interiors (Fixed Partitions)	69 (64) 31 (22)	29
0.575	Services (Lift) Interiors (Fixed Partitions)	48 (35) 37 (20)	58
0.875	Shell (Steel Connections) Interiors (Fixed Partitions)	38 (34) 34 (21)	130
1.175	Collapse	Collapse	Collapse (350)

Figure 5.5: component contribution to the total median repair time over the intensities range

At low-moderate intensities losses are driven mainly by non-structural components such as lift and fixed partitions. At higher intensities (0.875 g), the contribution of structural elements becomes dominant, marking the transition of vulnerable components with the increasing seismic demand. At 1.175 g global collapse governed the median response. Overall, the analyses confirm an optimum seismic performance of the designed building, resulting in high ductility, negligible collapse probability and a coherent losses distribution with the expected performance against increasing seismic demand. Finally, the infills' addition in the Openseespy non-linear model allowed to extend the previous assessment considering the additional stiffness provided by masonry panels. Infills presence modify the damage distribution over the seismic range (0.125g-1.175g) and thus the losses amount. "Figure 5.6" and "Figure 5.7" illustrate respectively the median repair cost and time variation considering the filled (with infills) and bare (no infills) frame.

MEDIAN REPAIR COST VARIATION (WITH/NO INFILLS)			
Intensity [g]	Median Repair Cost (No_Infills) [$]	Median Repair Cost (With_Infills) [$]	Median Repair Cost Variation [%]
0.125	70829	37075	-48
0.275	144319	107701	-25
0.425	201846	180943	-10
0.575	330975	236976	-28
0.725	504642	286499	-43
0.875	914908	554086	-39
1.025	1673998	1673998	NO INFLUENCE
1.175	1673998	1673998	NO INFLUENCE

Figure 5.6: median repair cost variation (with/no infills)

MEDIAN REPAIR TIME VARIATION (WITH/NO INFILLS)			
Intensity [g]	Median Repair Time (No_Infills) [days]	Median Repair Time (With_Infills)[days]	Median Repair Time Variation [%]
0.125	16	10	-39
0.275	29	24	-15
0.425	36	37	+4
0.575	58	45	-23
0.725	81	50	-38
0.875	130	90	-31
1.025	350	350	NO INFLUENCE
1.175	350	350	NO INFLUENCE

Figure 5.7: median repair time variation (with/no infills)

Results show losses decreasing up to 48% less in the filled situation with respected to the bare frame condition. Such benefit expires when seismic level achieves strong intensities (1.025g/1.175g) and the infills contribute become negligible. To conclude the assessment between the filled and bare system, “Figure 5.8” shows the resume of the average cost variation (considered in the seismic range 0.125g-0.875g, where the infills’ influence is still appreciable) of the individual component.

COMPONENT AVERAGE LOSSES VARIATION DUE TO INFILLS MODELLING (0.125g-0.875g)			
Component Category	Individual Component	Average Cost Variation [%]	Average Time Variation [%]
Shell	Steel Columns	-82	-77
	Steel Connections	-74	-67
	Curtain Wall	-72	-63
Interiors	Fixed Partitions	-44	-43
	Stairs	-54	-49
	Suspended Ceiling	+20	+9
	Indipendent Lighting	+14	+13
Services	Lift	-9	-9
	Air Distribution System Drops	+13	+10
	Air Distribution System VAV	+19	+21
	Sprinkler Water Supply	+5	-4

Figure 5.8: component average losses variation due to infills modelling

The analysis illustrates that drift-sensitive elements (such as steel elements, partitions, ecc) generally experience a losses reduction in terms of both repair cost and time. On the other hand, acceleration-sensitive elements (such as suspended ceiling, air distribution system, ecc) result in losses increase. This is due to the increased lateral stiffness provided by the panel integration, which conversely leads to increased floor accelerations and thus greater damage. Furthermore, structural elements are most influenced by infills integration, resulting in largest percentual losses reduction, followed by interiors components and finally by services elements. Overall, the combined assessment of the bare and filled system confirms how the losses evolve over the seismic range in the building life's period. The comparison between the 2 modelling solutions highlights that the inclusion of the masonry panels results in a more realistic and comprehensive losses distribution, showing the importance of properly account for the panel integration.

References

[1] A. Hassanzadeh, S. M. Asce, S. Moradi, A. M. Asce, H. V Burton, and M. Asce, "State-of-the-Art Review Performance-Based Design Optimization of Structures: State-of-the-Art Review," 2022, doi: 10.1061/JSENDH.

[2] E. Nastri and A. Pisapia, "Performance-Based Seismic Design," Mar. 01, 2025, *Multidisciplinary Digital Publishing Institute (MDPI)*. doi: 10.3390/app15052254.

[3] M. Mahoney and R. D. Hanson, "Seismic Performance Assessment of Buildings Volume 1-Methodology Second Edition Prepared for FEDERAL EMERGENCY MANAGEMENT AGENCY." [Online]. Available: www.ATCouncil.org

[4] G. A. P. D. E. B. Edmond V. Muho, "Deformation dependent equivalent modal damping ratios for the performance-based seismic design of plane R/C structures," *Soil Dynamics and Earthquake Engineering*, vol. 129, 2020.

[5] European Committee for Standardization (CEN), "Eurocode 8: Design of structures for earthquake resistance – Part 1: General rules, seismic actions and rules for buildings," Brussels, 2004.

[6] E. N. V. P. P. T. Rosario Montuori, "A simplified performance based approach for the evaluation of seismic performances of steel frames," *Eng Struct*, vol. 224, 2020.

[7] A.J Kappos, "Evaluation of behaviour factors on the basis of ductility and overstrength studies," vol. 21, no. 9, 1999.

[8] Z. Wang, "Seismic hazard assessment: Issues and alternatives," *Pure Appl Geophys*, vol. 168, no. 1–2, pp. 11–25, Jan. 2011, doi: 10.1007/s00024-010-0148-3.

[9] P. R. T E P R I M A and P. G. Verdi, "GAZZETTA UFFICIALE DELLA REPUBBLICA ITALIANA DIREZIONE E REDAZIONE PRESSO IL MINISTERO DELLA GIUSTIZIA-UFFICIO PUBBLICAZIONE LEGGI E DECRETI-VIA ARENULA, 70-00186 ROMA AMMINISTRAZIONE PRESSO L'ISTITUTO POLIGRAFICO E ZECCA DELLO STATO-VIA SALARIA, 691-00138 ROMA-CENTRALINO 06-85081-LIBRERIA DELLO STATO Aggiornamento delle «Norme tecniche per le costruzioni»," 2018.

[10] Pacific Earthquake Engineering Research Center (PEER), "NGA-East: Adjustments to Median Ground-Motion Models for Central and Eastern North America," 2015.

[11] D. Bindi *et al.*, "Ground motion prediction equations derived from the Italian strong motion database," *Bulletin of Earthquake Engineering*, vol. 9, no. 6, pp. 1899–1920, Dec. 2011, doi: 10.1007/s10518-011-9313-z.

[12] D. M. Boore and G. M. Atkinson, "Ground-motion prediction equations for the average horizontal component of PGA, PGV, and 5%-damped PSA at spectral periods between 0.01 s and 10.0 s," *Earthquake Spectra*, vol. 24, no. 1, pp. 99–138, 2008, doi: 10.1193/1.2830434.

[13] D. Vamvatsikos and C. Allin Cornell, "Incremental dynamic analysis," *Earthq Eng Struct Dyn*, vol. 31, no. 3, pp. 491–514, 2002, doi: 10.1002/eqe.141.

[14] European Committee for Standardization, *Eurocode 0: Basis of structural design. EN 1990:2002 + A1:2005 + A1:2008 + A1:2010*. Brussels, 2002.

[15] European Committee for Standardization (CEN), "Eurocode 3: Design of steel structures – Part 1-1: General rules and rules for buildings".

[16] A. M. Reinhorn and M. R. Willford, "Nonlinear Structural Analysis For Seismic Design A Guide for Practicing Engineers Gregory G. Deierlein." [Online]. Available: www.curee.org

[17] D. G. Lignos and H. Krawinkler, "Deterioration Modeling of Steel Components in Support of Collapse Prediction of Steel Moment Frames under Earthquake Loading," *Journal of Structural Engineering*, vol. 137, no. 11, pp. 1291–1302, Nov. 2011, doi: 10.1061/(asce)st.1943-541x.0000376.

[18] P. R. , R. E. , O. W. Luzi L., "Engineering strong motion database (ESM)," 2016.

[19] P. R. , P. F. , L. L. , R. E. , F. C. , L. G. , D. A. M. , B. R. , B. G. , I. I. Sgobba S., "REXELweb."

[20] F. Gutiérrez-Urzúa, F. Freddi, and L. Di Sarno, "Comparative analysis of code-based approaches for seismic assessment of existing steel moment resisting frames," *J Constr Steel Res*, vol. 181, Jun. 2021, doi: 10.1016/j.jcsr.2021.106589.

[21] M. Mahoney and R. D. Hanson, "FEMA P-58-2 / Seismic Performance Assessment of Buildings Volume 2-Implementation Guide Second Edition Prepared for FEDERAL EMERGENCY MANAGEMENT AGENCY," 2018. [Online]. Available: www.ATCouncil.org

[22] H. R. Mahoney M, "FEMA P-58-3 / Seismic Performance Assessment of Buildings, Volume 3 – Supporting Electronic Materials, Third Edition."

[23] J. Furley *et al.*, "Time-to-Functionality Fragilities for Performance Assessment of Buildings," *Journal of Structural Engineering*, vol. 147, no. 12, Dec. 2021, doi: 10.1061/(asce)st.1943-541x.0003195.

[24] M. De Iuliis, O. Kammouh, G. P. Cimellaro, and S. Tesfamariam, "Downtime estimation of building structures using fuzzy logic," *International Journal of Disaster Risk Reduction*, vol. 34, pp. 196–208, Mar. 2019, doi: 10.1016/j.ijdrr.2018.11.017.

[25] Danciu L.; Nandan S.; Reyes C.; Basili R.; Weatherill G.; Beauval C.; Rovida A.; Vilanova S.; Sesetyan K.; Bard P.-Y.; Cotton F.; Wiemer S.; Giardini D., "The 2020 update of the European Seismic Hazard Model: Model Overview," 2021.

[26] F. Gutiérrez-Urzúa *et al.*, "PRELIMINARY NUMERICAL ANALYSIS OF THE SEISMIC RESPONSE OF STEEL FRAMES WITH MASONRY INFILLS RETROFITTED BY BUCKLING RESTRAINED BRACES."